



Calhoun: The NPS Institutional Archive
DSpace Repository

Theses and Dissertations

1. Thesis and Dissertation Collection, all items

1983-09

Analysis of observed and modeled mixed layers: NOCAL region

Durban, Diane C.

Monterey, California. Naval Postgraduate School

<http://hdl.handle.net/10945/19630>

This publication is a work of the U.S. Government as defined in Title 17, United States Code, Section 101. Copyright protection is not available for this work in the United States.

Downloaded from NPS Archive: Calhoun



Calhoun is the Naval Postgraduate School's public access digital repository for research materials and institutional publications created by the NPS community. Calhoun is named for Professor of Mathematics Guy K. Calhoun, NPS's first appointed -- and published -- scholarly author.

Dudley Knox Library / Naval Postgraduate School
411 Dyer Road / 1 University Circle
Monterey, California USA 93943

<http://www.nps.edu/library>

NAVAL POSTGRADUATE SCHOOL

Monterey, California



THESIS

ANALYSIS OF OBSERVED AND MODELED MIXED
LAYERS: NOCAL REGION

by

Diane C. Durban

September 1983

Thesis Advisor:

C.N.K. Mooers

Approved for public release; distribution unlimited

Prepared for:
Office of Naval Research
Ocean Sciences and Technology Division (Code 422PO)
Arlington, Virginia 22217

T215154

NAVAL POSTGRADUATE SCHOOL
Monterey, California

Rear Admiral John J. Ekelund
Superintendent

David A. Schradly
Provost

This thesis prepared in conjunction with research supported
in part by the Office of Naval Research under RR031-03-01, RR032-02-0K.

Reproduction of all or part of this report is authorized.

Released as a
Technical Report by:

REPORT DOCUMENTATION PAGE		READ INSTRUCTIONS BEFORE COMPLETING FORM
1. REPORT NUMBER NPS-68-83-005	2. GOVT ACCESSION NO.	3. RECIPIENT'S CATALOG NUMBER
4. TITLE (and Subtitle) Analysis of Observed and Modeled Mixed Layers: NOCAL Region		5. TYPE OF REPORT & PERIOD COVERED Master's Thesis; September 1983
		6. PERFORMING ORG. REPORT NUMBER
7. AUTHOR(s) Diane C. Durban in conjunction with C.N.K. Mooers		8. CONTRACT OR GRANT NUMBER(s) N0001483AF00001
9. PERFORMING ORGANIZATION NAME AND ADDRESS Naval Postgraduate School Monterey, California 93943		10. PROGRAM ELEMENT, PROJECT, TASK AREA & WORK UNIT NUMBERS Program Element: 61153M Project: RRO31-03-01 RRO33-02-0K NR No.: 083-275(647-001X)
11. CONTROLLING OFFICE NAME AND ADDRESS Office of Naval Research, Arlington, VA Code 422PO Naval Postgraduate School, Monterey, CA 93943		12. REPORT DATE September 1983
		13. NUMBER OF PAGES 188
14. MONITORING AGENCY NAME & ADDRESS (if different from Controlling Office)		15. SECURITY CLASS. (of this report) UNCLASSIFIED
		15a. DECLASSIFICATION/ DOWNGRADING SCHEDULE
16. DISTRIBUTION STATEMENT (of this Report) Approved for public release; distribution unlimited		
17. DISTRIBUTION STATEMENT (of the abstract entered in Block 20, if different from Report)		
18. SUPPLEMENTARY NOTES		
19. KEY WORDS (Continue on reverse side if necessary and identify by block number) mixed layer; mixed layer modeling; wind mixing; ocean prediction		
20. ABSTRACT (Continue on reverse side if necessary and identify by block number) Surface mixed layer properties off Northern California (NOCAL) were analyzed statistically and numerically. The observations were acquired on three cruises as part of the Pilot Ocean Prediction Study of the California Current eddies centered ca. 37 to 39N, 125 to 127W during March and August 1982. Mixed layer depth, averaging 33+14m, and a horizontal correlation scale of no more than 35km, which has significance for relating thermal structure		

information from individual temperature profiles to that of Fleet Numerical Oceanography Center's (FNOC) analyses based on a grid length of approximately 300km. Simulations and sensitivity tests were made using the Garwood bulk mixed layer model and the Mellor Level-2.5 diffusion model with the initial and boundary conditions acquired at sea and from FNOC. Upper ocean thermal structure analyses and forecasts were also obtained from the Navy's TOPS/TOPS-EOTS diffusion model, which has since become operational at FNOC. Comparisons of observations, analyses, and model solutions reveal consistent cooling and deepening by the former two models and excessive warming by the latter model. These significant differences are believed to be related to model resolution, model sensitivity, oceanic and atmospheric data quality, and spatial variability.

Approved for public release; distribution unlimited

Analysis of Observed and Modeled Mixed

Layers: NOCAL Region

by

Diane C. Durban
Lieutenant(junior grade)⁷, United States Navy
B.S., United States Naval Academy, 1981

Submitted in partial fulfillment of the
requirements for the degree of

MASTER OF SCIENCE IN METEOROLOGY AND OCEANOGRAPHY

from the

NAVAL POSTGRADUATE SCHOOL
September 1983

ABSTRACT

Surface mixed layer properties off Northern California (NOCAL) were analyzed statistically and numerically. The observations were acquired on three cruises as part of the Pilot Ocean Prediction Study of the California Current eddies centered ca. 37 to 39N, 125 to 127W during March and August 1982. Mixed layer depth, averaging 33 ± 14 m, had a horizontal correlation scale of no more than 35 km, which has significance for relating thermal structure information from individual temperature profiles to that of Fleet Numerical Oceanography Center's (FNOC) analyses based on a grid length of approximately 300 km. Simulations and sensitivity tests were made using the Garwood bulk mixed layer model and the Mellor Level-2.5 diffusion model with the initial and boundary conditions acquired at sea and from FNOC. Upper ocean thermal structure analyses and forecasts were also obtained from the Navy's TOPS/TOPS-EOTS diffusion model, which has since become operational at FNOC. Comparisons of observations, analyses, and model solutions reveal consistent cooling and deepening by the former two models and excessive warming by the latter model. These significant differences are believed to be related to model resolution, model sensitivity, oceanic and atmospheric data quality, and spatial variability.

TABLE OF CONTENTS

I.	INTRODUCTION-----	18
A.	BACKGROUND AND OBJECTIVES-----	18
B.	LITERATURE REVIEW-----	22
1.	Bulk Models-----	22
2.	Summary of Bulk Models-----	26
3.	Garwood Model-----	31
4.	Diffusion Models-----	36
5.	Summary of Diffusion Models-----	39
6.	TOPS/TOPS-EOTS-----	41
7.	Verification Testing of Mixed Layer Models-----	47
C.	STUDY AREA AND ITS CLIMATOLOGY-----	57
II.	THE OBSERVATIONS-----	76
A.	DATA ACQUISITION-----	76
B.	DESCRIPTION OF DATA AVAILABLE-----	80
C.	FORCING FUNCTIONS FOR THE GARWOOD AND MELLOR LEVEL-2.5 MODELS-----	82
III.	STATISTICS-----	94
A.	DETERMINATION OF THE OBSERVED VARIABLE MIXED LAYER DEPTH-----	94
B.	STATISTICAL CHARACTERIZATION-----	99
IV.	ANALYSIS OF OBSERVED AND SIMULATED TEMPERATURE STRUCTURE-----	117
V.	SUMMARY AND CONCLUSIONS-----	169
VI.	RECOMMENDATIONS-----	170

APPENDIX A-----	172
A. DATA PROCESSING PROCEDURES-----	172
APPENDIX B-----	177
LIST OF REFERENCES-----	179
BIBLIOGRAPHY-----	180
INITIAL DISTRIBUTION LIST-----	186

LIST OF TABLES

TABLE I	SUMMARY OF TERMS USED IN BULK MODELS-----	31
TABLE II	SUMMARY OF TERMS USED IN DIFFUSION MODELS----	41
TABLE III	BASIC STATISTICS-----	104
TABLE IV	TEMPERATURE ANOMALIES-----	167
TABLE V	VERTICAL RESOLUTION OF TOPS-----	177

LIST OF FIGURES

1	California Current study domain for Mar. 1982 OPTOMA cruise: (X)'s denote CCSI XBT stations-----	20
2	California Current study domain for Aug. 1982 OPTOMA cruises: (X)'s denote CCSII and CCSIII XBT stations-----	21
3	Temperature versus depth profile with old and new MLD's; h_1 =new mixed layer depth, h_2 =old mixed layer depth-----	25
4	MILE observations versus simulations: NI '77, Dashed curves: observed hour average T(5m) and depth where T is 0.1C colder than T(5m); solid curves: modeled values of mixed layer temperature and depth-----	49
5	Time series of predicted (dashed line) and observed (solid line) temperatures at 6M depth at <u>R.V. Discoverer</u> during the BOMEX Experiment-----	51
6	Skill of advective and nonadvective TOPS over persistence and climatology as indicated from TRANSPAC data-----	56
7	Study domain in relation to bathymetry off Northern and Central California (Contour interval: 200m)-----	58
8	CalCOFI map of mean August geostrophic flow at the surface for years 1950-1965 (Dyn. m; interval: 0.04m)-----	60
9	Dynamic topography of study domain during CCSI (Dyn. cm, interval 1.0, surface relative to 450m)----	61
10	Dynamic topography of study domain during CCSII (Dyn. cm, interval 1.0, surface relative to 450m)----	62
11	Distribution of observations per 1-degree square; the contour interval is 2,500 observations; Values greater than 5,000 are shaded-----	63
12	Long term mean August wind stress vectors: 1857-1972-----	64
13	Long term mean August wind stress curl field: 1857-1972-----	65

14	Long term mean August incident solar radiation: 1901-1972-----	68
15	Long term mean August effective back radiation: 1901-1972-----	69
16	Long term mean August sensible heat flux: 1901-1972-----	70
17	Long term mean August latent heat flux: 1901-1972-----	71
18	Long term mean August net heat exchange: 1901-1972-----	72
19	(Wind Speed)**3, Thermocline Strength, and MLD Mean distributions of wind speed cubed (m**3s**-3) indicating the rate of turbulent energy production, thermocline strength (C), and mixed layer depth (m) for (A) winter (December-February) and (B) summer (June-August)-----	75
20	CCSII cruise track and the nearest TOPS/TOPS-EOTS gridpoints-----	78
21	CCSIII cruise track and the nearest TOPS/TOPS-EOTS gridpoints-----	79
22	Average SST for last half of July 1982-----	83
23	Time series of three hourly averaged DAS recorded air temperatures used in computing forcing functions for the Garwood and Mellor Level-2.5 model simulations-----	85
24	Time series of calculated dewpoint temperatures used to compute forcing functions for the Garwood and Mellor Level-2.5 model simulations-----	86
25	Time series of FNOC analyzed wind components and speeds for 39.05N, 127.72W-----	87
26	Time series of interpolated FNOC analyzed winds -interpolated to the necessary time step-----	88
27	Time series of XBT SST used to compute the forcing functions for the Garwood and Mellor Level-2.5 model simulations-----	90
28	Time series of cloud cover in octals-----	91

29	Time series of net heat flux (Watt/m**2) (Julian days correspond with 31 July-14 August 1982)-----	92
30	Time series of wind speed cubed (cm/sec)**3 (Julian days correspond with 31 July-14 August 1982)-----	93
31	XBT trace depicting an "excellent" new/old mixed layer-----	95
32	XBT trace depicting an "excellent" new and old mixed layer-----	96
33	Histograms of CCSI Bucket and SST, CCSII SST, and CCSIII SST (Temperatures in degrees Celsius)-----	101
34	Autocorrelations function for CCSI bucket temperatures with respect to distance; results depicted are for detrended data; also indicated are the number of data pairs-----	102
35	Autocorrelation function for CCSI XBT SST with respect to distance: results depicted are for detrended data and 'raw' data (with trend); also indicated are the number of data pairs-----	103
36	Autocorrelation functions for CCSII XBT SST with respect to distance; results depicted are for detrended data and 'raw' data; also indicated are the number of data pairs and the 95% confidence limits-----	106
37	Autocorrelation functions for CCSIII XBT SST with respect to distance; results depicted are for detrended data and 'raw' data; also indicated are the number of data pairs and the 95% confidence limits-----	107
38	Histograms of NMLD (meters) for CCSI, CCSII, and CCSIII-----	109
39	Histograms of QMLD (meters) for CCSI, CCSII, and CCSIII-----	110
40	Autocorrelation function for CCSI old mixed layer depth-----	111
41	Autocorrelation functions for CCSII old mixed layer depth-----	112

42	Autocorrelation function for CCSIII old mixed layer depth-----	114
43	Computer contoured old mixed layer depths (meters) from CCSIII Data were interpolated to a regular rotated grid and contoured; Rotation origin: 37.33N, 126.25W; Subplot origin:38.10N, 126.38W-----	115
44	Hand contoured old mixed layer depths (meters) from CCSIII-----	116
45	Overall average profile from Garwood model (Temperature in degrees Celsius)-----	118
46	Average 1 August profile from Garwood model (Temperature in degrees Celsius) initialized with FNOC analyzed profile. (Temperature in degrees Celsius)-----	119
47	Average 2 August profile from Garwood model initialized with FNOC analyzed profile (Temperature in degrees Celsius)-----	120
48	Average 3 August profile from Garwood model initialized with FNOC analyzed profile (Temperature in degrees Celsius)-----	121
49	Average 4 August profile from Garwood model initialized with FNOC analyzed profile (Temperature in degrees Celsius)-----	122
50	Average 5 August profile from Garwood model initialized with FNOC analyzed profile (Temperature in degrees Celsius)-----	123
51	Average 6 August profile from Garwood model initialized with FNOC analyzed profile (Temperature in degrees Celsius)-----	124
52	Average 7 August profile from Garwood model initialized with FNOC analyzed profile (Temperature in degrees Celsius)-----	125
53	Average 8 August profile from Garwood model initialized with FNOC analyzed profile (Temperature in degrees Celsius)-----	126
54	Average 9 August profile from Garwood model initialized with FNOC analyzed profile (Temperature in degrees Celsius)-----	127

55	Average 10 August profile from Garwood model initialized with FNOC analyzed profile (Temperature in degrees Celsius)-----	128
56	Average 11 August profile from Garwood model initialized with FNOC analyzed profile (Temperature in degrees Celsius)-----	129
57	Average 12 August profile from Garwood model initialized with FNOC analyzed profile (Temperature in degrees Celsius)-----	130
58	Average 13 August profile from Garwood model initialized with FNOC analyzed profile (Temperature in degrees Celsius)-----	131
59	Contoured Garwood model simulated T/Z Field-----	133
60	TOPS and TEOTS profiles for 1 August 1982 (Temperature in degrees Celsius)-----	134
61	TOPS and TEOTS profiles for 13 August 1982 (Temperature in degrees Celsius)-----	135
62	Contoured T/Z field composed of TOPS profiles-----	136
63	Average XBT and standard deviation plot for 1 August 1982 (Temperature in degrees Celsius)-----	138
64	Average XBT and standard deviation plot for 2 August 1982 (Temperature in degrees Celsius)-----	139
65	Average XBT and standard deviation plot for 12 August 1982 (Temperature in degrees Celsius)-----	140
66	Average XBT and standard deviation plot for 13 August 1982 (Temperature in degrees Celsius)-----	141
67	Averaging XBT's with steep thermoclines A) Right panel: XBT's to be averages; B) Left panel: Average and median XBT's (shallow (indicated by arrow) and deep, respectively)-----	143
68	Averaging XBT's with less steep thermoclines A) Right panel: XBT's to be averaged; B) Left panel: Average and median XBT's (shallow (indicated by arrow) and deep, respectively)-----	144
69	Contoured temperature/depth of 1800Z XBT's-----	146

70	Daily average and average tuned Garwood profiles: 1 August (Temperature in degrees Celsius)-----	148
71	Daily average and average tuned Garwood profiles: 13 August (Temperature in degrees Celsius)-----	149
72	XBT's 96 and 216 (Temperature in degrees Celsius) Launched at approximately the same location on 4 and 10 August, respectively-----	151
73	August 1 composite of simulated and observed profiles-----	152
74	August 2 composite of simulated and observed profiles-----	153
75	August 3 composite of simulated and observed profiles-----	154
76	August 4 composite of simulated and observed profiles-----	155
77	August 5 composite of simulated and observed profiles-----	156
78	August 6 composite of simulated and observed profiles-----	157
79	August 7 composite of simulated and observed profiles-----	158
80	August 8 composite of simulated and observed profiles-----	159
81	August 9 composite of simulated and observed profiles-----	160
82	August 10 composite of simulated and observed profiles-----	161
83	August 11 composite of simulated and observed profiles-----	162
84	August 12 composite of simulated and observed profiles-----	163
85	August 13 composite of simulated and observed profiles-----	164
86	Time series of FNOC analyzed winds vs DAS logged winds-----	175

GLOSSARY OF NOTATIONS*

A	Horizontal eddy diffusivity coefficient
b	Buoyancy
B	Mean buoyancy
b_*	Nondimensional buoyancy
\overline{bw}	Turbulent buoyancy flux (cm^2/s^3)
c_D	Drag coefficient
c, c_p	Specific heat of seawater (cal/gm-C)
C	Complex mean momentum
\overline{cw}	Flux of complex momentum
D	Damping coefficient for inertial oscillations
dz	Depth increment
e	Total turbulent kinetic energy (TKE)
E_o	TKE flux from atmosphere to ocean produced by breaking waves
E_h	Downward TKE flux at base of homogeneous layer
f	Coriolis parameter (sec^{-1})
F	Downward flux of solar radiation
g	Acceleration due to gravity (m/s^2)
G	Rate of energy production due to mean shear
h	Mixed layer depth
k	Wavenumber of interfacial disturbance
K_H	Vertical eddy diffusion coefficient for heat and salinity
K_M	Vertical eddy diffusion coefficient for momentum
L, ℓ	Obukhov length scale

$m_1 - m_6$ Universal constants computed and used in Garwood model
 ML Mixed layer
 MLD Mixed layer depth
 p Pressure
 q Square root of twice the turbulent kinetic energy
 Q_o Heat flux through sea surface
 Q_h Heat flux through base of ML
 $Q(B)$ Back radiation (cal/sec*cm**2)
 $Q(C)$ Sensible heat flux (cal/sec*cm**2)
 $Q(E)$ Latent heat flux (cal/sec*cm**2)
 $Q(N)$ Net surface heat flux (cal/sec*cm**2)
 $Q(S)$ Clear sky radiation (cal/sec*cm**2)
 Rf Flux Richardson number
 Ri Gradient Richardson number
 R_o Rossby number
 S Salinity
 S_H Stability function for vertical eddy fluxes of heat and salinity
 S_N Stability function for vertical eddy fluxes of momentum
 SST Sea surface temperature (C)
 $\overline{s'w'}$ Vertical eddy flux of salinity
 t Time
 T_o Temperature (C) corresponding with sea surface
 T Temperature (C)
 TKE Turbulent kinetic energy
 $\overline{T'w'}$ Turbulent temperature flux (mwatts/cm**2)

u_*	Friction velocity
U_{10}, W_{10}	Wind speed at 10m (m/sec)
u, v	x and y components of current velocity
U, V	x and y components of mean current velocity
$\overline{u'w'}, \overline{v'w'}$	Momentum fluxes
w	z component of current velocity
x, y	Grid-referenced horizontal coordinates, positive toward east and north, respectively
z	Vertical coordinate, positive upward from sea surface
ρ_w, ρ_o	Reference density for water
ρ	Density of seawater
ν	Molecular diffusivity coefficient
α	Expansion coefficient for heat
β	Expansion coefficient for salt
$\overline{\langle \rangle}$	Vertical average
$(\bar{})$	Ensemble mean
$'$	Departure from mean
τ	Surface wind stress (dynes/cm**2)
τ_ϵ	Dissipation time scale
τ_e	Time scale of TKE transport
ϵ	Dissipation

* Attempts have been made to maintain original notations.

ACKNOWLEDGMENT

I would like to express my appreciation to Professor C.N.K. Mooers, my thesis advisor, for his thoroughness and unbounded enthusiasm through the study; to Professor R.W. Garwood, my first reader, whose guidance and time were most appreciated; to Dr. Michele Reinecker, whose help and patience were essential to the task; to Mr. Ken Pollak of FNOC for his role in acquiring the necessary TOPS/TOPS-ETOS data; to Professor G. Mellor for his down-to-earth guidance; and to the numerous faculty and staff members whose understanding and advice helped lighten the load. Finally, thanks to my family, for their crucial unwavering support, and to my classmates, whose acceptance and friendship helped make this an enjoyable experience.

I. INTRODUCTION

A. BACKGROUND AND OBJECTIVES

Over the past few years, the ocean research community and the Navy have become increasingly aware of the need and measures for ocean thermal structure modeling. Not only has the ocean response to atmospheric forcing become of importance because of its feedback to the atmosphere, but also because of the importance of ocean thermal structure in acoustic propagation. For these and other reasons, a growing study has centered on the upper ocean- "that layer bounded by the surface which exhibits strong seasonal variations...most notable in the local temperature profile of the water column." [Grabowski, et.al., 1982] The nearsurface structure called the mixed- or mixing layer has received significant emphasis. The Glossary of Meteorology defines this structure "as a surface layer of virtually isothermal water due to wind induced turbulent motion and/or free convection which frequently exists above the thermocline". To understand the form and dynamics of the mixed layer and the upper ocean thermocline in general, numerous models have come into use.

The objective of this research is first of all to obtain a description of the characteristics of the mixed layer in a 'test block' of the ocean (ca. 37 to 39N; 125 to 127W)

surveyed during the first and second OPTOMA cruises (Figs. 1, 2) occurring during the second week of March and the first two weeks in August 1982, respectively. (OPTOMA- Ocean Prediction Through Observations, Modeling, and Analysis, -is a joint Harvard/NPS project 'intended to acquire field data to characterize synoptic scale eddies over a domain in the California Current off Northern California, and to 'set up' an eddy-resolving, statistical/dynamical, limited-domain, open boundary numerical ocean prediction model'.) The next objective was to evaluate the thermal structure analysis of the Navy's TOPS model over the second cruise period in comparison with the Mellor level-2.5 model and the Garwood (1976, 1977) bulk mixed layer model. Finally, the results of the three basically single point models were compared with the observations. (Note: TOPS is often considered a quasi-three-dimensional model, because it includes advection by climatological geostrophic currents and wind drift.)

The idea that the vertical distribution of temperature, salinity, and current in the upper ocean layers generally appears to be governed largely by the vertical heat, momentum, and salt fluxes imposed by local air-sea transfer [cf. Camp and Elsberry, 1978] has led to one-dimensional time dependent models which assume horizontal homogeneity. [Klein, 1980] The reliance upon this assumption varies among models as well as regions of applicability.

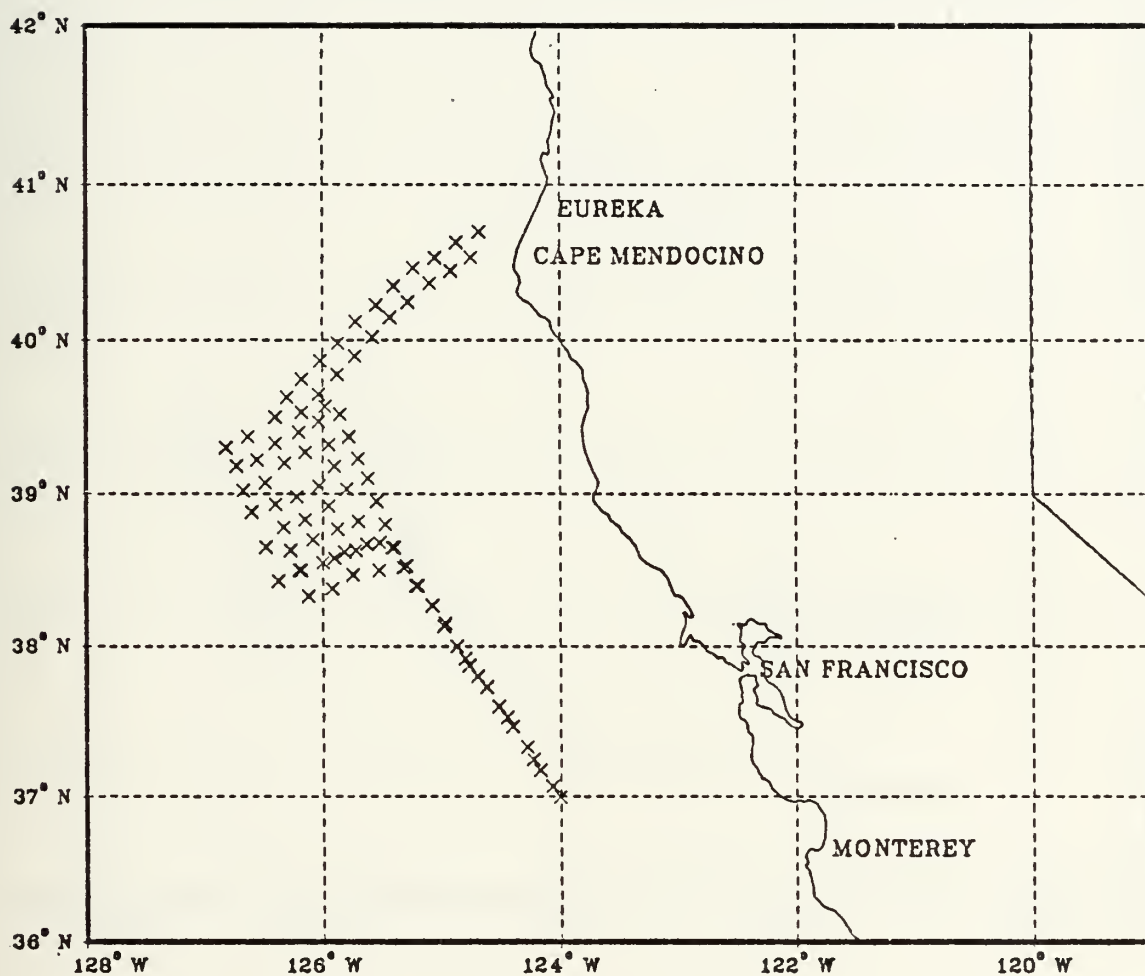


Figure 1. California Current study domain for Mar. 1982 OPTOMA cruise: (X)'s denote CCSI XBT stations

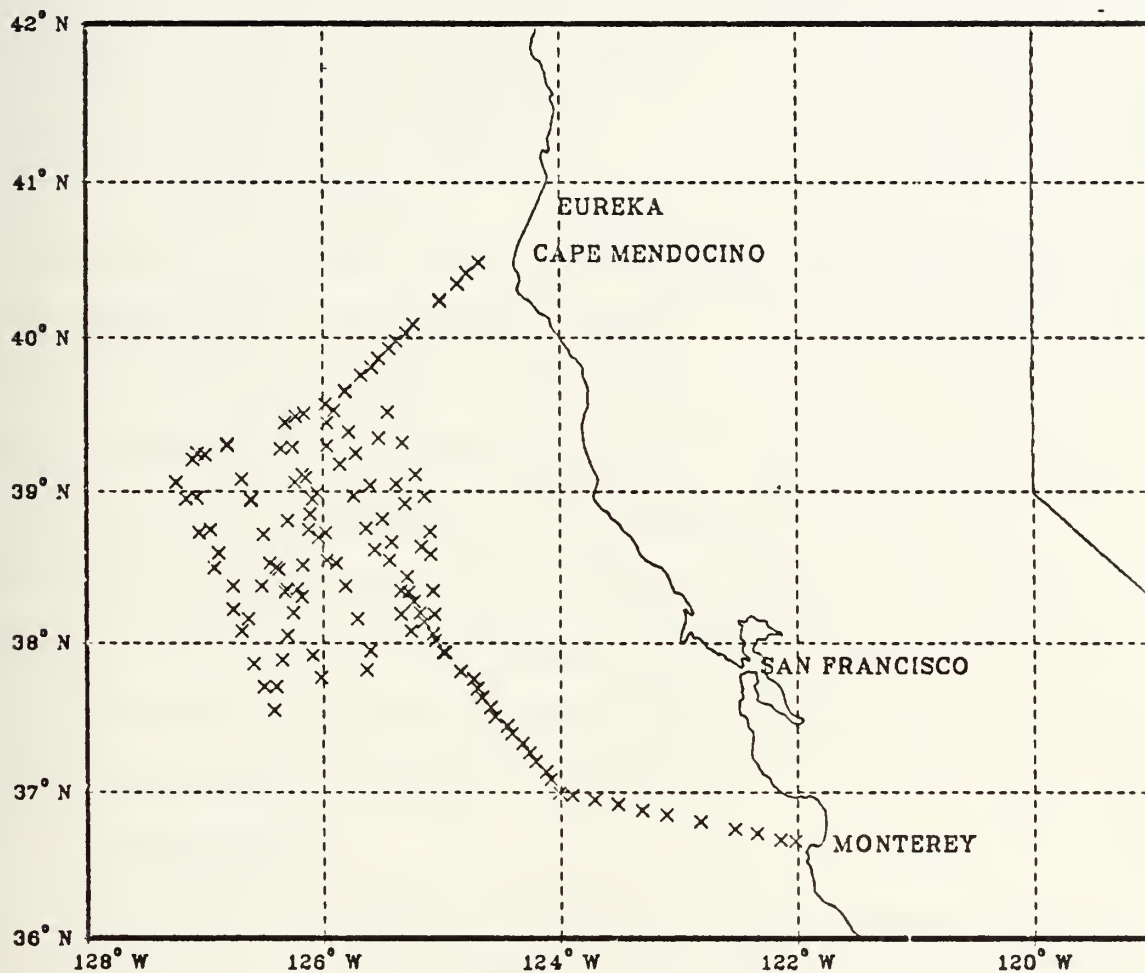


Figure 2. California Current study domain for Aug. 1982 OPTOMA cruises: (X)'s denote CCSII and CCSIII XBT stations

B. LITERATURE REVIEW

Techniques for modeling vary significantly in the degree to which they attempt to represent the upper ocean features and dynamics. The existing models may be categorized as belonging to one of two broad classes:

- a. Bulk Mixed-Layer Models
- b. Diffusion Models

Each class of models will be described with some reference to its components. No attempt, however, will be made to cover all of the models in great detail or to describe each of the existing models or model modifications. The only exceptions to this will be the Garwood (1977) and TOPS [Mellor and Durbin, 1975] models which are of direct interest in this study. The structure of the Mellor Level-2.5 model will not be specifically discussed, because it is very similar to the TOPS (Mellor Level-2) model.

1. Bulk Models

The first category of models, the bulk models, are often referred to as slab models. The reason for this is that Pollard and Millard (1970) and Halpern (1974) showed, with the occurrence of strong wind-forced vertical mixing, the mixed layer responds at the inertial frequency as a rigid slab. This description may be misleading, for it implies that T , S , and V are uniform throughout the layer. (Glossary of Terms) Such, however, is not the case. Instead, the models are based on the assumption that values of the

aforementioned parameters are 'quasi-uniform' within a 'well-mixed layer'. [Klein, 1980] Provided the assumption holds (as it may away from fronts and eddies), the values can be 'lumped' into integrals. [Niiler and Kraus, 1977; Zilitinkevitch et.al, 1979] That is, the 'bulk' models predict integral (or average mixed layer) values for all variables. (Garwood, personal communication)-hence, the perhaps 'better' term -'integral model' is frequently used.

This type of modeling requires an a priori assumption that a mixed layer exists. [Marchuk, et.al., 1977] To describe the layer requires only knowledge of the fluxes at the surface and the base of the mixing layer (i.e., surface and entrainment fluxes). The mathematics of the modeling is, therefore, greatly simplified from partial differential equations to ordinary differential equations.

Basically, mixed layer modeling is founded on two fundamental hypotheses. The first is that the mixed layer is formed as a result of the upper ocean response to forced and free convection. Atmospheric forcing in the form of applied wind stress converts mean kinetic and potential energy to turbulent kinetic energy within the upper ocean. This turbulent motion, in turn, entrains below-layer water into the layer, thereby changing the layer's characteristics. Strong solar heating works against the forced convection to increase the potential energy, and form a shallow turbulent boundary layer. This heating in effect alters only the near

surface water, for invoking the Second Law of Thermodynamics, water cannot be unmixed. Thus, solar heating results in a new mixed layer in addition to the 'old mixed layer'.

(Fig. 3) This distinction between new and old mixed layers will be discussed and utilized in the following sections.

The second hypothesis of importance, a topic of much controversy, invokes the use of some form of the mechanical energy budget as essential in the closure scheme of the more recent models. The disagreement, and consequently a difference in some models, lies in the question as to whether the kinetic energy of the mean flow or the turbulent kinetic energy plays the main role in driving the downward buoyancy flux at the base of the turbulent boundary layer, i.e., in controlling the mixed layer dynamics and entrainment.

Thompson (1976), Pollard (1977), and Price (1977) advocate that the mean kinetic energy is converted directly to potential energy by an instability in the mean flow that causes the bulk Richardson number to be less than some constant of order one. Advocates of the turbulent kinetic energy budget, following the original argument of Kraus and Turner (1967), disagree that this will be the dominant mechanism, reasoning that turbulence-generated instabilities normally have the capacity to erode the interface to the extent that they preclude the existence of mean flow instabilities.

[Garwood, 1979]

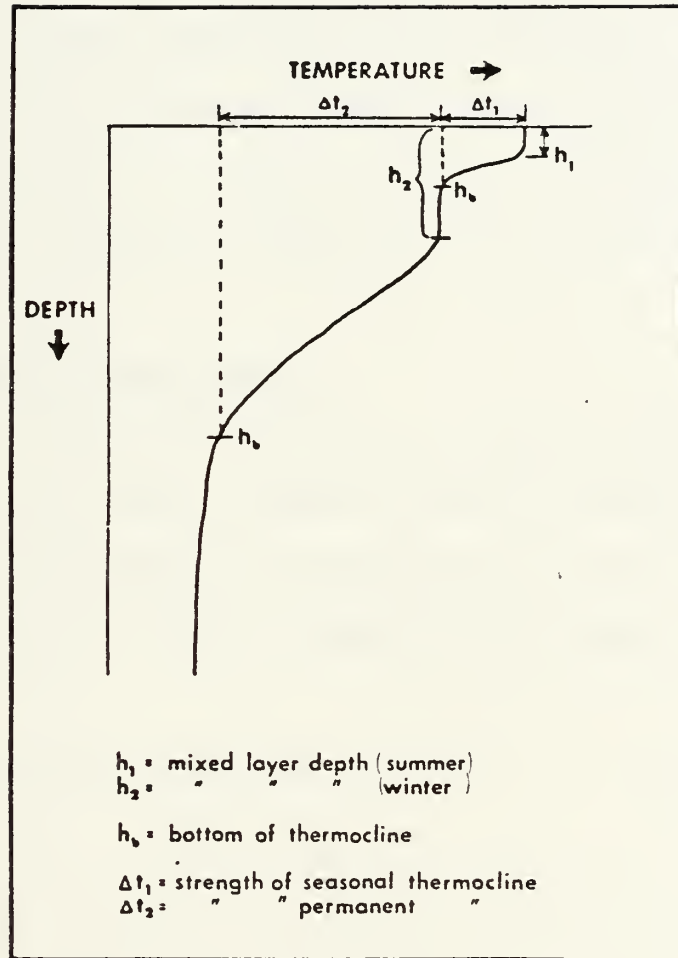


Figure 3. Temperature versus depth profile with old and new MLD's; h_1 = new mixed layer depth, h_2 = old mixed layer depth [Husby and Nelson, 1982]

Differences in the views by no means end there; for example, there is no unanimous approach to parameterization of the kinetic energy budget. The gross parameterization approach is commonly used in closure schemes. However, second order closure schemes have been developed, for example, Launder (1975). Such closure schemes, though applied in only one of the bulk models - Garwood (1976, 1977)-are receiving increasing use. Garwood's scheme will be described in a later section.

2. Summary of Bulk Models

The structure of all simple one-dimensional bulk models may be described in terms of two fundamental equations: the vertically integrated heat equation and the vertically integrated turbulent kinetic energy (TKE) budget.

$$(1) \quad \underbrace{h(\partial T_o / \partial t)}_A = \underbrace{Q_o}_B - \underbrace{Q_h}_C$$

$$(2) \quad P = \underbrace{\int_0^h G dz}_D + \underbrace{E_o}_E - \underbrace{E_h}_F + \underbrace{\beta \left(\int_0^h F dz \right)}_G - \underbrace{\frac{1}{2} h F|_{z=h}}_{H_1} \quad \underbrace{H_2}$$

$$\underbrace{- \int_0^h \epsilon dz}_I - \underbrace{\int_0^h \frac{\partial e}{\partial t} dz}_J.$$

where indicated terms are:

A: Mixed layer depth (MLD) times the local time rate of change of mixed layer temperature (MLT).

B: Net heat flux through the sea surface.

C: Net heat flux through the base of the ML.

D: $P = \frac{1}{2} \rho h (Q_o + Q_h)$

Vertically integrated generation or dissipation of TKE by buoyancy forces.

E: Rate of TKE production due to transfer from mean current shear.

F: E_o is the downward TKE flux at the top of the ML (i.e., from the atmosphere to the ocean and produced by wave breaking at the sea surface).

G: E_h is the downward turbulent energy flux at the base of the ML.

H_1 and H_2 : Effect of penetrative solar radiation.

I: Net turbulent layer dissipation over the ML.

J: Net local time rate of change of TKE over the ML.

The main differences between the various bulk models are in the definitions of the heat flux, Q , and the turbulent entrainment across the interface. Some of the main features of several bulk models are listed below.

Kraus and Turner (KT) (1967): KT developed the first bulk model capable of addressing the time evolution of a mixed layer/seasonal thermocline system; they were the first to propose a TKE budget to close the system. Kraus and Turner

assumed a steady state turbulent regime and neglected dissipation. They parameterized penetrative solar radiation with an exponential decay law and shear production in terms of the frictional velocity.

Denman (DN) (1973): DN rederived the KT model, following Kraus' advice that the rate of increase of potential energy by mixing should be a small constant fraction, m , of the rate at which turbulent kinetic energy is transferred downward by the wind stress. (He used $m=.0012$) Denman also included absorption of solar radiation below the mixed layer. He showed that for sufficiently long model runs, the eventual depth of the mixed layer depended as much upon the temperature gradient below the mixed layer as upon the generation of turbulent kinetic energy. Unlike KT, DN included some turbulent dissipation.

Pollard, et.al. (PRT) (1973): As DN and KT, PRT assumed a steady state regime. The rate of work done by the wind stress on the mean motion was equated with the rate of increase of the energy of the mean field. The mixed layer deepened rapidly to a maximum within half of an inertial period from the time of the instantaneous increase in the wind speed (which then was held constant). Forty percent of the incoming energy was found to directly increase the mean kinetic energy while the rate of change of the mean potential energy was three times smaller than that of the mean kinetic energy. This result reinforced their

hypothesis that the shear instability of non-steady 'wind drift currents' is the main mechanism in turbulence production. They neglected turbulent dissipation and penetrative solar radiation.

Niiler (NI '75) (1975): NI recognized that instantaneous sharp wind changes were not realistic, and that in a steady regime, the surface energy fluxes from the breaking waves could be an order of magnitude greater than the energy fluxes from the wind to the currents. Thus, NI extended the PRT model so that at the beginning and final stages of a model run, TKE generation through surface fluxes was most important, while at intermediate times the drift current velocity shear was dominant. As with the PRT, NI'75 assumed a steady state, no penetrative solar radiation, and no energy flux through the base of the mixed layer. Turbulent dissipation was parameterized as a function of the frictional velocity.

Kim (KIM) (1976): KIM proposed a model more complex than KT which included TKE storage as well as the same parameterization for penetrative solar radiation as in DN. An additional feature of importance was the use of a background, depth-dependent turbulent dissipation rate to avoid infinite deepening.

DeSzoeker and Rhines (DR) (1976): They used the NI model with the addition of a TKE storage term (term J) to show

that the KT and PRT models yielded results that are asymptotes for a single model equation.

Gill and Turner (GT) (1976): They simulated oceanic seasonal cycles, and showed that the cyclical behavior of the potential energy content, heat content, and the surface temperature could be recovered if all or some portion of the potential energy released during the runs was dissipated. They neglected terms G , H_1 , H_2 , and J .

Niiler (NI '77) (1977): This model is similar to NI '75. Additions include a TKE storage term (term J) and background dissipation identical to that employed by Kim.

Niiler and Kraus (NK) (1977): The NK model is a conglomerate of several of the models described above. For example, the radiation term is the same as that used in the KT model; terms E and F are similar to those used previously by Niiler with the only difference being in the coefficients; and the turbulent dissipation term is similar to that used by Resnyansky (1975) and the shear production term of the GT model. The NK model does not include the storage term, J . Unlike previous models, it includes the downward flux of TKE through the mixed layer base (term G).

Garwood (GWD) (1977): (to be discussed in Section 3)

TABLE I**

SUMMARY OF TERMS USED IN BULK MODELS

	E	F	G	H	I	J
KT	*	+		*		
DN	*	+		*	*	
PRT	*					
NI '75	*	*			*	
KIM	+	*		*	*	*
DR	*	*			*	*
GT	*	*				
NI '77	*	*			*	*
NK	*	*	*	*	*	
GWD	*	*		*	*	

* Appears explicitly

+ Appears implicitly, i.e., in one of the other terms

** Modified (Zilitinkevich, et.al., 1979)

3. Garwood Model

The Garwood (1977) bulk mixed layer model is composed of a closed system of seven equations:

The entrainment flux equation:

$$(3) \quad - \overline{bw}(-h) = \frac{m_4 \overline{w^2}^{\frac{1}{2}} \langle \overline{E} \rangle}{h}$$

The horizontal component of the turbulent kinetic energy equation:

$$(4) \quad \frac{1}{2} \frac{\partial}{\partial t} (h \overline{u^2 + v^2}) = m_3 u_*^3 \frac{\overline{bw}(-h) |\Delta C|^2}{2 \Delta B} - m_3 (\langle \bar{E} \rangle - 3 \langle \overline{w^2} \rangle) \langle \bar{E} \rangle^{1/2} - \frac{2m_1}{3} (\langle \bar{E} \rangle^{1/2} + \frac{m_5}{m_1} fh) \langle \bar{E} \rangle.$$

The vertical component of the turbulent kinetic energy equation:

$$(5) \quad \frac{1}{2} \frac{\partial}{\partial t} (h \langle \overline{w^2} \rangle) = \frac{1}{2} h \overline{bw}(-h) - \frac{1}{2} h u_* b_* + m_2 (\langle \bar{E} \rangle - 3 \langle \overline{w^2} \rangle) \langle \bar{E} \rangle^{1/2} - \frac{m_1}{3} (\langle \bar{E} \rangle^{1/2} + \frac{m_5}{m_1} fh) \langle \bar{E} \rangle.$$

The mean buoyancy and complex mean momentum equations:

$$(6) \quad h \frac{\partial \langle B \rangle}{\partial t} = \overline{bw}(-h) - \overline{bw}(0) + \frac{\alpha g}{\rho_o C_p} Q_o,$$

$$(7) \quad h \frac{\partial \langle C \rangle}{\partial t} = \overline{cw}(-h) - \overline{cw}(0) - if \langle C \rangle h.$$

The jump conditions (relating entrainment fluxes to mean buoyancy, rate of deepening, and mean momentum):

$$(8) \quad -\overline{bw}(-h) = \Delta B \frac{\partial h}{\partial t} .$$

$$(9) \quad -\overline{cw}(-h) = \Delta C \frac{\partial h}{\partial t} ,$$

Depending on which version of the model is used, one needs either to provide surface momentum and buoyancy fluxes, mean buoyancy and momentum below the mixed layer along with the radiation absorption or else the observed variables from which these fluxes can be computed. Closure is achieved with the bulk buoyancy and momentum equations and the vertically-integrated individual turbulent kinetic energy components.

A number of significant differences exist between this model and other bulk mixed layer models that may not be obvious from the preceding summarization or the matrix of terms describing which terms are included in each model. Some of these will be made explicit in the following discussion of the mechanics of, and ideas behind, the Garwood model.

According to Garwood (1977), the basis for the initial interface destabilization and the resulting entrainment

is the shear across the interface (base of the mixed layer). This shear is hypothesized by Garwood to be the result of local turbulent eddies (wind generated turbulent kinetic energy available for mixing is explicitly parameterized as dependent on h/L) with the mean flow only making a minor contribution to the achievement of this critical shear value. (The instability related to this criterion is often called a Kelvin-Helmholtz instability or a Benjamin (1963) Class C instability.) By using the familiar equation for the flux Richardson number:

$$(10) \quad R_f = \overline{b w} / (\overline{u w} \partial U / \partial z + \overline{v w} \partial V / \partial z), \text{ and}$$

taking into account the jump conditions (8, 9), shear production can be shown to be only a fixed fraction of the buoyant damping in the entrainment zone. This zone may in fact have a $R_f > 1$, and still possess enough turbulent kinetic energy for entrainment to proceed. Garwood's reasoning, in contrast to that of Pollard, et.al. (1973), is that the mean shear production is only a secondary energy source for mixing. This secondary source of energy can only be made available by entrainment which is initiated by another source. This other and more significant source is the convergence of the flux of turbulent energy from above by the term:

$$(11) \quad \frac{\partial}{\partial z} \left[w \left(\frac{E}{2} + \frac{P}{\rho_0} \right) \right]$$

Therefore, the critical number in the Garwood model is not the flux Richardson number, but instead the ratio of the buoyancy flux to the convergence of turbulent energy, P:

$$(12) \quad P = \overline{bw} / \frac{\partial}{\partial z} \left[\overline{w \left(\frac{\overline{E}}{2} + \frac{P}{\rho_0} \right)} \right]$$

The time, τ_e ,

$$(13) \quad \tau_e = a_1 h \overline{w^2}^{-1/2}.$$

required to transport the available turbulent energy, $\langle \overline{E} \rangle$, to the entrainment zone is important in relation to dissipation, and to the idea that not all available TKE contributes to increasing the potential energy of the system. According to Tennekes and Lumley (1972), the viscous dissipation of geophysical flows with large Reynolds numbers is proportional to the reciprocal of the time scale of the largest eddies. Garwood developed the idea that for the deeper mixed layers ($R_0 \sim 1$), the planetary rotation introduces a second time scale of importance: $(1/f)$. Not only did the inclusion of this second time scale enable Garwood to more explicitly parameterize viscous dissipation in relation to the local Rossby number, but the very role of the time scale in the entrainment equation enabled Garwood's model to simulate a wider range of conditions, i.e., diurnal and annual ranges

of mixed layer stability. (The PRT model can simulate a wide range of changes, though the deepening of the mixed layer is in accordance only with the mean shear production.)

Another difference over most previous models was in Garwood's method of using the turbulent kinetic energy equation. The model uses the component equations (4, 5) vice the typical use of the total equation. This facilitates analyzing the retreat or shallowing of the turbulent boundary layer which depends on only the vertical component of turbulence being inadequate to transport heat, momentum, and TKE to the earlier depth of mixing. (Fig. 3) Thus, using the equation in component form allows for a more explicit and satisfactory treatment of the mixing process.

4. Diffusion Models

The second category of mixed layer models, the diffusion models, has received less attention from the oceanographic community than the simpler bulk models. Yet, the interest that exists has grown greatly with the increasingly powerful computers and the development of methods for solving nonlinear partial differential equations. [Marchuk, et.al 1977] The diffusion models are both complex to interpret and to program. They require the numerical solution of partial differential equations of temperature, salinity, and momentum in time and depth for closely spaced vertical arrays of gridpoints. Unlike bulk models, the 'gridpoint models' do not require the a priori assumption of the existence of a mixed layer. Mixed layer depths, are, on the

contrary, diagnosed from the examination of the turbulence flux predictions as well as the predicted temperature and salinity profiles.

Mathematically, the 'mixed layer' in a diffusion model's vertical profile is treated in the same manner as is the thermocline. This allows for a more detailed analysis of the vertical structure (mixed layers, thermoclines, etc.), the mixing processes throughout the water column, and a more complete simulation of the vertical fluxes of temperature, salinity, and momentum. The latter is a basic concern in the diffusion models which attempt to represent the turbulent fluxes $\overline{w'u}$, $\overline{w'T}$, and $\overline{w'S}$ by algebraic or differential equations in terms of the gradients of mean temperature, salinity, and momentum. These fluxes in conjunction with the necessary boundary conditions for T, S and u provide a solution for the basic conservation equations of temperature, salinity, and momentum. Thus, the system of turbulence and thermodynamic equations are closed in order to solve for the vertical distributions of thermodynamic and turbulence variables. [Grabowski, 1980; Kondo, et.al., 1978]

Diffusion models may be further categorized by complexity, i.e., a) no-equation models; b) one-equation or k-models; c) two equation or k-l-models; and d) second order closure models.

A no-equation model is based on the turbulence transport being parameterized by a buoyancy influenced eddy

viscosity coefficient. The one-equation or k-models are similar to the no-equation models though they include a relationship between eddy diffusion and the local turbulence. The two-equation or k-l-models include a transport differential equation. The second order closure models, first proposed by Chou [1945], are based on transport equations for all of the Reynolds stresses derived from the Navier Stokes equations. They also include turbulent heat and salinity fluxes and the variance derived from the latter in conjunction with the heat conservation equation.

A detailed profile is sought to represent the oceanic vertical structure as completely as possible. For example, Halpern (1976) among others, noted the existence of shear in the top of the water column, a characteristic assumed not to exist in bulk models. Subsequently, the necessity of using numerical models to determine a more realistic distribution of variables such as the velocity, temperature, turbulence intensity, dissipation, and the like was recognized [Phillips, 1977].

The first ocean diffusion model was implemented by Ekman in 1905. It was a type A model, that is, it was a no-equation model that neglected buoyancy and salinity. A notable result from this model was the famous Ekman spiral. Because of its neglect of density stratification, this model will not be discussed further. The major difference between the diffusion models, beyond the number of equations

employed, lies in whether they are based on observations, dimensional analysis, and simple stability arguments or on some form of the TKE energy equation. Of the five models to be briefly discussed below, the first two are of the former type, while the other three are of the latter type.

5. Summary of Diffusion Models

Munk and Anderson (MA): 1949: The MA model is a no-equation model wherein the eddy diffusion coefficients for heat and momentum are functions of the gradient Richardson number. No salinity is included in this model.

Kondo, Sasano, and Ishii (KSI): 1979: The main feature of the SKI model is that constant flux formulations are applied to regions of varying fluxes. Formulation of diffusion coefficients based on studies of the atmospheric boundary layer are cast in Monin Obukhov formalism and applied to the upper oceans. Eddy diffusion coefficients for salt are assumed to be the same as those for heat.

Vager and Zilitinkevich (VZ): 1968: This model is a one-equation or k-model based on Prandtl's extension of the mixing length theory for homogeneous flow. Salinity is ignored.

Mellor and Yamada (MY): 1974: Mellor and Yamada formulated a sequence of models with varying degrees of complexity using second order closure. This discussion will deal with the level-2 model, because the TOPS/TOPS-EOTS

model (to be discussed in the next section) is based on the level-2 MY turbulence closure scheme, and because it is simpler than the level-2.5 model. (The level-2.5 MY model was also used though its mechanics are quite similar to those of the level-2 MY model. The main difference is the inclusion of additional complexity as, for instance, the retention of the TKE storage term in the level-2.5 MY model.) (To avoid repetition, TOPS/TOPS-EOTS will not be mentioned in this section except to say that the 'Clancy version' employed includes salinity, solar radiation, and horizontal advection by instantaneous wind drift and climatologically averaged geostrophic currents.) The level-2 MY model neglects horizontal advection and diffusion terms. The TKE budget is consequently a balance between the production and dissipation of TKE and the conversion to potential energy as seen in Table II. A similar balance exists between the turbulent heat flux, the temperature variance, and the individual stress components. Unlike the other two models described in Table II, the MY level-2 model neglects the turbulent transport term.

Kochergin, Klimok, and Sukhoruks (KKS): 1976: The KKS model is a two equation or a k-l-model. Its TKE budget parameterizes the time rates of change of TKE and the turbulence dissipation rate.

TABLE II
SUMMARY OF TERMS USED IN DIFFUSION MODELS
(Modified: Grabowski, et.al. 1980)

	TKE Prod/ dissip rate	Shear Produc- tion	Buoyancy Conver- sion of PE to TKE	Vertical Transport of TKE Work Done against Pres- sure Gradient	Dissipation
VZ	*	*	*	* 0	*
MY	0	*	*	0 0	*
KKS	*	*	*	* 0	*

*: includes term

0: does not include term explicitly

6. TOPS/TOPS-EOTS

TOPS/TOPS-EOTS is the Navy's new real-time ocean thermal structure analysis/forecast system in use at the Fleet Numerical Oceanography Center (FNOC). (Operational as of March 1983) It was developed by the Naval Ocean Research and Development Activity (NORDA) as part of the Navy's automated environmental prediction system (AEPS). The goal behind TEOTS is to produce reliable, accurate, real-time representations of the ocean thermal structure. The motivation for the way the model is organized (to be discussed below) lies in the available sources of data and the operational nature

of the model. Given that the upper ocean is primarily atmospherically forced, and the assessment that the mixed layer depths have proved 'highly predictable with a variety of models', such as, the Denman (1973) or Mellor and Durbin (MD) (1975) models, NORDA has developed an operational model based largely on the use of the rather well-defined atmospheric variables to drive a model to describe the relatively data sparse oceans. Surface wind, solar heat fluxes, and precipitation fields are among those necessary to drive TOPS/TEOTS.

For vertical structure, TOPS has seventeen levels from the surface to 500 meters, with the majority of the levels placed within the first 100m to enhance the vertical resolution where most needed. (Appendix B) The horizontal grid is typical of many operational atmospheric models, i.e., 381 km at 60N. The input fields on this grid are smoothed spatially by the TOPS modified EOTS. Spatial averaging of the fields also smooths the temporal variability of the fields. Of course, horizontal features smaller than the spacing cannot be resolved so that the capabilities are limited in enclosed seas, in the vicinity of fronts and eddies, and near boundary currents. [Clancy and Pollak, 1982] This last point is important to keep in mind for the simulation comparisons in Chapter IV.

As its name implies, TOPS/TOPS-EOTS is made up of two components: TOPS and TOPS-EOTS. They are coupled in a cyclical fashion.

TOPS-EOTS is an improved, updated version of the Navy's conventional objective analysis component, EOTS (Expanded Ocean Thermal Structure). It supplies TOPS with updated (real-time) initial conditions for a twenty-four hour forecast. Its improvement over conventional EOTS lies in the fact that the TOPS forecast is fed back into TOPS-EOTS as a first guess field for the following day's analysis. This not only reduces the noise resulting from the introduction of data into the analysis, and makes the analysis dynamically and thermodynamically consistent with the atmospheric forcing, but it also allows the model to be run for an extended period of time within data-sparse regions prior to being updated, provided atmospheric forcing data are available.

TOPS (Thermodynamic Ocean Prediction System), the forecast component, is a thermodynamic model for vertical structure which is forced by surface fluxes supplied by NOGAPS (Naval Operational Global Atmospheric Prediction System). It uses the MY level-2 turbulence scheme previously described with the added effects of advection by instantaneous wind drift and climatologically averaged geostrophic currents.

The prognostic equations used by the model are the conservation equations of temperature, salinity and momentum:

$$(14) \quad \frac{\partial \bar{T}}{\partial t} = \frac{\partial}{\partial z} (\overline{-w'T'}) + v \frac{\partial \bar{T}}{\partial z} + \frac{1}{\rho_w c} \frac{\partial \bar{F}}{\partial z} \\ - \frac{\partial}{\partial x} (u_a \bar{T}) - \frac{\partial}{\partial y} (v_a \bar{T}) - \frac{\partial}{\partial z} (w_a \bar{T}) + A \left(\frac{\partial^2 \bar{T}}{\partial x^2} + \frac{\partial^2 \bar{T}}{\partial y^2} \right)$$

$$(15) \quad \frac{\partial \bar{S}}{\partial t} = \frac{\partial}{\partial z} (\overline{-w'S'}) + v \frac{\partial \bar{S}}{\partial z} \\ - \frac{\partial}{\partial x} (u_a \bar{S}) - \frac{\partial}{\partial y} (v_a \bar{S}) - \frac{\partial}{\partial z} (w_a \bar{S}) + A \left(\frac{\partial^2 \bar{S}}{\partial x^2} + \frac{\partial^2 \bar{S}}{\partial y^2} \right)$$

$$(16) \quad \frac{\partial \bar{u}}{\partial t} = f \bar{v} + \frac{\partial}{\partial z} (\overline{-w'u'}) + v \frac{\partial \bar{u}}{\partial z} - D \bar{u}$$

$$\frac{\partial \bar{v}}{\partial t} = -f \bar{u} + \frac{\partial}{\partial z} (\overline{-w'v'}) + v \frac{\partial \bar{v}}{\partial z} - D \bar{v}$$

where:

'D' is a damping coefficient representing the drag force by radiational stress at the base of the mixed layer associated with the propagation of internal waves downward and away from the wind-forced region. 'A' is the background

horizontal eddy diffusion associated with the intermittent breaking of internal waves. [Clancy, et.al., 1982]

There are no horizontal pressure gradients in the last two equations so that the u and v represent wind drift current. The geostrophic advection is provided to the u_a and v_a terms in the T and S equations.

Within the MY level-2 closure scheme, the vertical eddy fluxes of T , S , and momentum are parameterized (Mellor and Durbin (1975); Clancy and Pollak (1983)) as follows:

$$(17) \quad \overline{w'T'} = -\lambda q S_H \frac{\partial \overline{T}}{\partial z} \equiv -K_H \frac{\partial \overline{T}}{\partial z}$$

$$(18) \quad \overline{w'S'} = -\lambda q S_H \frac{\partial \overline{S}}{\partial z} \equiv -K_H \frac{\partial \overline{S}}{\partial z}$$

$$(19) \quad \overline{w'u'} = -\lambda q S_M \frac{\partial \overline{u}}{\partial z} \equiv -K_M \frac{\partial \overline{u}}{\partial z}$$

$$\overline{w'v'} = -\lambda q S_M \frac{\partial \overline{v}}{\partial z} \equiv -K_M \frac{\partial \overline{v}}{\partial z}$$

where K_M and K_H are eddy diffusion coefficients; λ is a turbulence length scale; $q = \sqrt{(2) * TKE}$; S_H and S_M are functions of the bulk Richardson number:

$$(20) \quad Ri \equiv \frac{-\frac{g}{\rho_w} \frac{\partial \bar{\rho}}{\partial z}}{[(\frac{\partial \bar{u}}{\partial z})^2 + (\frac{\partial \bar{v}}{\partial z})^2]}$$

There is an implied cutoff Richardson number such that one can determine the three empirical constants. The TKE budget used to obtain q is:

$$(21) \quad \ell q S_M [(\frac{\partial \bar{u}}{\partial z})^2 + (\frac{\partial \bar{v}}{\partial z})^2] + \ell q S_H (\frac{g}{\rho_w} \frac{\partial \bar{\rho}}{\partial z}) - \frac{q^3}{15\ell} = 0$$

and the equation for ℓ is:

$$(22) \quad \ell = \frac{0.1 \int_{-\infty}^0 |z| q dz}{\int_{-\infty}^0 q dz}$$

The solar radiation flux is parameterized by using an extinction profile for the most common water type. (For the level-2.5 model, the solar radiation flux is applied at the surface.)

As mentioned previously, boundary conditions are mainly provided by the FNOG atmospheric models. XBT profiles are included in the analysis when they are available. (The

ocean data used in the TOPS runs will be briefly mentioned in later sections when the model results are discussed.)

7. Verification Testing of Mixed Layer Models

Numerous tests have been completed or are in the planning stages for verification of the forecasting abilities of the Garwood, TOPS, and Level-2 Mellor or Mellor-Durbin (MD) models as well as for the other models previously discussed. A review of any mixed layer model verification testing would not be complete without at least mention of MILE, the Mixed Layer Experiment, which consisted of an intensive examination of the upper ocean in the environs of Ocean Station P during a 20-day period in autumn 1977. Excepting that brief discussion, the mainstay of the review of verification testing will encompass the three models directly involved in this study. (Though the MD model is essentially the core of the TOPS model, each will be reviewed separately, for TOPS, a first generation operational model, has its own inherent verification problems.)

Mixed Layer Experiment, 1977: The Mixed Layer Experiment (MILE), 1977, is a noteworthy example wherein data were acquired, and compared initially against simulations produced using the NI'77 model and subsequently other model simulations. Davis, et.al. (1981) used velocity profiles, measurements not usually available in ML verification studies in an attempt to not only obtain a firm understanding of the dynamics and thermodynamics involved, but in so doing, to also confirm

the applicability of the bulk approach to the study domain. They failed to acquire such a confirmation in all cases except those involving strong storms wherein the upper oceanic shear became localized a short distance below the isothermal layer. However, by accounting for the vertical advection and horizontal pressure gradient within the domain, Davis, et.al. (1981) were able to indicate a 'reasonable balance' in both the heat and momentum budgets, respectively. Two major difficulties encountered were a) the need to acquire accurate data representing changes below the mixed layer so as to better understand the vertical distribution of heat and momentum within the mixed layer, and b) the need to acquire better expertise in being able to separate effects of internal waves, energetic inertial motions and internal tides from responses of the upper ocean to storms. [Davis, et.al., 1981] Despite the numerous weaknesses in the study described by Davis, et.al. (1981), simulations encouragingly seem to agree with the observations. Their 'most favorable' result (Fig. 4) was for $m_1 = 0.39$ and $m_2 = 0.48$, where m_1 and m_2 are tuned coefficients determining 'limits of excursion' and 'rate of response', respectively.

a. Review of Verification Testing of Three Models

The Level-2 Mellor model and similar models have been evaluated in numerous and varied simulation experiments. Mellor and Durbin (1975) obtained favorable results from tests using five weeks of data acquired at Ocean Station Papa

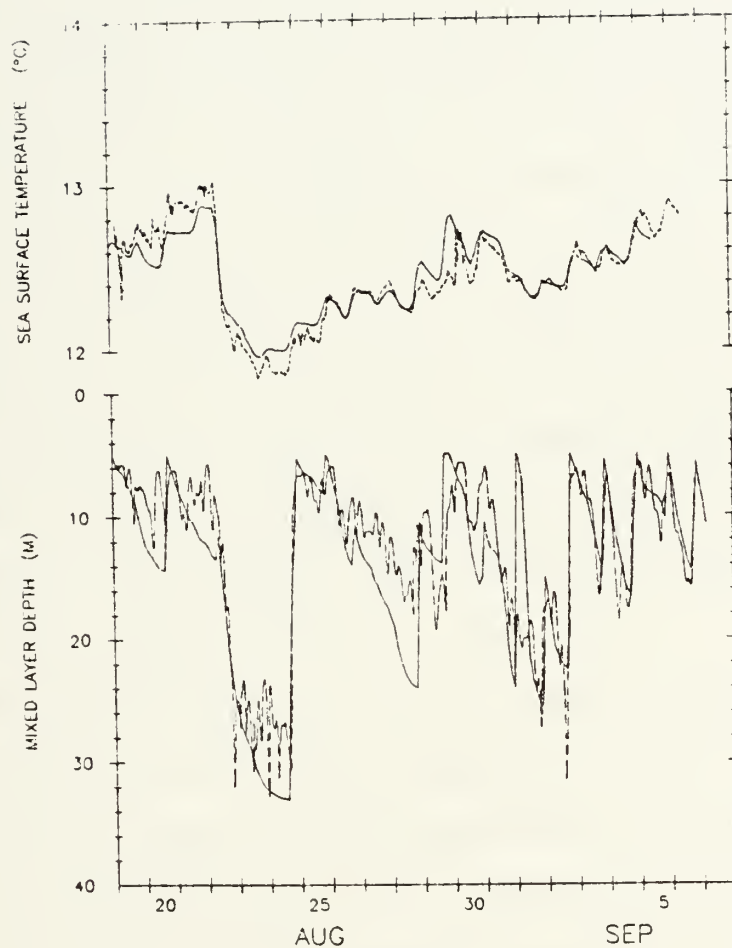


Figure 4. MILE observations versus simulations:
 NI '77, Dashed curves: observed hour
 average T(5m) and depth where T is 0.1C
 colder than T(5m); solid curves:
 modeled values of mixed layer temperature
 and depth [David, et.al., 1981]

(50N, 145W), as well as that data acquired nearby during MILE. The model's ability to handle the response of the upper ocean to an atmospheric low pressure system, i.e., the observed versus the predicted SST during and after frontal passage, was explored by Price et.al (1978) for the Gulf of Mexico region. The model's ability to amply predict the ocean's response to stronger atmospheric forcing was verified in the case of the passage of hurricane Eloise by the fortunate existence of a NOAA data buoy, EB10, located on the track of the hurricane. Klein (1980) used the MD model to simulate the variability of the mixed layer depths in the Mediterranean Sea. The model favorably simulated (Fig. 5) [Clancy, et.al., 1981] the diurnal mixed layer response observed during BOMEX. (The Barbados Oceanographic and Meteorological Experiment.)

The Garwood model has also undergone, and is still undergoing, verification testing, though by a more limited populus. One of the most notable simulations extended over 17 years of Ocean Station Papa data. Not only was this the first simulation of its kind in length, and in the handling of interannual variability in mixed layer response, but it was also the first simulation conducted for the period of the spring transition. (Comparison of the hindcasts with the observations lends encouragement to the ability of one-dimensional (bulk) models to account for a large part of the variance on time scales from the synoptic to greater than a



Figure 5. Time series of predicted (dashed line) and observed (solid line) temperatures at 6M depth at R.V. Discoverer during the BOMEX Experiment [Clancy, et.al., 1981]

year. [Garwood and Adamec, 1982] Additional verification testing includes various studies of model performance along the shipping track between San Francisco and Hawaii [Steiner, 1981], and during POLEX, a component of the North Pacific Experiment. [Shook, 1980] Data assimilation tests were performed by Warrenfeltz (1980) and by Larsen (1981).

Because the MD model is at the core of TOPS, one might say that the TOPS model has undergone extensive testing and evaluation. Such, however, is not the case in that TOPS is a first generation operational model, and as such is subject to inherent problems not experienced by other one-dimensional or quasi-three-dimensional models. The TOPS verification is, for the most part, a test of the quality of the FNOC operational data base, the source of not only the initial and upper boundary conditions, but also the verification fields. These verification fields have necessarily been extracted from the objective analysis or TOPS modified objective analysis scheme, for observations have rarely been available near the model's widely spaced gridpoints. The distribution of observations is neither uniform nor constant. The model is, therefore, subject to not only a wide range of testing conditions, but also to a greatly fluctuating source of observations. When considering the advective version of TOPS, one must also consider possible three-dimensional processes.

Thus, meaningful quantitative forecast verification seems reasonable only in regions containing an adequate supply of data. The verification fields must be obtained from the same scheme used to acquire initial conditions, because different schemes applied to the same data set are likely to produce varying verification fields. [Barnett, et.al., 1980] The present FNOC daily global intake of data consists of approximately 200 XBT's, 2,000 'bucket' temperatures, and approximately 20,000 satellite SST's from TIROS-N. This apparent lack of sufficient subsurface definition has resulted in much of the verification effort centering on the SST.

TOPS is an operational model, one component of a resource-limited naval facility model network. As such, it neither has number one priority in the FNOC objectives list, nor can it avoid being impacted by the ever evolving computational environment. The rate of personnel change, in combination with the shortage of oceanographers on the staff, has resulted in most of the verification testing being left as a milestone to be achieved in the future.

One of the major changes which has recently occurred at FNOC, and which will alter the workings of TOPS, is the replacement of the old atmospheric primitive equation (PE) model with the Naval Operational Global Atmospheric Prediction System (NOGAPS). This change took place on 3 August 1982, midway during the model simulation runs of

interest in this thesis. The change was made to improve the higher priority atmospheric products supplied to the fleet. A study of the effects of NOGAPS on TOPS results is in the plans for the near future. It is hoped that NOGAPS will provide more accurate heat fluxes for ocean prediction analysis.

The analysis system has evolved from OTS (Ocean Thermal Structure) analysis system to EOTS (Expanded Ocean Thermal Structure) analysis system and finally to TEOTS or TOPS-EOTS (TOPS modified EOTS). The last change in the evolutionary sequence was implemented in full on 22 March 1983- that is, TEOTS replaced EOTS as a bottom boundary condition for the atmospheric models. Previously, EOTS was the bottom boundary condition of the atmospheric models so that there was only a one-way influence between the atmospheric and oceanic models, i.e., the atmospheric model drove the oceanic model. With the implementation of TEOTS, the feedback loop is complete. Thus, the bottom boundary condition of the atmospheric model is more influenced by the physics of the situation.

Another change to be more fully discussed later was a more resilient return of the model to climatology. This change took place on 20 September 1982. [Pollak, personal communication] Though not yet documented, the change supposedly results in the model forecast of SST remaining within approximately 3C of climatology with any deviations

being suppressed within approximately a two-week period. (The scientific basis for this criterion is unknown.) (The climatology receives a weight in the process such that sharp deviations from climatology are reduced by an increase of the weighting applied to the climatological factor.)

Most of the published verification reports describe TOPS model performance prior to these aforementioned changes. For example, Warn Varnas, et.al. (1982) performed a 60-day simulation in the TRANSPAC region of the central North Pacific for November and December 1976. This was done using TOPS in conjunction with OTS. Comparison of SST results from both the advective and nonadvective versions of the model revealed consistent skill over both climatology and persistence. (Fig. 6) (As will be discussed later, results also revealed a heat flux bias confirmed previously by comparisons of the heat fluxes with those calculated by Nate Clark.) Clancy, et.al., (1981) performed a short time scale synoptic verification of TOPS/EOTS (nonadvective version on Cyber 175) using both pattern-of-change correlation techniques [Dobryshman, 1972], and the apparent forecast error technique. The former techniques demonstrated TOPS' ability to routinely produce real-time forecasts of large scale changes of SST. The latter technique indicated that, with adequate data coverage and limited domains of strong atmospheric forcing, the model could achieve a skill twice that of persistence.

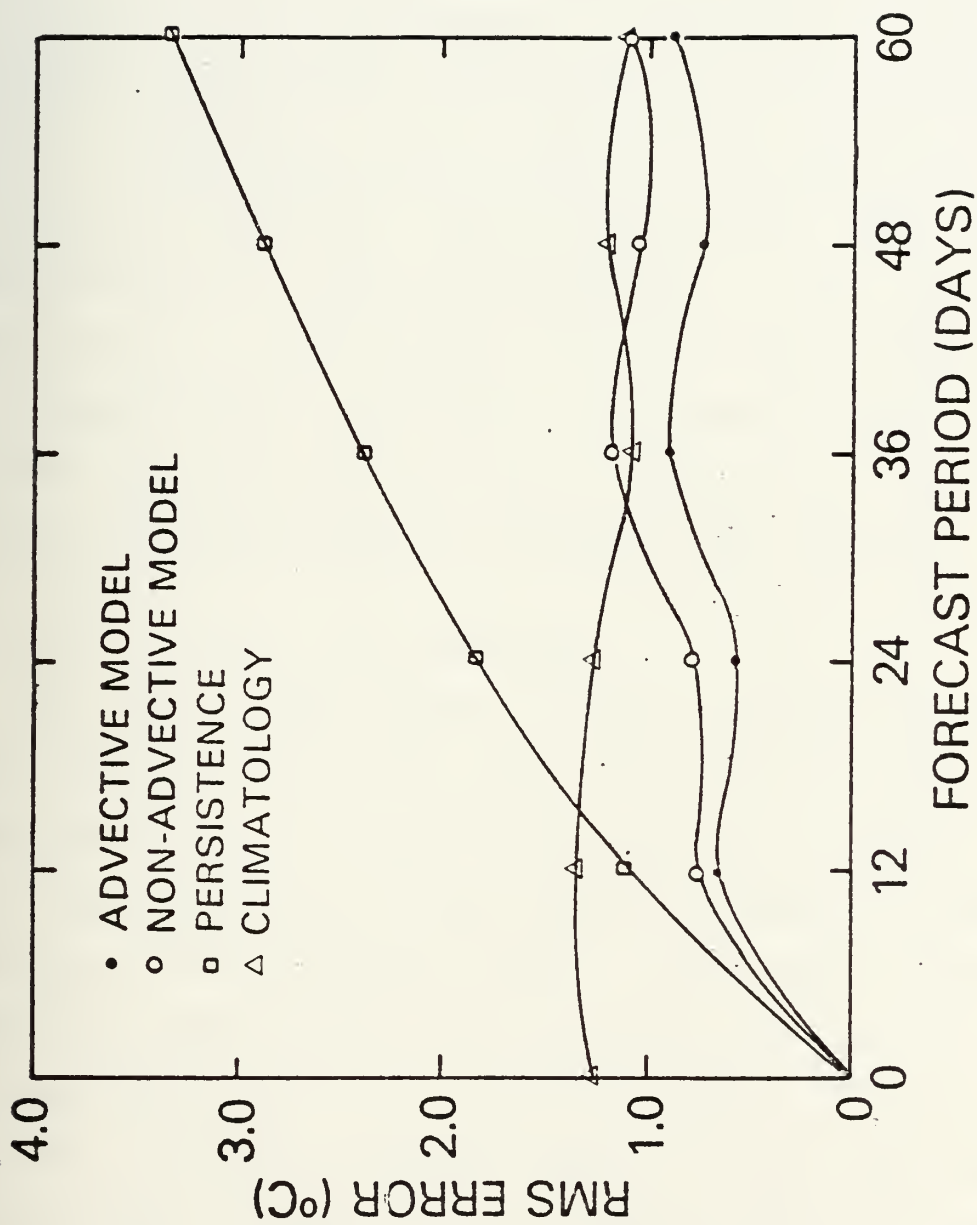


Figure 6. Skill of adjective and nonadjective TOPS over persistence and climatology as indicated from TRANSPAC data [Warn-Varnas, et.al., 1982]

The latest verifications of the coupled TOPS include TOPS/TEOTS vice TOPS linked with EOTS. TEOTS has proved to be less noisy and more consistent with the predictions of TOPS and atmospheric forcing; this result is especially true in relation to the spring transition. Composites of forecast verification statistics for May 1981 indicate the skill of TOPS in forecasting both MLD and SST change out to 72 hours. RMS errors indicate TOPS better persistence out to (but not including) 72 hours for MLD, but only out to 24 hours for SST. The latter deficiency is believed to be the result of the possible heat bias of the FNOC primitive equation model. It is yet to be determined whether NOGAPS can resolve this problem.

C. STUDY AREA AND ITS CLIMATOLOGY

The domain investigated is (Figs. 1, 2) located in the California Current System, just south of the Mendocino Escarpment (Fig. 7) in the region from approximately 37.5 to 39.6N and 125 to 127W. This system is composed of four currents: the California Current, the Davidson Current, the California Undercurrent, and the Southern California Current. Of main influence in the designated domain is the California Current, the eastern boundary current of the large anti-cyclonic gyre centered near the Hawaiian Islands. The current, an extension of the Westwind Drift (Sverdrup, et.al., 1942), occurs between the North Pacific atmospheric

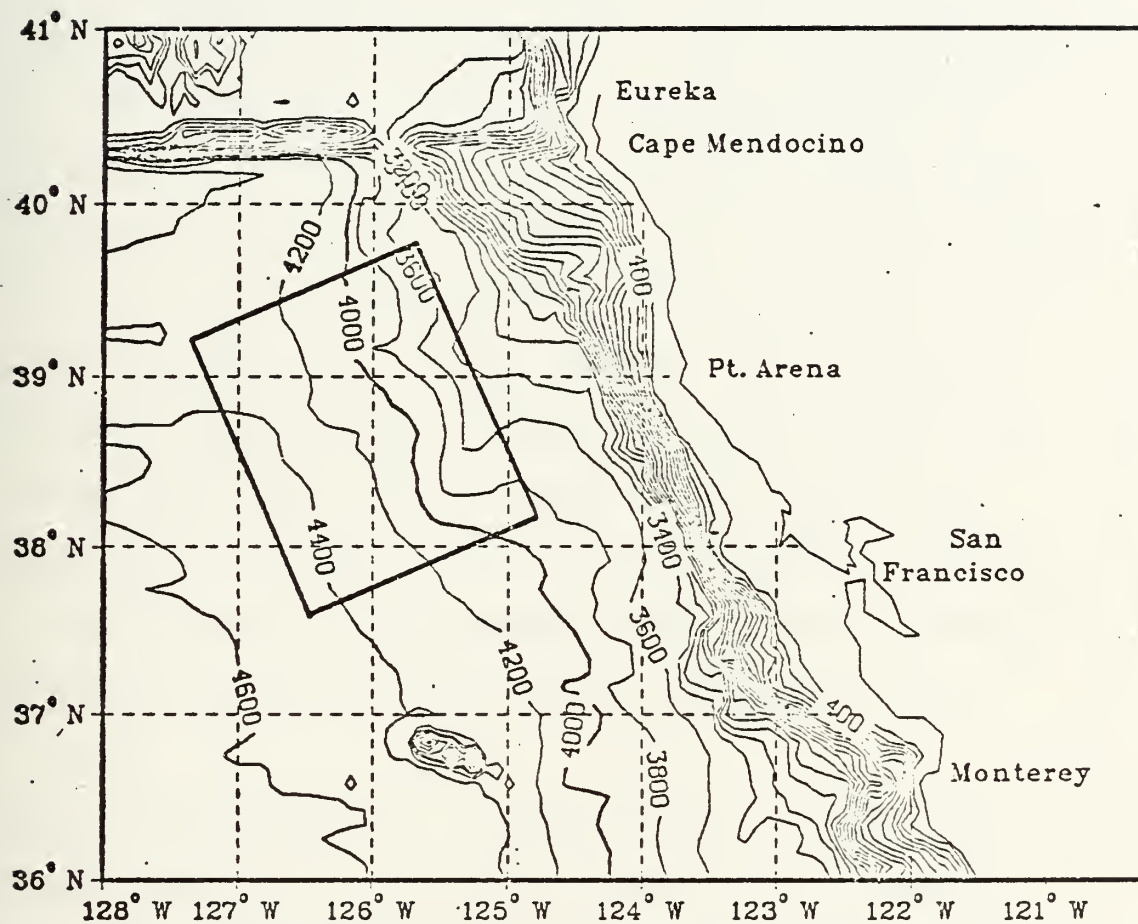


Figure 7. Study domain in relation to bathymetry off Northern and Central California (Contour Interval: 200m)

high system and the semipermanent thermal low positioned over central California. Geostrophic and surface Ekman components of the flow are consistent with the temperature distribution, and the atmospheric high pressure system with its associated wind stress. An anticyclonic eddy is the major feature depicted by the dynamic topography computed for the CCSI domain. The dynamic topography for CCSII clearly depicts the anticyclonic and cyclonic eddies toward the northeast and southwest regions of the study domain which dominated the region during that time period and into CCSIII. [Reid, et.al, 1958] (Figs. 8-10) Nelson (1977) compiled a climatological description of the surface wind stress and wind stress curl over the California Current System, by computing the wind stress using the bulk formula in one degree squares from marine weather observations, primarily ship reports, archived by the National Climatic Center. (Figs. 11-13)

Nelson encountered many of the typical problems that arise when dealing with multi-source data as, for example, uneven and dissimilar sampling in space and time. Only approximately 12% of the observations were actually measured. The resulting values provide a climatological view of the area. The domain of interest falls within a region of monthly mean maximum wind stress values for August. (approximately 1 dyne/cm^2) The upper ocean is undoubtedly influenced by such forcing. Past evidence has indicated

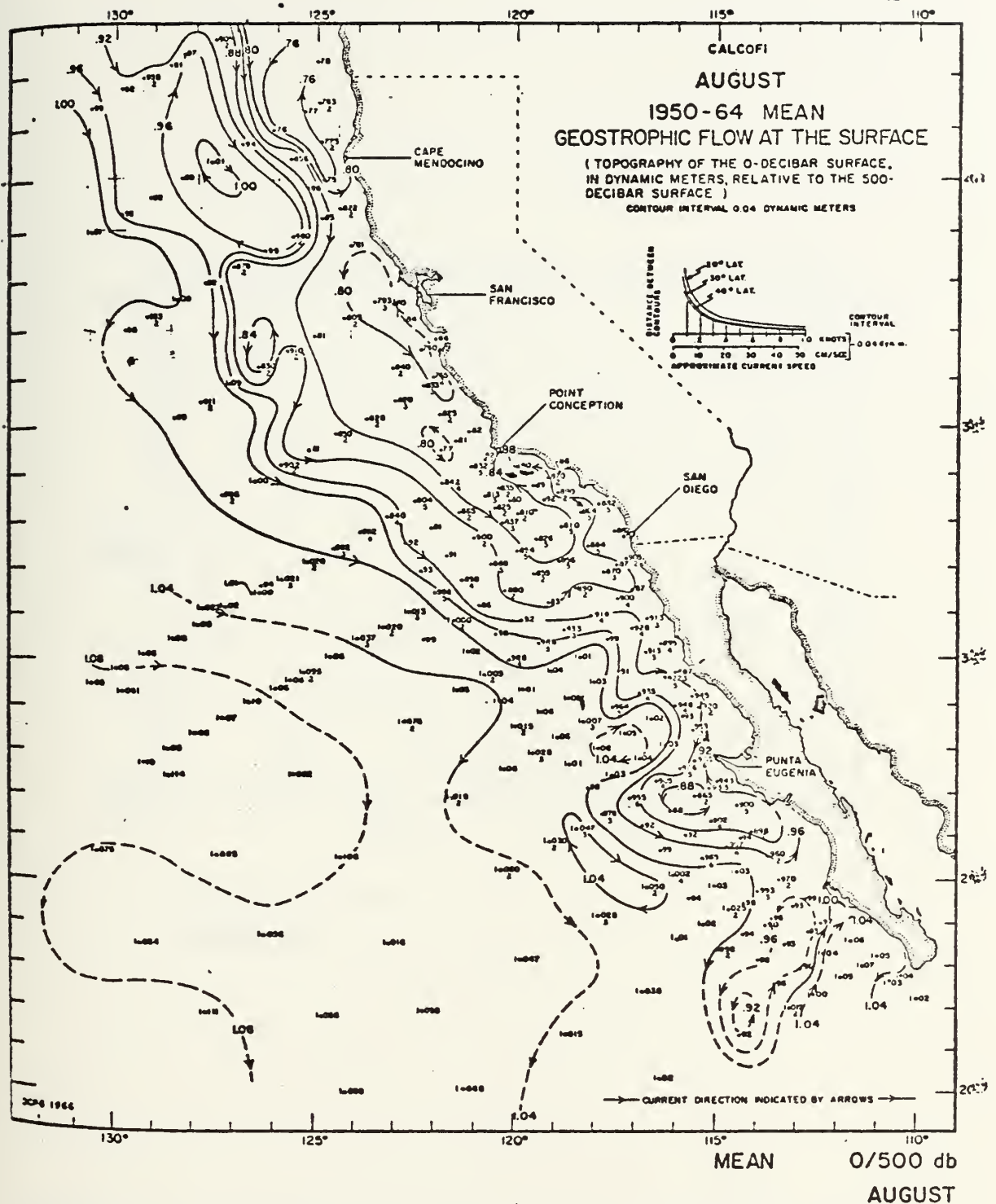


Figure 8. CalCOFI map of mean August geostrophic flow at the surface for years 1950-1965 (Dyn. m; interval: 0.04m)

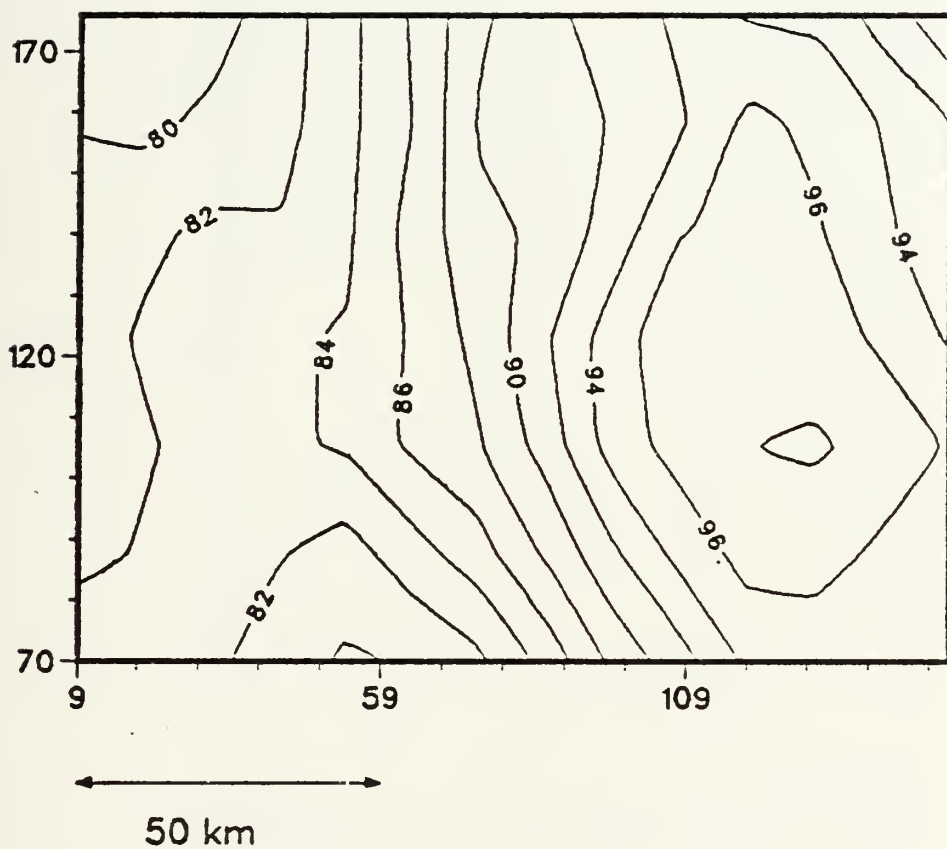


Figure 9. Dynamic topography of study domain during CCSI (Dyn. cm, interval 1.0, surface relative to 450m)

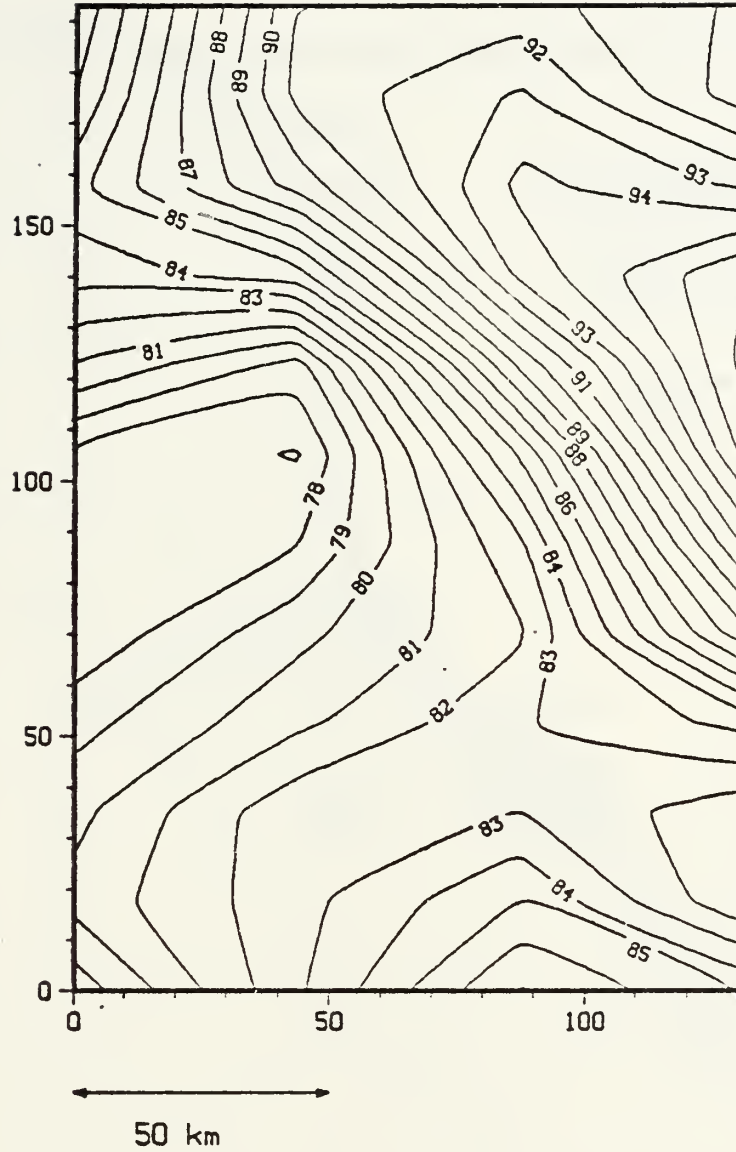


Figure 10. Dynamic topography of study domain during CCSII (Dyn. cm, interval 1.0, surface relative to 450m)

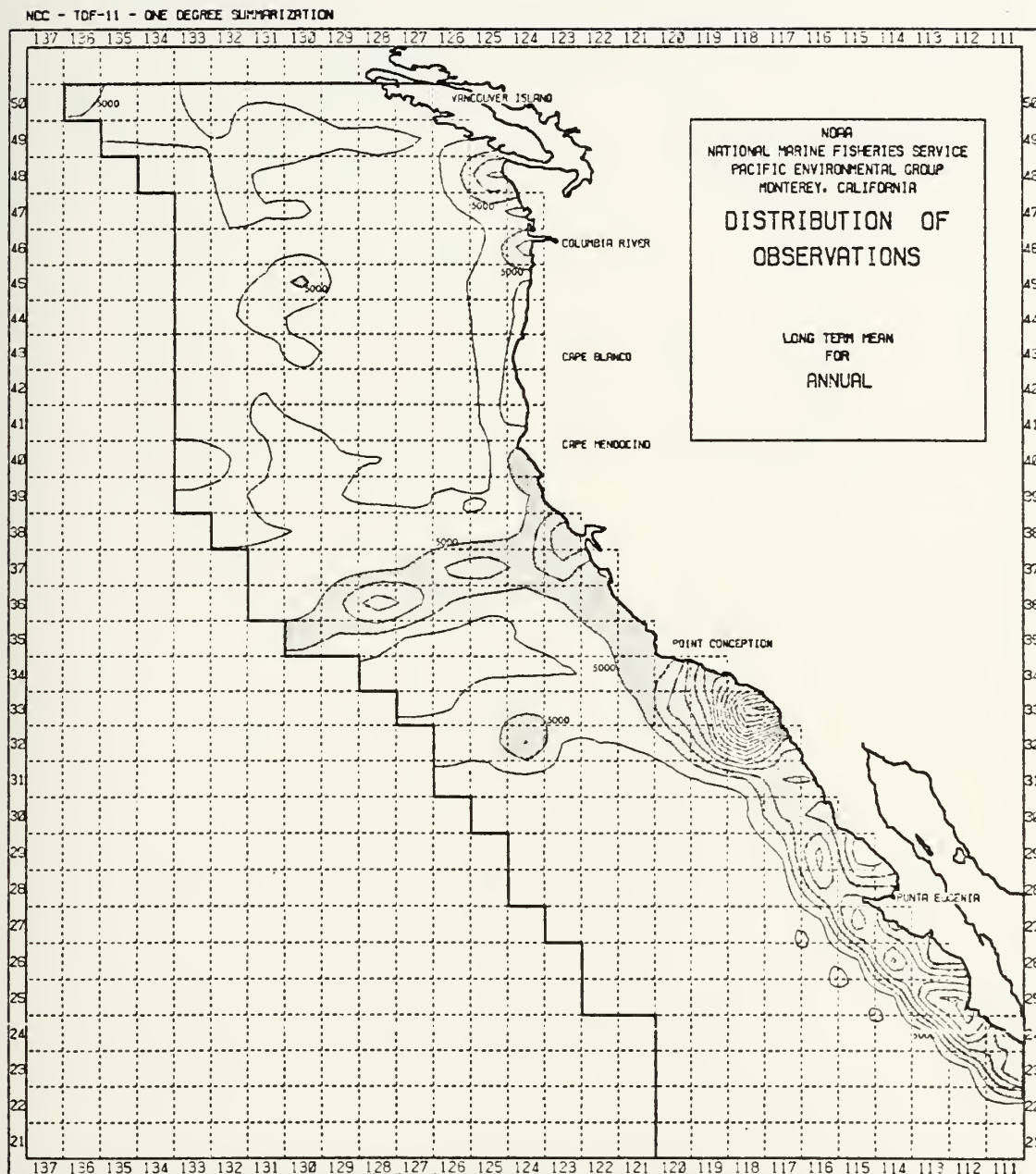


Figure 11. Distribution of observations per 1-degree square; the contour interval is 2,500 observations; Values greater than 5,000 are shaded [Nelson, 1977]

NCC - TOF-11 - ONE DEGREE SUMMARIZATION

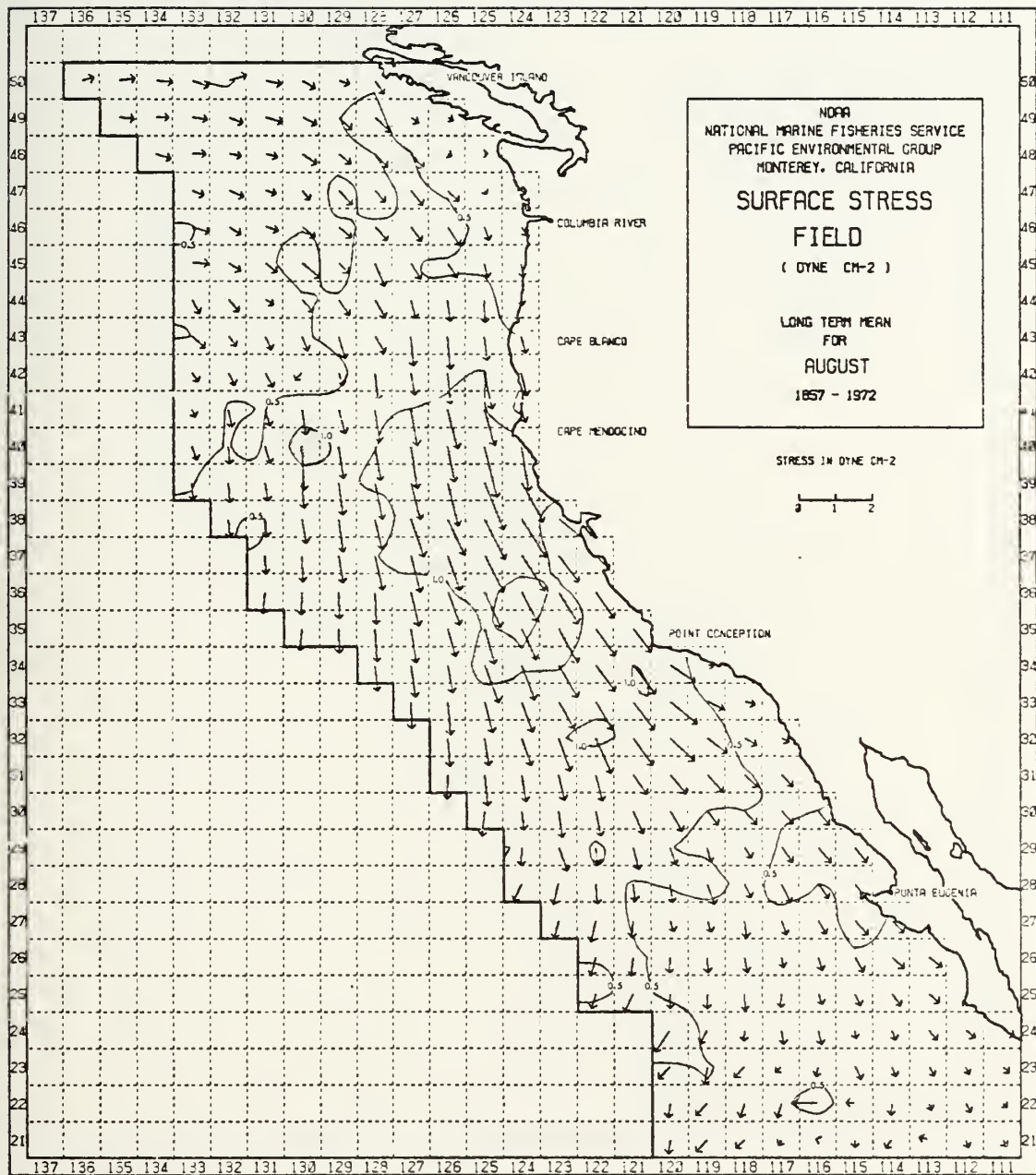
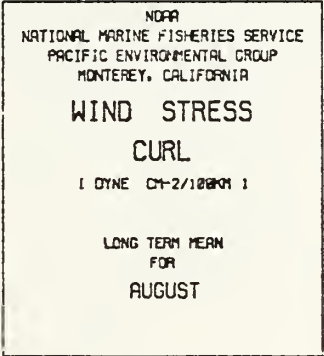


Figure 12. Long term mean August wind stress vectors: 1857-1972. [Nelson, 1977]

137 136 135 134 133 132 131 130 129 128 127 126 125 124 123 122 121 120 119 118 117 116 115 114 113 112 11



65

that the responsiveness of the coastal regime to such forcing. It is speculated that elements of the coastal response may be advected into offshore regions (and vice versa) by the predominance of jets within the region. (The small negative value for wind stress curl indicates slight open ocean downwelling within the study domain itself, whereas the coastal regions indicate strong upwelling tendencies.) Another point of speculation is the direct forcing of the subsurface eddy field by the wind stress curl mechanism [Mooers, personal communication, 1983].

Thermodynamical atmospheric forcing fields are also important to mixed layer evolution. Nelson and Husby (1981) compiled monthly mean heat flux fields over the California Current region. As with the mean wind fields, the monthly mean radiative and turbulent heat fluxes were computed from archived surface marine weather reports ranging from 1921-1972. The marine weather observations incorporated in the heat flux calculations were of a highly diverse nature. The distribution of the observations was nonrandom and highly biased toward fair weather. Also problems existed due to sampling errors and methods of computation. Thus, large errors were possible in the heat flux estimates. Errors of 10% in each of the components of heat exchange could conceivably have resulted in an error of anywhere from 10 to 70% in the net heat flux, $Q(N)$.

$$Q(N)=Q(S) - Q(B) - Q(E) - Q(C)$$

Despite the questionable magnitude of the long term monthly means, however, Nelson and Husby (1981) concluded that the temporal and spatial consistency of the independent surface heat flux estimates 'indicates that the geographic patterns are realistic and significant'. The wind fields were of similar or better quality.

The mean fields for August of $Q(S)$, $Q(B)$, $Q(E)$, $Q(C)$, and $Q(N)$ (Figs. 14-18), provide insight into heat gain and loss within the current, and more specifically within the study domain. Values at the domain center (38N, 126W), are:

$$Q(S)=216.3 \text{ Watts/M}^2$$

$$Q(B)=32.77 \text{ Watts/M}^2$$

$$Q(E)=35.92 \text{ Watts/M}^2$$

$$Q(C)=-7.24 \text{ Watts/M}^2$$

$$Q(N)=154.9 \text{ Watts/M}^2$$

Standard errors of the means evaluated using

$$SE(Q)=SD(Q)/\sqrt{N}$$

where $SD(Q)$ is the standard deviation and N is the number of observations (253 within the study domain region), are:

$$Q(S) : \text{Error}=3.80 \text{ (Watts/M}^2)$$

$$Q(B) : \text{Error}=1.41 \text{ (Watts/M}^2)$$

$$Q(E) : \text{Error}=3.28 \text{ (Watts/M}^2)$$

$$Q(C) : \text{Error}=1.47 \text{ (Watts/M}^2)$$

$$Q(N) : \text{Error}=5.20 \text{ (Watts/M}^2)$$

As expected, the incoming solar incidence corrected for clouds and the sea surface albedo dominates the heat budget. The effective back radiation and the latent heat

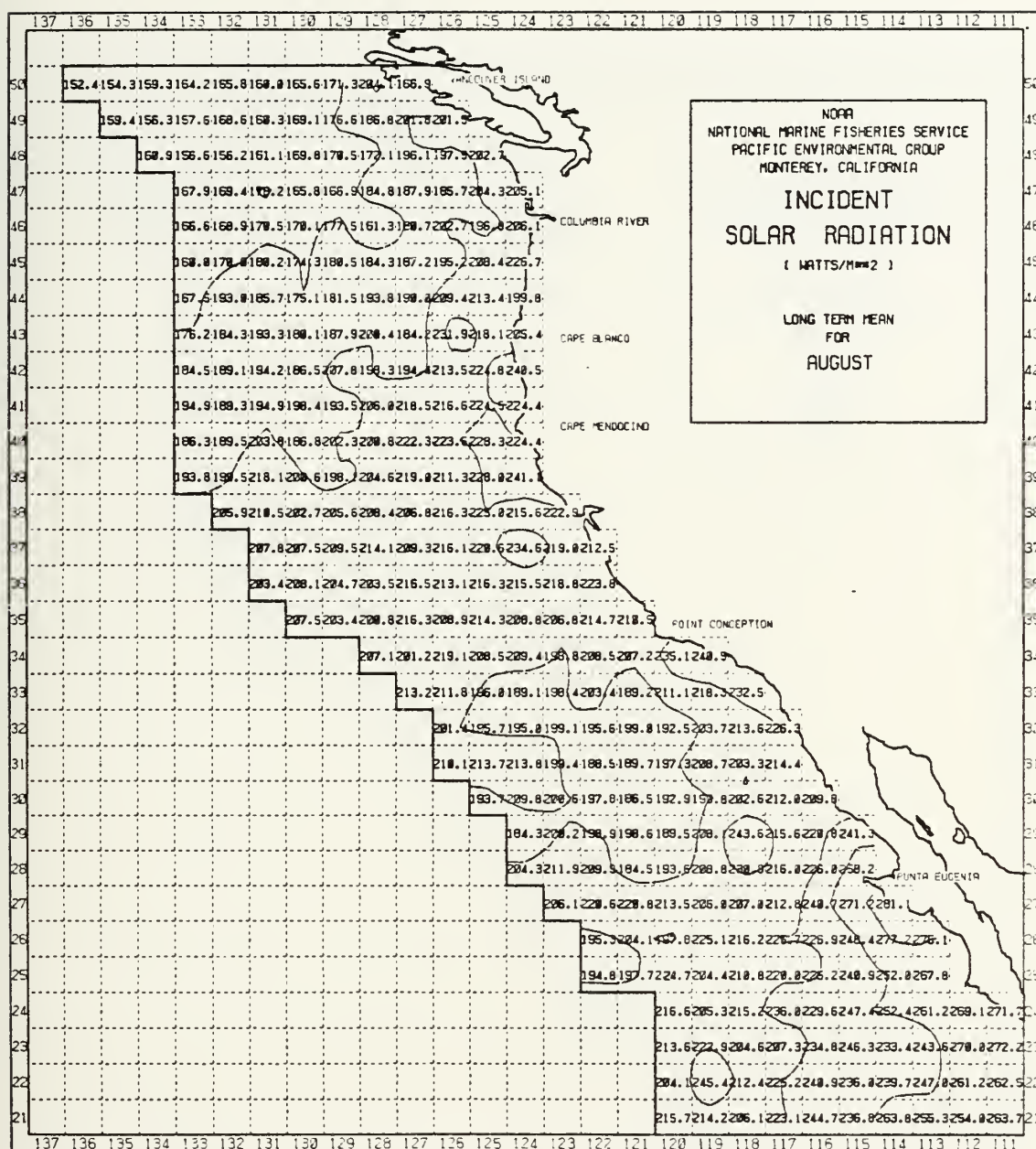


Figure 14. Long term mean August incident solar radiation: 1901-1972 [Nelson and Husby, 1983]

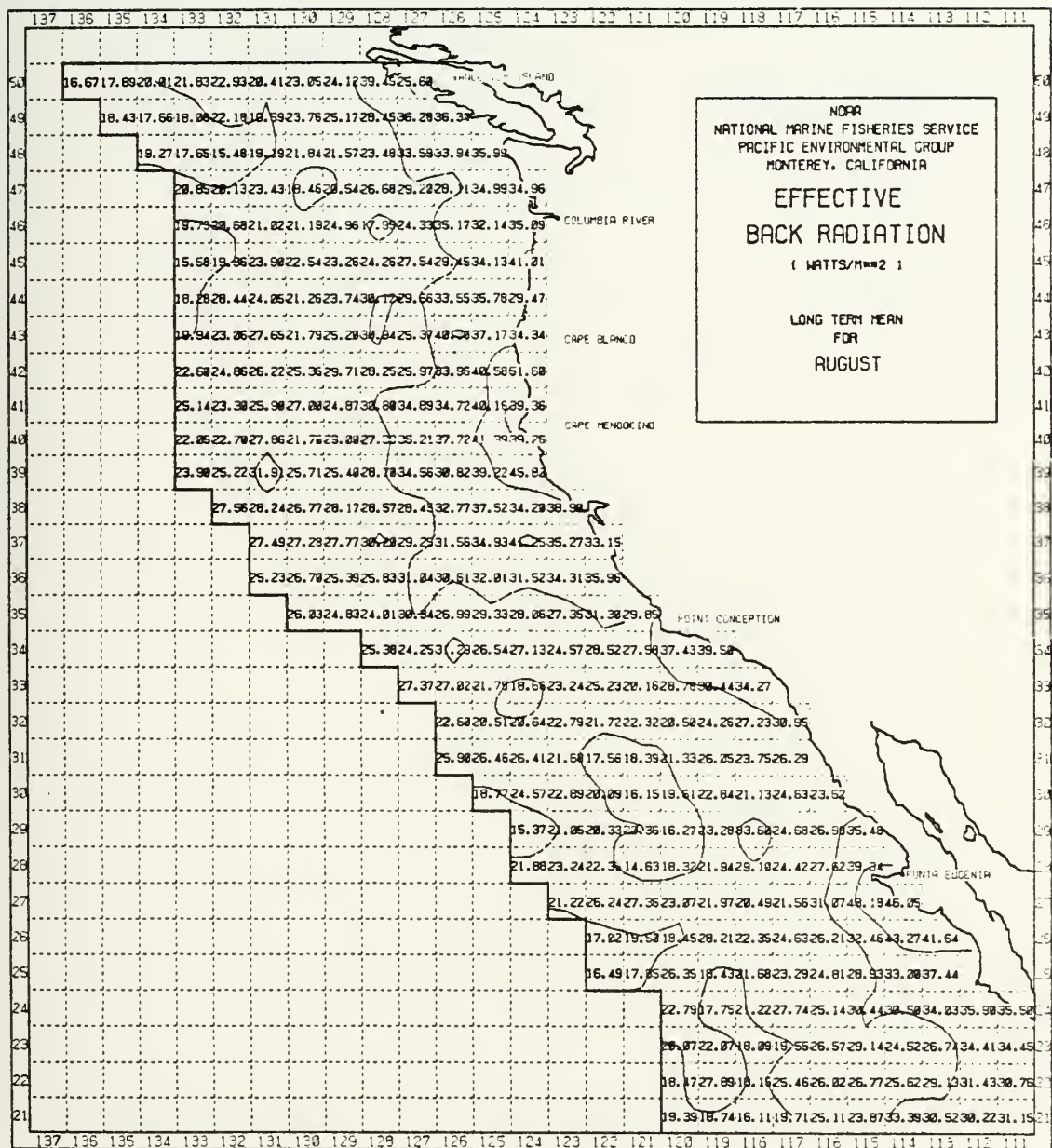


Figure 15. Long term mean August effective back radiation: 1901-1972 [Nelson and Husby, 1983]

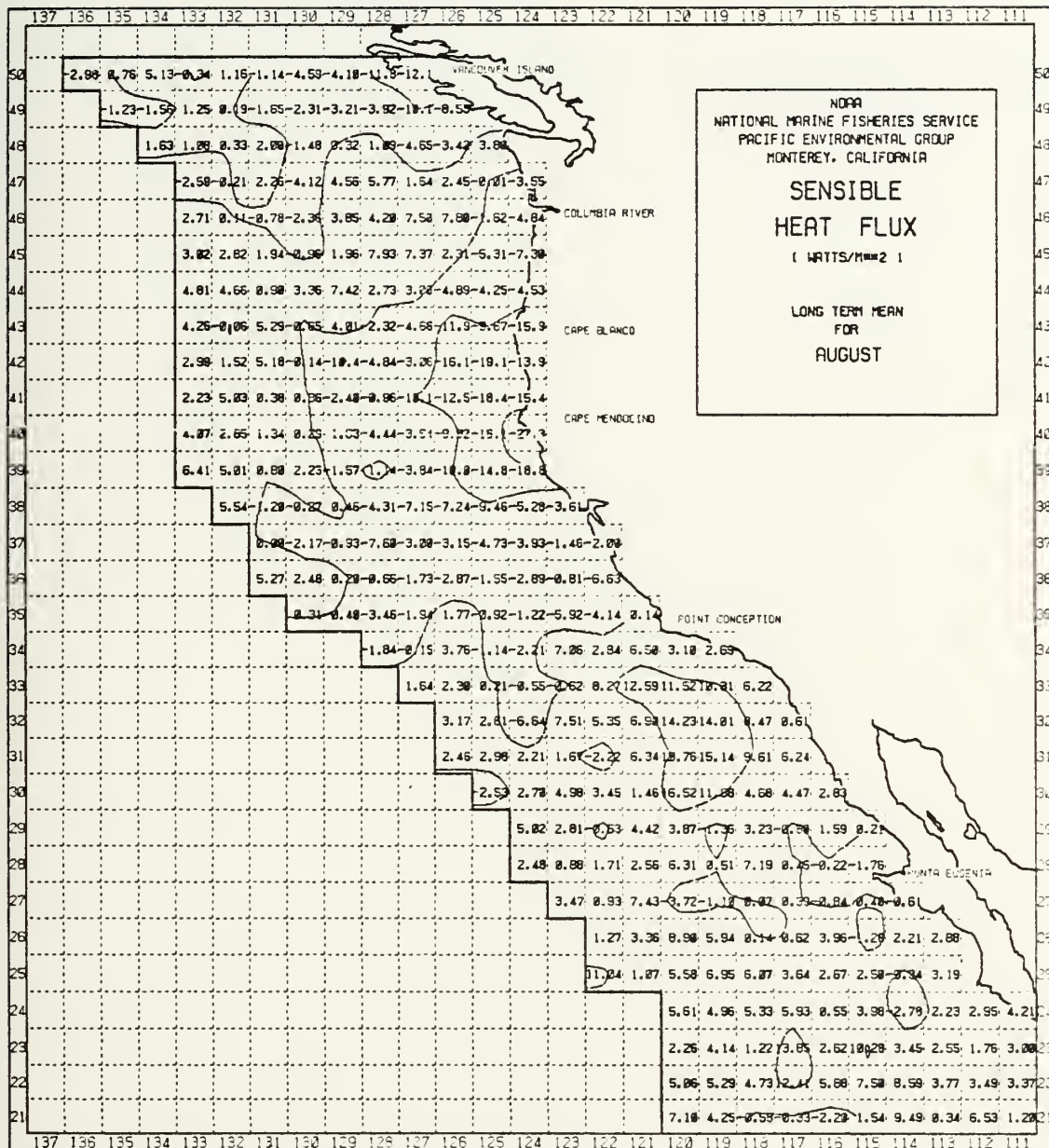


Figure 16. Long term mean August sensible heat flux: 1901-1972 [Nelson and Husby, 1983]

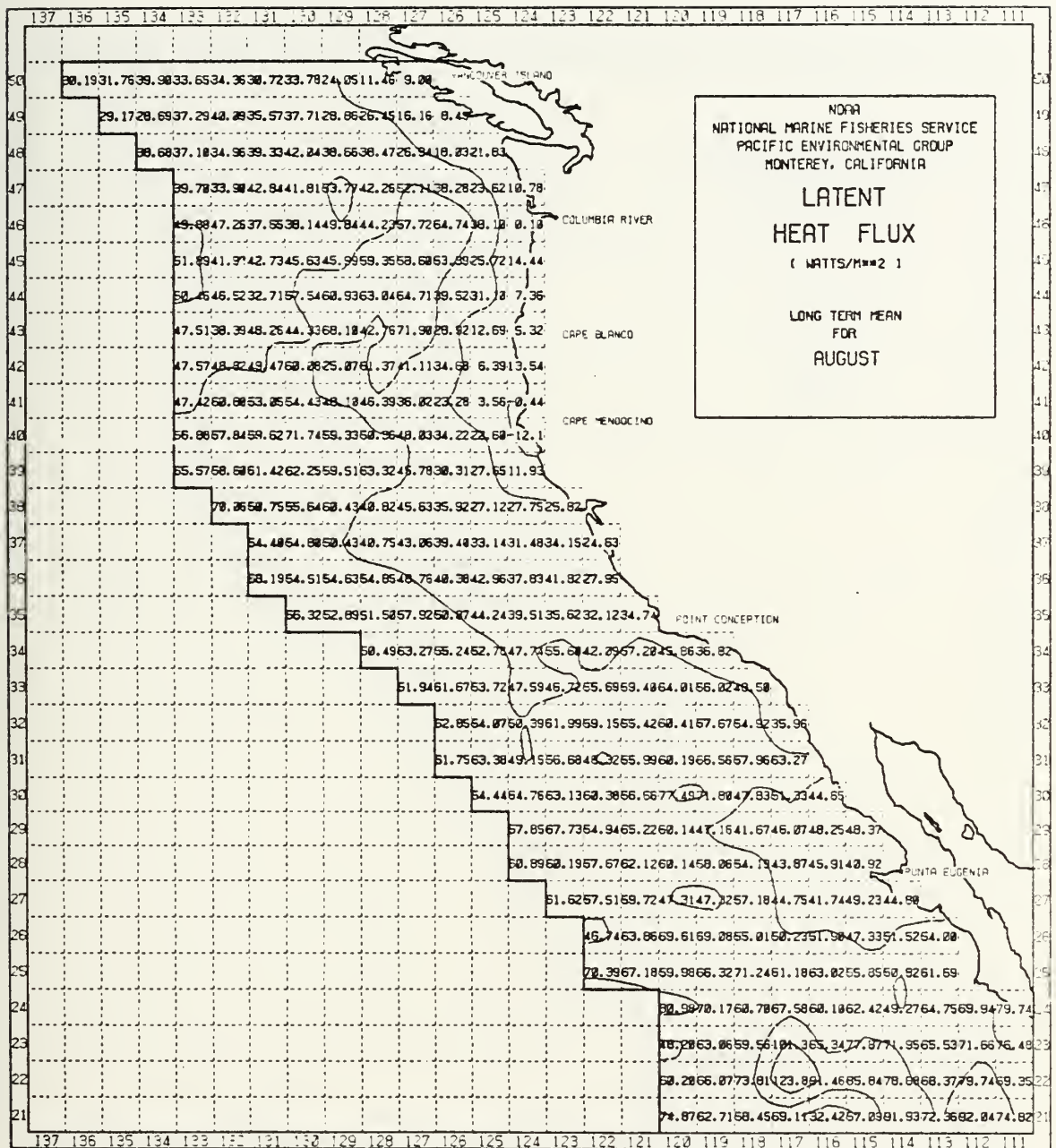


Figure 17. Long term mean August latent heat flux: 1901-1972 [Nelson and Husby, 1983]

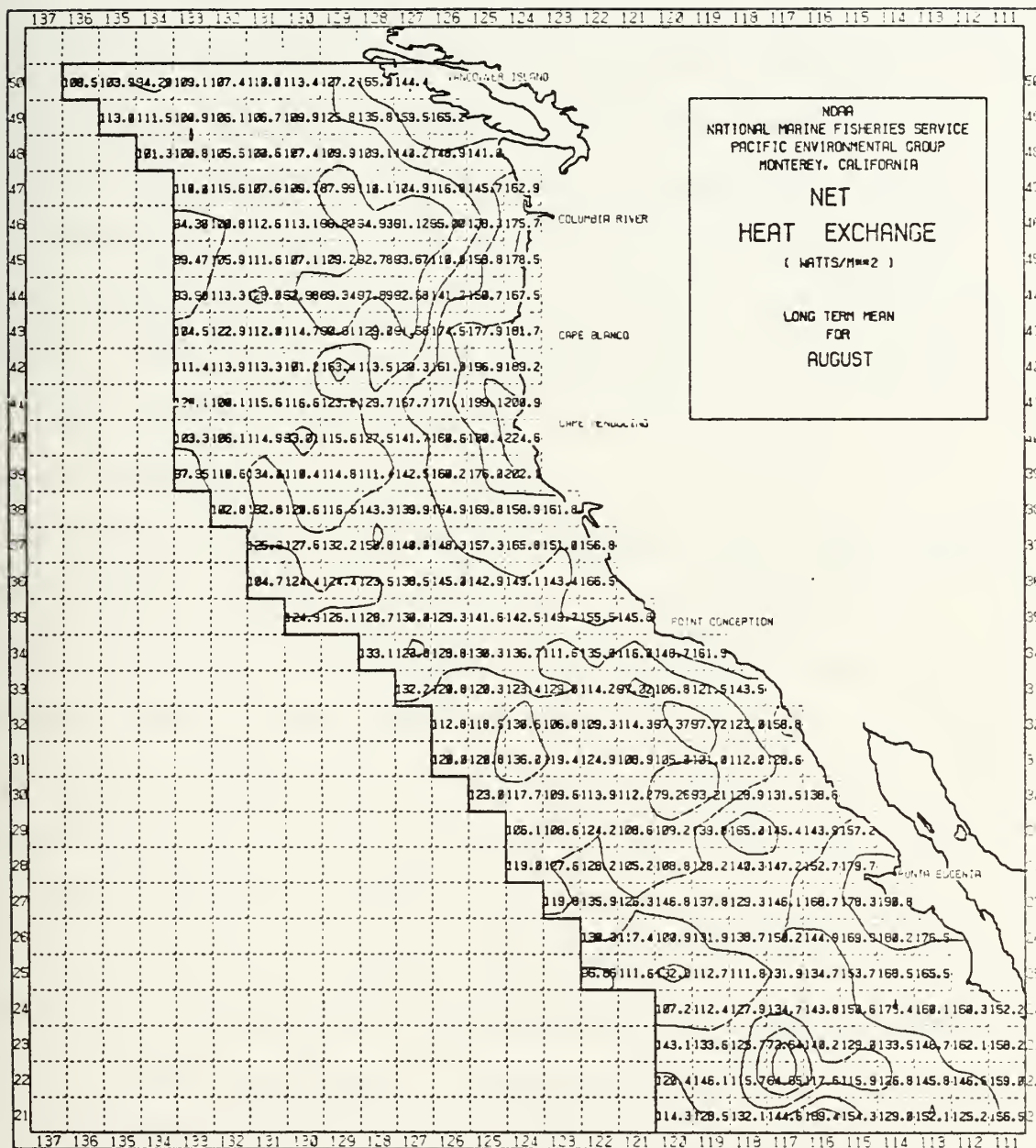


Figure 18. Long term mean August net heat exchange: 1901-1972 [Nelson and Husby, 1983]

term are essentially of equal climatological value within the region of interest. As will be seen in the following discussions, the climatological value of net heat flux is far greater than that computed from acquired synoptic atmospheric data due to frequently overcast conditions. The climatological $Q(N)$ is, however, somewhat less (approximately 30 Watts/m^2) than the value 'backed out' from the transition depicted in the acquired TOPS/TOPS-EOTS profiles. Heat fluxes and wind stress values, the boundary conditions required for the model simulations, are to be further discussed in Chapter IV.

Wind speed cubed, thermocline strength, and mixed layer depth fields are also included here to demonstrate the spatial and seasonal characteristics of wind generated turbulent kinetic energy and the associated upper ocean stability based on Husby and Nelson (1982). Winds used in the computations of the wind speed cubed fields were the same as winds used in the calculations of wind stress and wind stress curl. The wind speed cubed fields were computed as an indicator of the turbulent kinetic energy transferred from the air to the upper ocean, a common procedure.

In producing the other two fields, Husby, et.al. (1982) were faced with some of the typical problems one encounters when working with mixed layers, more specifically with interpreting temperature profiles (mainly XBT). It was necessary to establish the criterion for the extraction of the desired features. A typical vertical temperature profile

with characteristics of interest is depicted in Fig. 3. (This profile and some actual XBT profiles will be discussed in more detail in Chapter III, Section A.) That BT profiles comprising their data base were digitized at five meter intervals plays an important role in the type of criterion used. They chose to select their mixed layer depths as the upper limit of the first five meter interval in which the temperature gradient exceeded $-0.3\text{C}/5\text{m}$ ($-0.06\text{C}/\text{m}$). The bottom of the thermocline was obtained by choosing the upper depth of the two successive five meter intervals within which the temperature gradient did not exceed $-0.3/5\text{m}$. The strength of the thermocline was then obtained by taking the difference of the temperature at the bottom of the thermocline from the mixed layer temperature. These values were then summarized into one degree squares and mapped. (Fig. 19)

The practice of using the wind speed cubed as an indicator as described above does not seem to apply to the study domain in August, for in using an above average estimate of 6 m/s wind, the resulting wind speed cubed is $216 (\text{m/s})^3$; a value quite a bit less than that depicted in the climatology. The mean observed mixed layer is, however, quite consistent with the corresponding climatological mixed layer depicted in Fig. 19. The discrepancy between turbulence indicator (wind) and mixed layer depth leads one to consider the probable importance of convective activity and horizontal advection within the region.

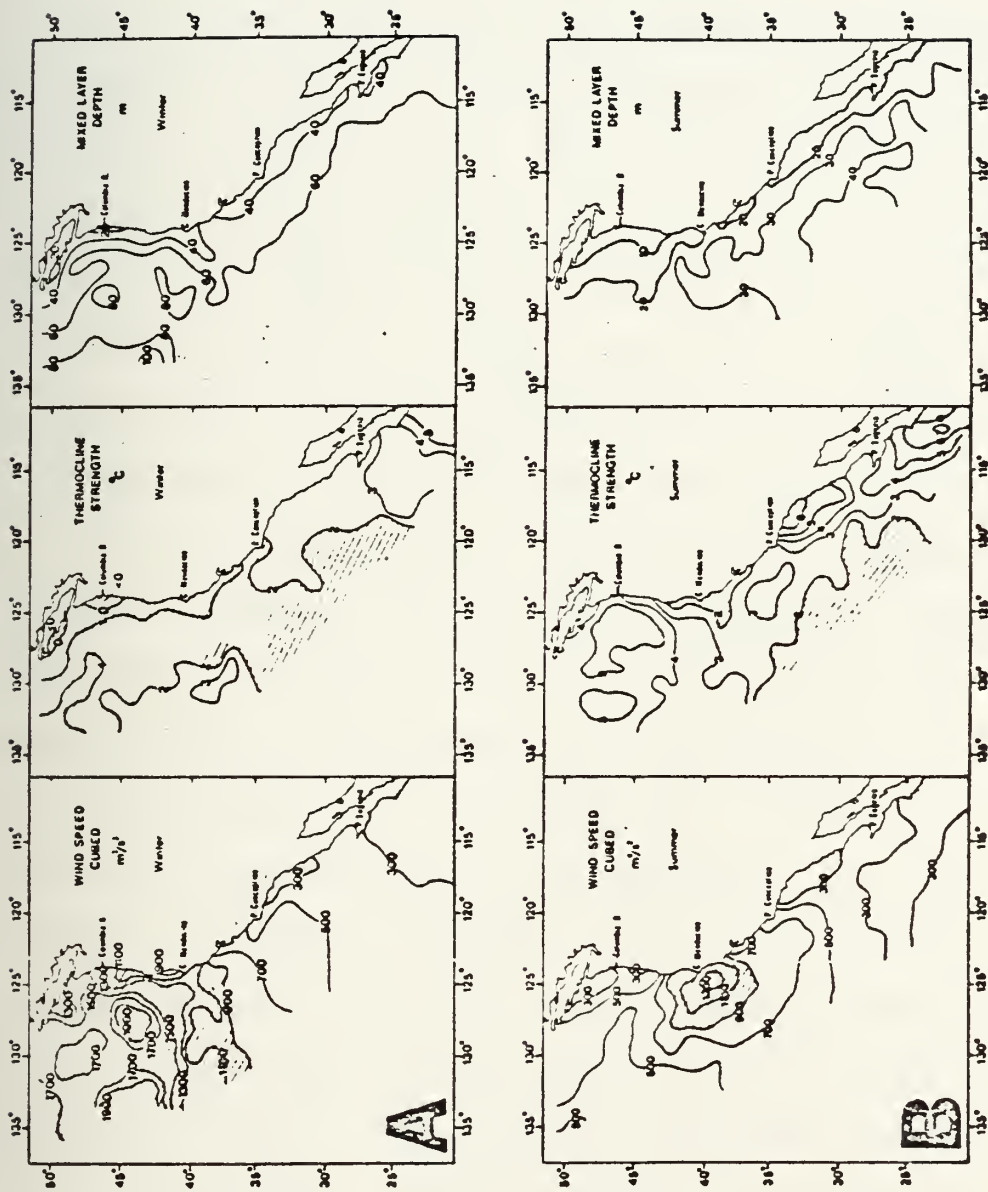


Figure 19. (Wind Speed)³, Thermocline Strength, and MLD Mean distributions of wind speed cubed (m/s^3), indicating the rate of turbulent energy production, thermocline strength (C), and mixed layer depth (m) for (A) winter (December-February) and (B) summer (June-August) [Husby and Nelson, 1982]

II. THE OBSERVATIONS

A. DATA ACQUISITION

The analyzed data were acquired aboard the R/V ACANIA in support of the Pilot Ocean Prediction Study of California Current Eddies, which has since become known as the OPTOMA program sponsored by ONR. The cruises designated CCS1 and CCS2 (Legs I and II) covered time intervals 8 to 12 March, 30 July to 5 August, and 9 to 14 August 1982, respectively. (For the convenience of this thesis, CCS1 will be called CCSI, CCS2 legs I and II will be called CCSII and CCSIII, respectively.) Each had as its domain of interest, a region off Point Arena centered at approximately 38N, 126W. CCSII was devoted to sampling the largest domain, approximately 180 km square with line spacing of ca. 44km. and station spacing of approximately a quarter of the baroclinic Rossby radius of deformation, i.e., 9 km. This allowed for better resolution over a scale neither so large as that of the CalCOFI data nor as small as that used during CCSI. (120 km with line spacing of ca. 18 km and station spacing of 9 km.) CCSIII was for the most part a resampling of the CCSII grid. Station spacing on a whole was maintained at small enough intervals (ca. 9 km for August cruises) to minimize aliasing by the smaller scale activity.

On all three cruises, continuous sampling was achieved using the shipboard DAS (Digital Data Acquisition System). T-4 XBT's (expendable bathythermographs) maximum depth of 450 m, were launched at each station. (Figs. 1, 2) 189 XBT's were deployed on CCSI, while approximately twice that number, 353, were deployed in the combined latter two cruises. No CTD casts were made during CCSI. Interspersed along the track on CCSII and CCSIII were 500 and 1500m CTD casts. During CCSII and CCSIII, 100 CTD casts were made prior to equipment failure due to rough weather. In addition to logging these vertical profiles, DAS stored station and interstation "underway" values of position, time, ship's speed, ship's roll, and surface atmospheric data; such as, dewpoint temperature, air temperature, barometric pressure, wind direction, and wind speed. Fractional cloud cover was recorded in the ship's log on an hourly basis by the deck watchstander.

Winds for each day of the August cruises in the vicinity of the cruise tracks (nine gridpoints) were supplied by FNOC. (Figs. 20, 21) In addition, TOPS and TOPS-EOTS produced ocean temperature profiles associated with eight of the nine points of interest which were archived by FNOC for later evaluation with in situ data. (The ninth point was located on land.)

Satellite IR imagery was available from NOAA/NESS (Redwood City) for cruise planning and preliminary analysis.

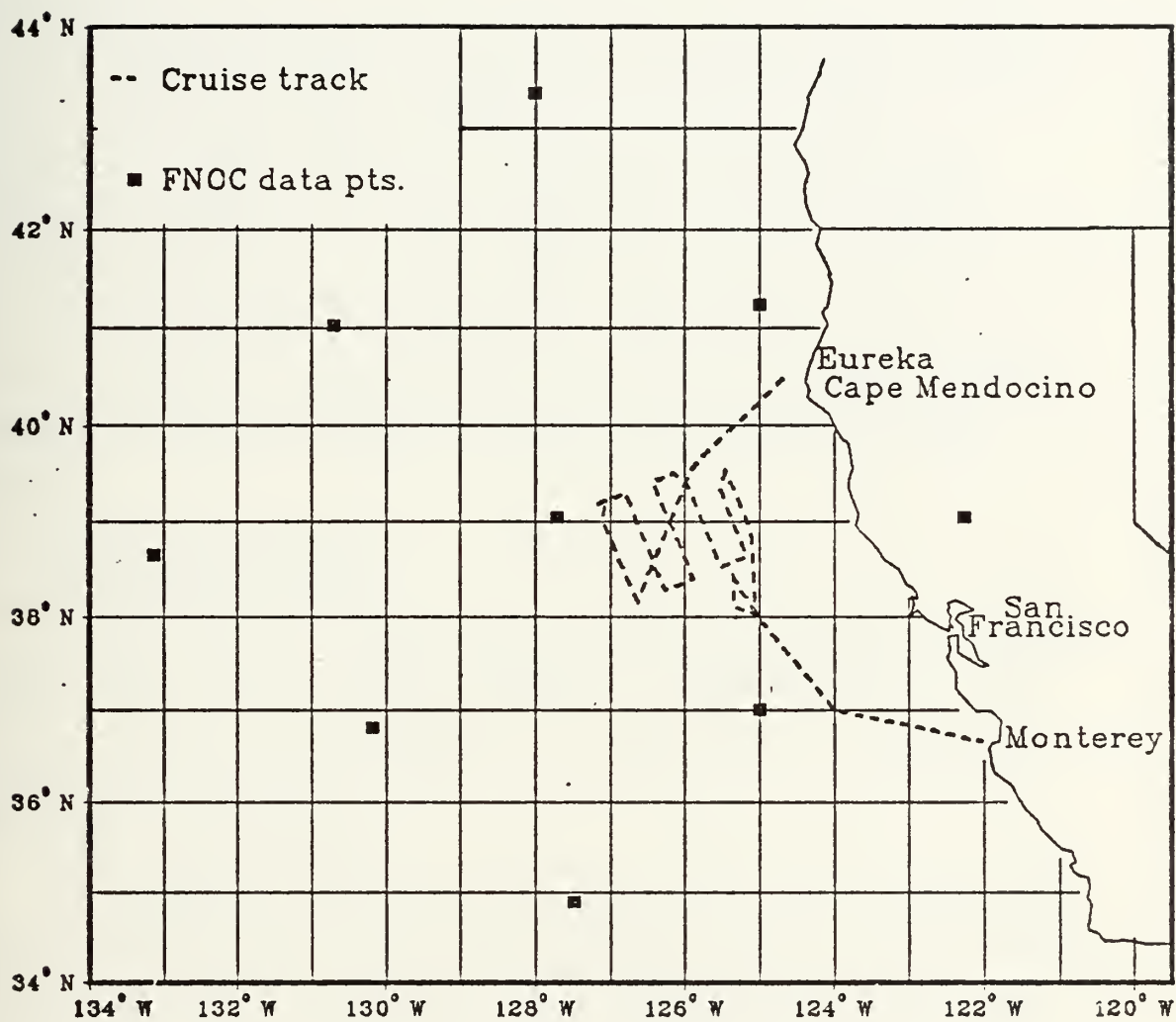


Figure 21. CCSIII cruise track and the nearest TOPS/
TOPS-EOTS gridpoints

Higher quality imagery was supplied by SOSF (Scripps Ocean Satellite Facility) for post analysis.

B. DESCRIPTION OF DATA AVAILABLE

1. CCSI

The XBT data are of primary interest from the March cruise. 189 XBT's were deployed, of which 180 were 'successful'. Each trace was digitized by FNOC because DAS had malfunctioned. Final selection left 105 XBT's within the grid region. Data files consisted of date, time, latitude, longitude, and vertical profiles of depth versus the corresponding temperature and climatologically-based salinity.

2. CCSII and CCSIII

These cruises contained more data of present interest. The XBT count was 257 after editing. Digitization by FNOC in this case was not necessary. Of these XBT's, 198 were located within the grid.

The data, similar to that of CCSI with the exception that the salinity was not climatologically-based, were recorded on DAS cartridges. Data from these tapes were subsequently made accessible from CMS (Conversational Monitor System) on the NPS IBM 3033. The original traces and XBT logs were used for comparison and error checks.

DAS log data, stored and accessed in the same way as the XBT data, though in the standard DAS header file format,

were the source of the majority of the atmospheric data acquired during CCSII and CCSIII. Numerous runs in various editing modes were made to delete blocks of zeros, erroneous values, and data not applicable to the grid region. (see Appendix A)

Additional atmospheric data, such as cloud cover, were recorded on an hourly basis in the ship's log. Any additional data pertaining to the ocean, such as bucket temperatures, were logged in the CTD log or on the XBT traces.

Finally, atmospheric as well as oceanic analyses in the vicinity of the experimental domain were archived by FNOG. They consisted of daily wind values, one for each of the nine selected FNOG gridpoints, as well as daily analyses and 24-hour forecasts of the ocean temperature profiles for the eight gridpoints located over the ocean. Since TOPS/TOPS-EOTS runs on a Northern Hemispheric polar stereographic grid with a grid spacing of approximately 300 km in the midlatitudes, it was not possible to obtain analyses from numerous points in the cruise region. In fact, of the eight points located over the ocean, none of them fell directly within the cruise domain. (Figs. 20, 21) The use of the standard FNOG gridpoint was an unnecessary limitation that was imposed for convenience. (Subsequently, it was learned that FNOG has the capacity to interpolate their analyses to produce a vertical temperature profile at a specified point.) The analyses and TOPS

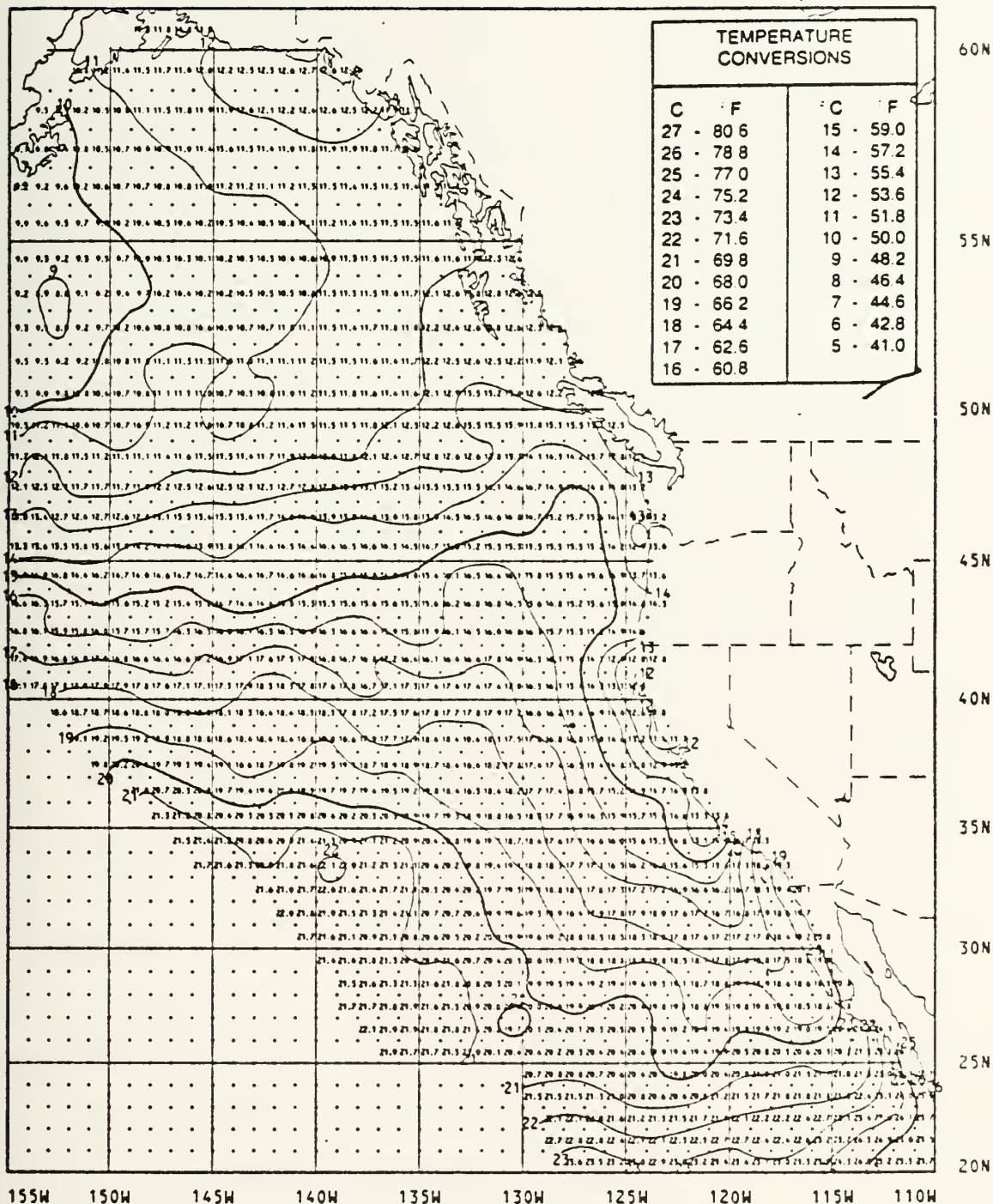
predictions used in this study were from the point closest to the study domain. Based on the SST climatology (Fig. 22), the chosen FNOG gridpoint at 39.05N, 127.75W was not expected to have a SST much greater (at most 1C) than that of the XBT's within the cruise area.

C. FORCING FUNCTIONS FOR THE GARWOOD AND MELLOR LEVEL-2.5 MODELS

The version of the Garwood model utilized required an initial vertical temperature profile as well as three-hourly values of air temperature, dewpoint temperature, wind speed, and cloud cover for the computation of the boundary conditions to be used in both the Garwood and the Mellor 2.5 models: the momentum and heat fluxes.

For the first run, initialization was done with the FNOG analyzed ocean temperature profile at 39.0N, 127.75W. This initialization permitted comparison of the forecasted TOPS/TOPS-EOTS ocean temperature profile with that obtained from the Garwood model over the same time span. All other runs were made using XBT 96 as the initial temperature profile.

The three-hourly air temperature was obtained by averaging the DAS underway data. Averages were made over 6 to 299 values. The resulting standard deviations range from a high of 1.67C to a low of 0.0005C. Only three values had a standard deviation over 1.0C. Averaging was done under the assumption that the air temperature varied little over the



West Coast
15 DAY SST MEAN (°C)

Semi-monthly means of sea surface temperature
compiled by the National Meteorological Center
of the National Weather Service.

Figure 22. Average SST for last half of July 1982

relatively small cruise grid at any given time. In addition, it was assumed in the case of missing or erroneous data that, at a given time of day, the values did not vary much over the course of a couple of days. Thus, for missing 0001-0300 readings, the 0300 input to the model was assumed equal to that of the previous day. (Fig. 23)

The dewpoint temperatures were to be acquired in a similar manner, however, faulty instrumentation precluded this. Dewpoint temperatures were instead computed using a technique described by Bolton (1980). (Fig. 24) To use the method, relative humidities (also unavailable) were required. As recommended by Davidson (personal communication), a relative humidity of 90% was assumed throughout to correspond with the foggy/hazy conditions which existed intermittently through the cruises.

Wind speeds (Fig. 25) from the nearest FNOC point were used consistent with the location of initial values. The region of interest was considered to be too small to require interpolation of winds. (Fig. 26) Ship winds available from DAS are relative winds, but true winds could be calculated by correcting for ship's velocity. This was not necessary for the runs described. Instead, the applicability of the FNOC winds was checked by comparing them with the DAS winds recorded at CTD stations because the ship was then 'stationary'. (see Appendix A)

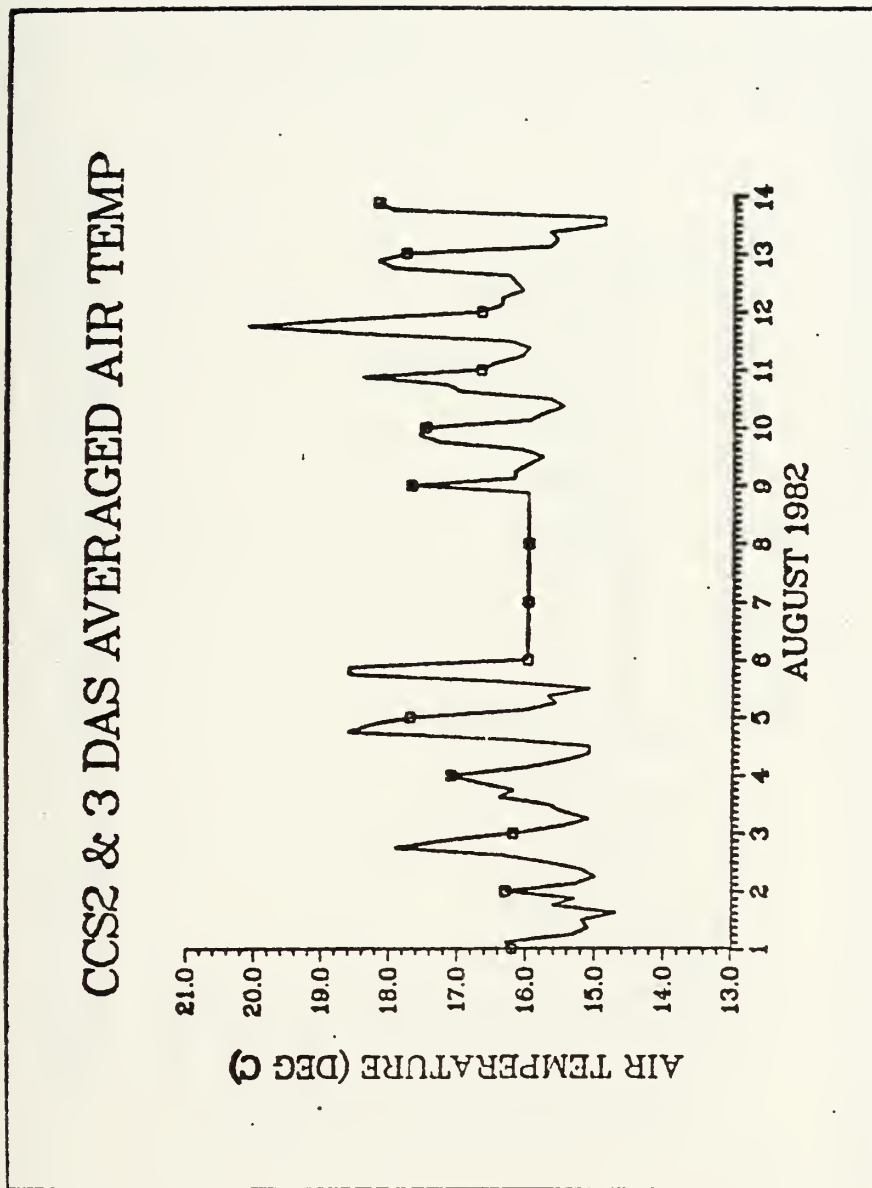


Figure 23. Time series of three hourly averaged DAS recorded air temperatures used in computing forcing functions for the Garwood and Mellor Level-2.5 model simulations

CCS2 & 3 DAS AVERAGED DEWPT TEMP

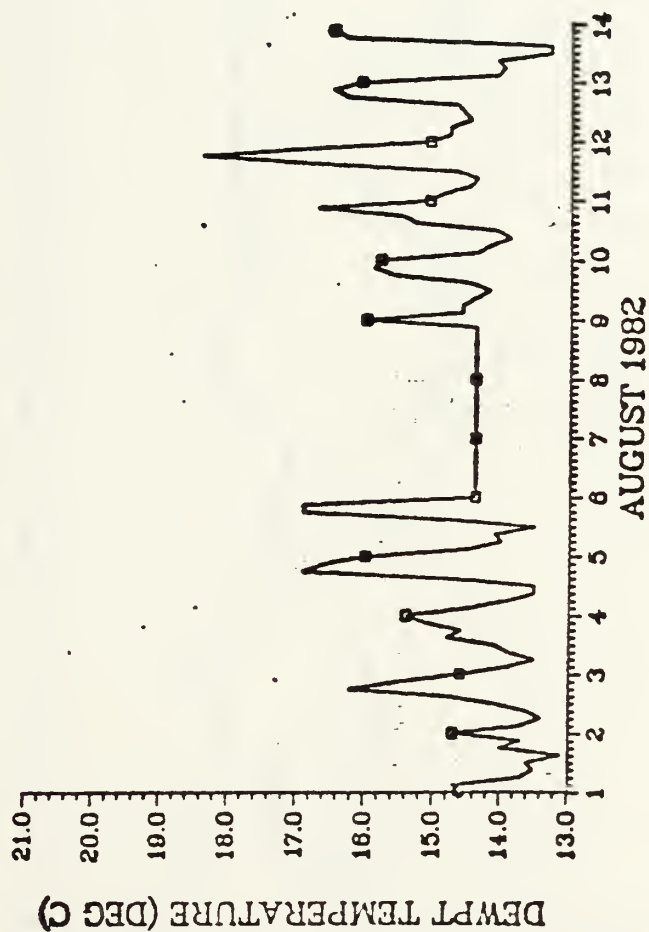


Figure 24. Time series of calculated dewpoint temperatures used to compute forcing functions for the Garwood and Mellor Level-2.5 model simulations

ANALYZED WINDS: 39.05N,127.72W

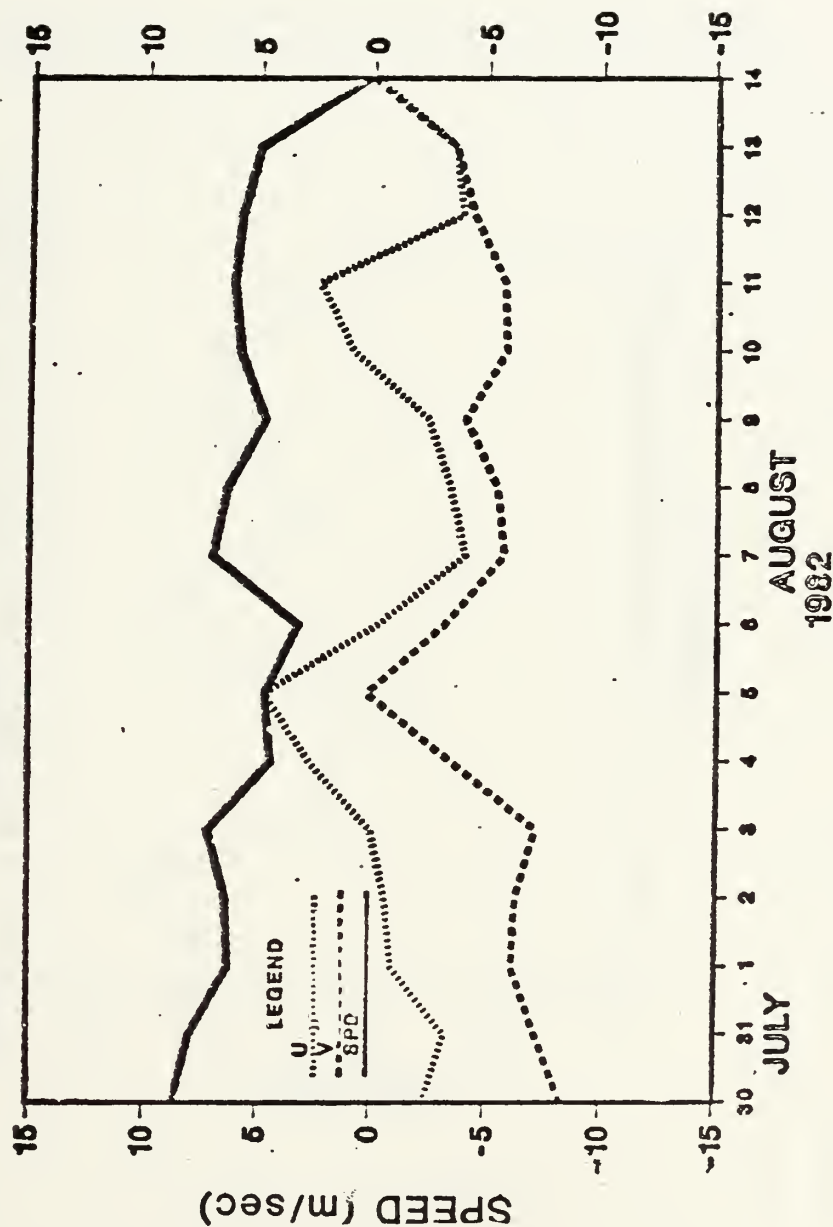


Figure 25. Time series of FNOc analyzed wind components and speeds for 39.05N, 127.72W

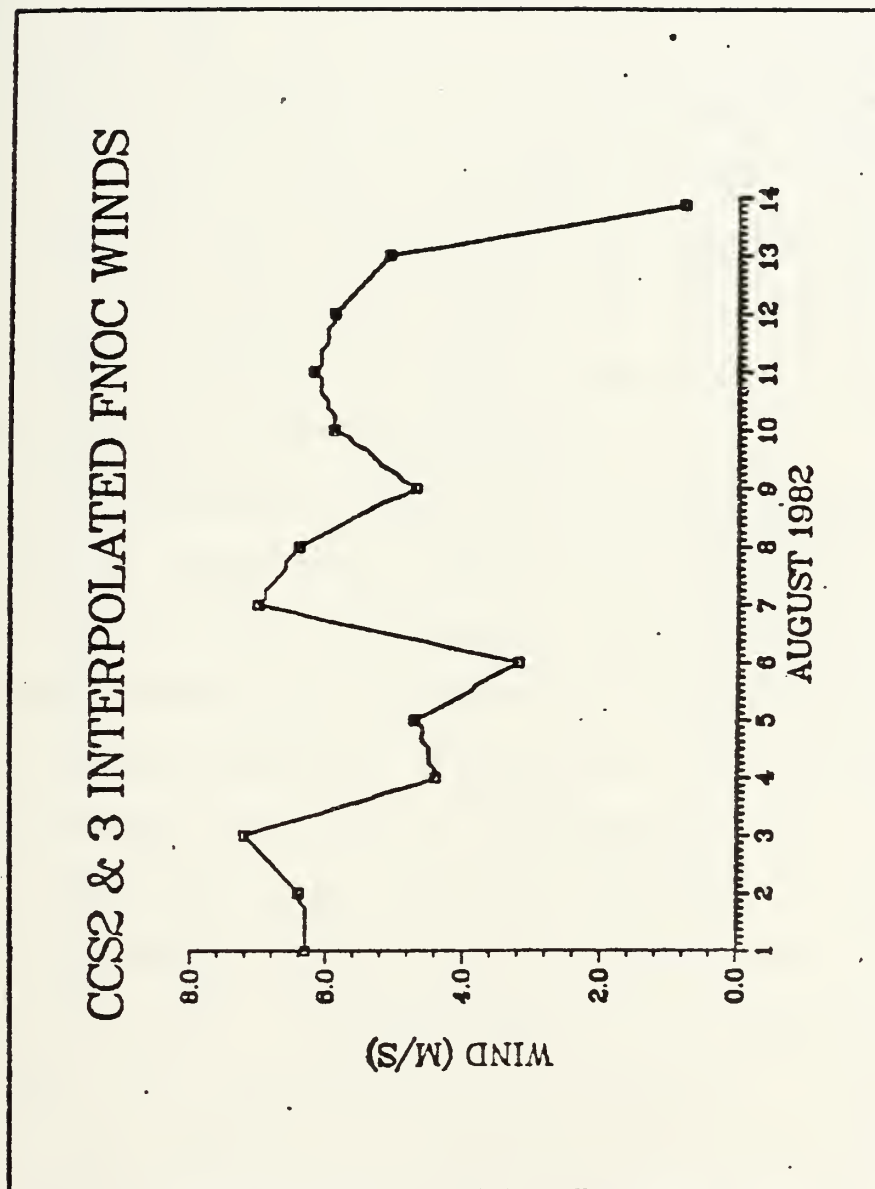


Figure 26. Time series of interpolated FNOC analyzed winds-
interpolated to the necessary time step

Sea surface temperatures were obtained from individual XBT's along the track. (Fig 27) The XBT's used were those launched within half an hour of the necessary input time.

The final input, cloud cover in octals, was acquired from hourly observations, and averaged over three-hour intervals. (Fig. 28)

The boundary conditions, i.e., heat and momentum fluxes, applied were computed within the program. (Figs. 29, 30) As will be discussed later, the average daily net heat flux forcing the Garwood and Mellor models over the thirteen days was $+4.25 \text{ W/m}^2$. (where positive is upward flux, i.e., the ocean was losing heat to the atmosphere)

Additional information required by the Garwood model includes various coefficients; such as, the extinction coefficient and the drag coefficient. For the most part, they were set from previous model usage. The Garwood model contains two 'tuning parameters' (resulting in essentially two degrees of freedom) which had to be addressed prior to model simulations with each 'new host point' [Garwood, et.al., 1982] The parameters, AM and AZR had already been set upon receipt of the model. (A tuning analysis is presently underway within the Ocean Prediction Laboratory. The procedure and results will probably be documented at some future time.)

Coefficients, such as the diffusion coefficients, used in the Mellor level-2.5 model are 'universal' constants, and so required no alterations.

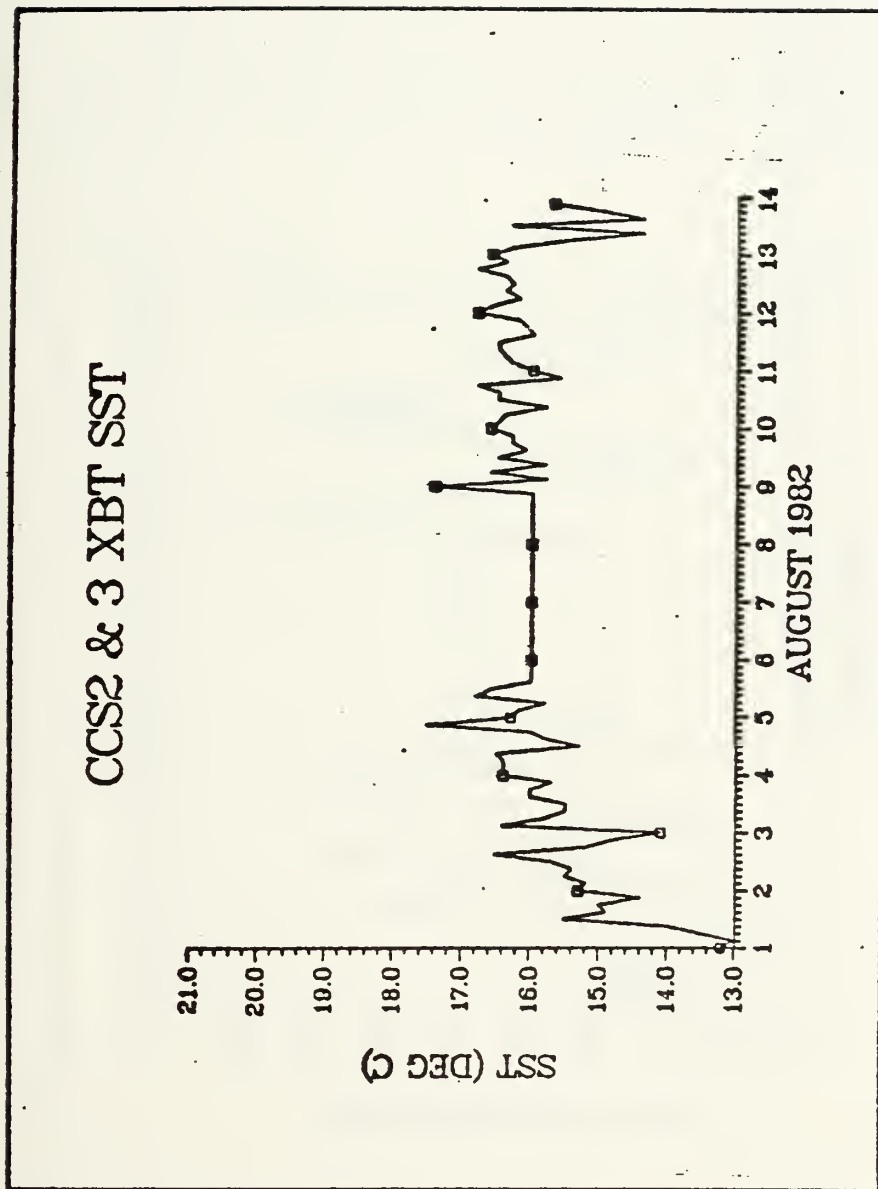


Figure 27. Time series of XBT SST used to compute the forcing functions for the Garwood and Mellor Level-2.5 model simulations

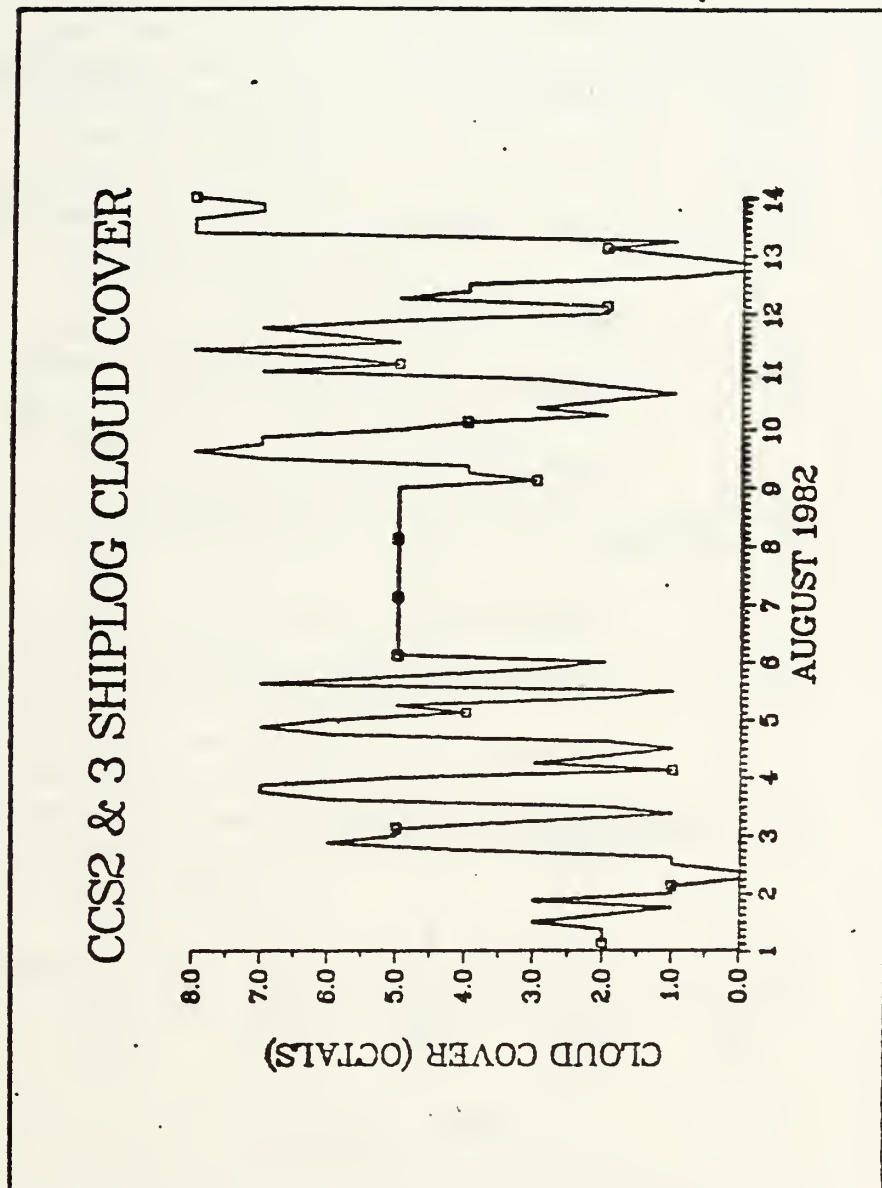


Figure 28. Time series of cloud cover in octals

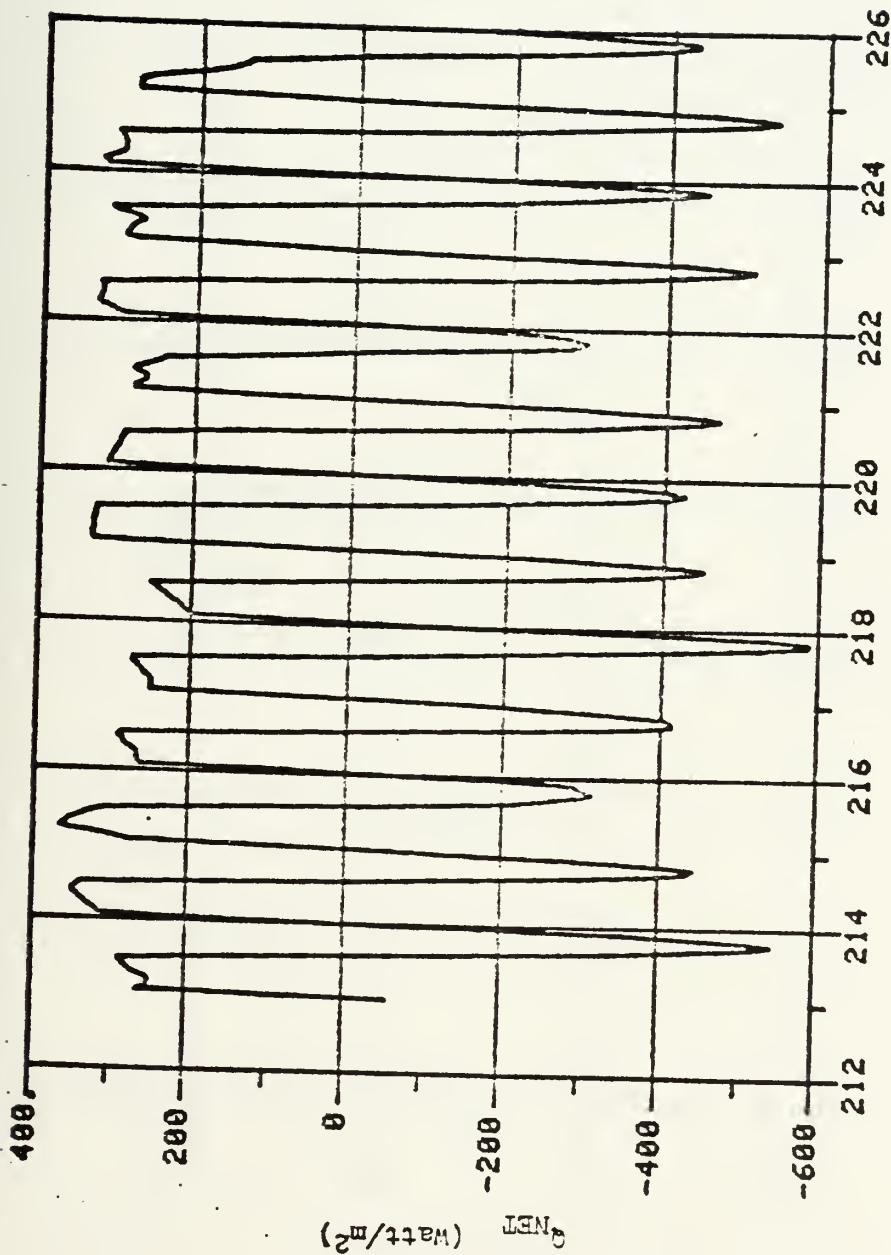


Figure 29. Time series of net heat flux (Watt/m²)
(Julian days correspond with 31 July-14
August 1982)

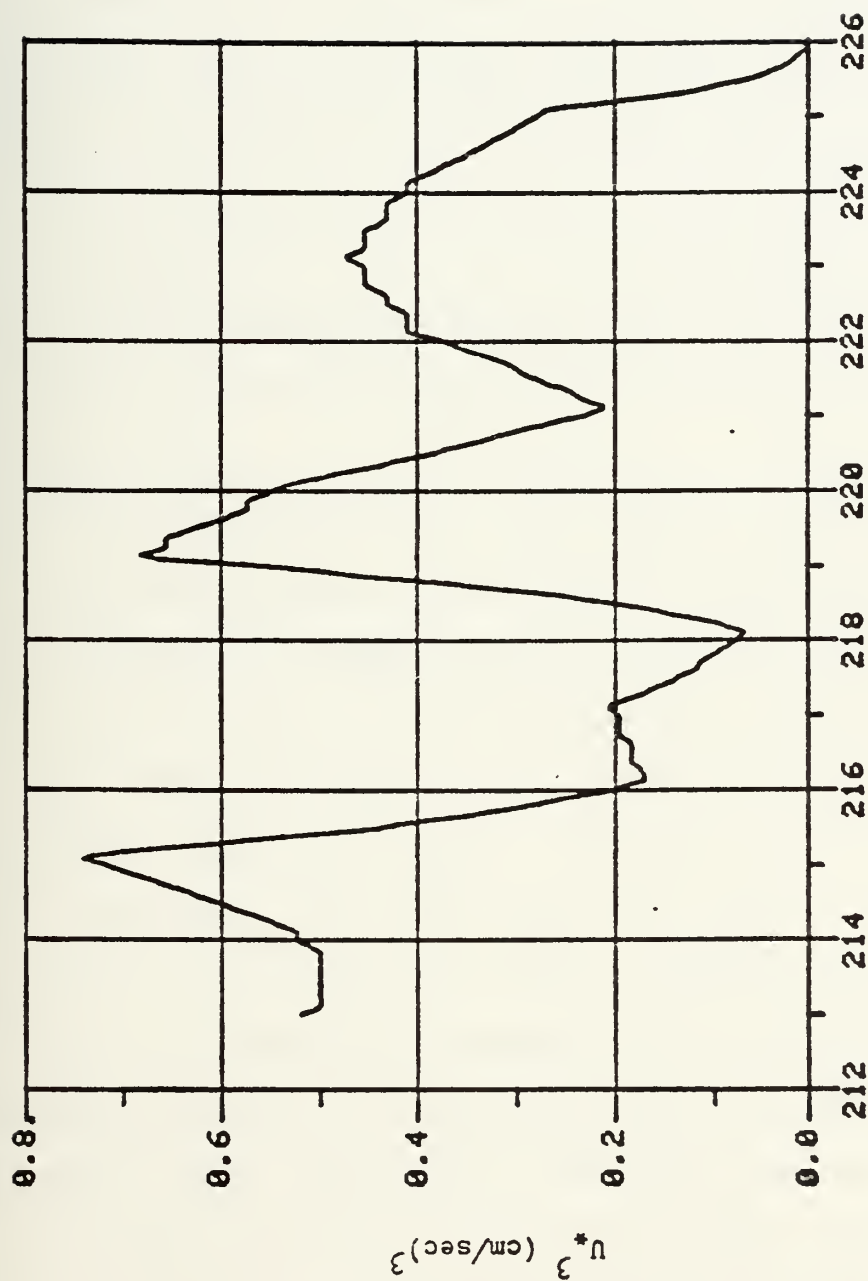


Figure 30. Time series of friction velocity cubed (cm/sec)³ (Julian days correspond with 31 July-14 August 1982)

III. STATISTICS

A. DETERMINATION OF THE OBSERVED VARIABLE MIXED LAYER DEPTH

Obtaining mixed layer depths from DAS or FNOC digitized profiles or even from the original XBT traces is no easy task. Criteria employed vary greatly, and there is a tendency to change one's criterion with each new exception that arises. Further complexity occurs with the desire to isolate new (shallow) mixed layer depths in addition to the numerous old (deep) ones.

The new mixed layer is a layer formed over the old one due to the mixing being insufficient to reach the level of the old (previously formed) mixed layer. This may be the result of weak winds and surface heating. The old mixed layer will remain in place until turbulent diffusion of the interface or some other process dissipates it or strong mixing deepens the layer. The main reason for this is that the Second Law of Thermodynamics does not permit the unmixing of the fluid. An 'excellent' example of an old mixed layer recorded during CCSI is depicted in Fig. 31. (This layer is also the new mixed layer for it has replaced the old one which would have existed at an earlier time.) An old mixed layer extending to approximately 63m with an overlying new mixed layer extending to approximately 41m is depicted in Fig. 32. In Fig. 3, h_1 would be considered a new mixed layer

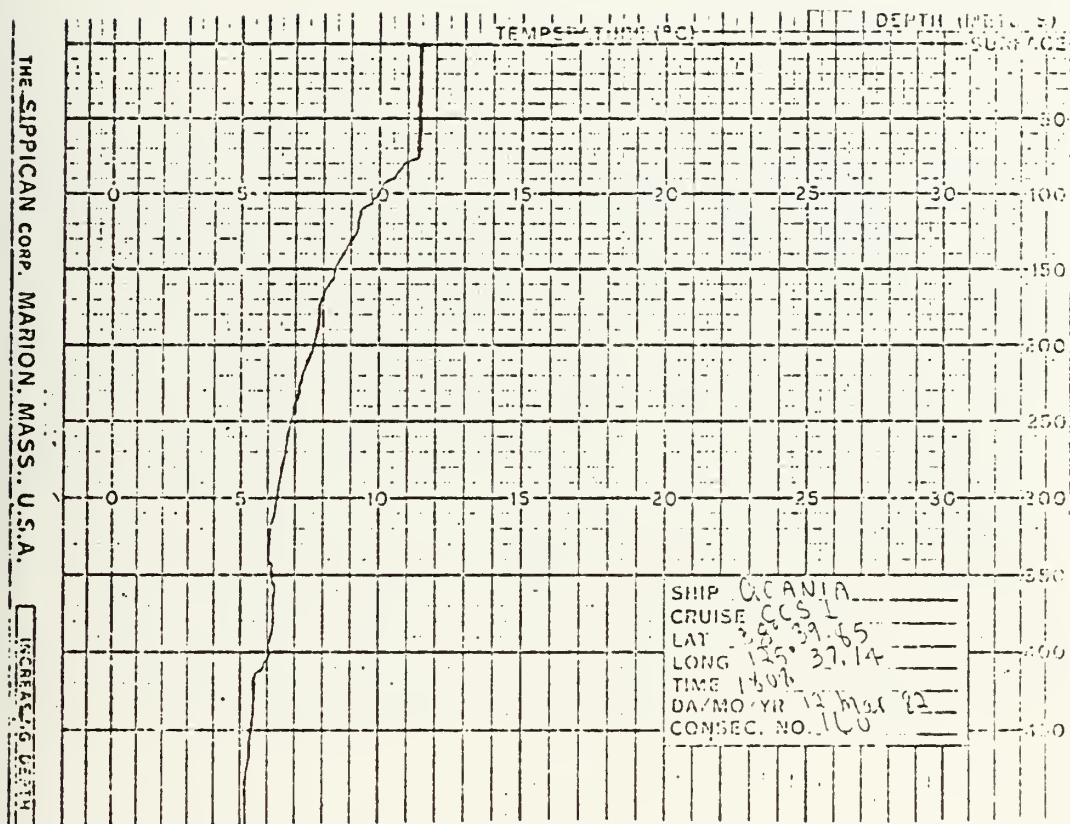


Figure 31. XBT trace depicting an "excellent" new/old mixed layer

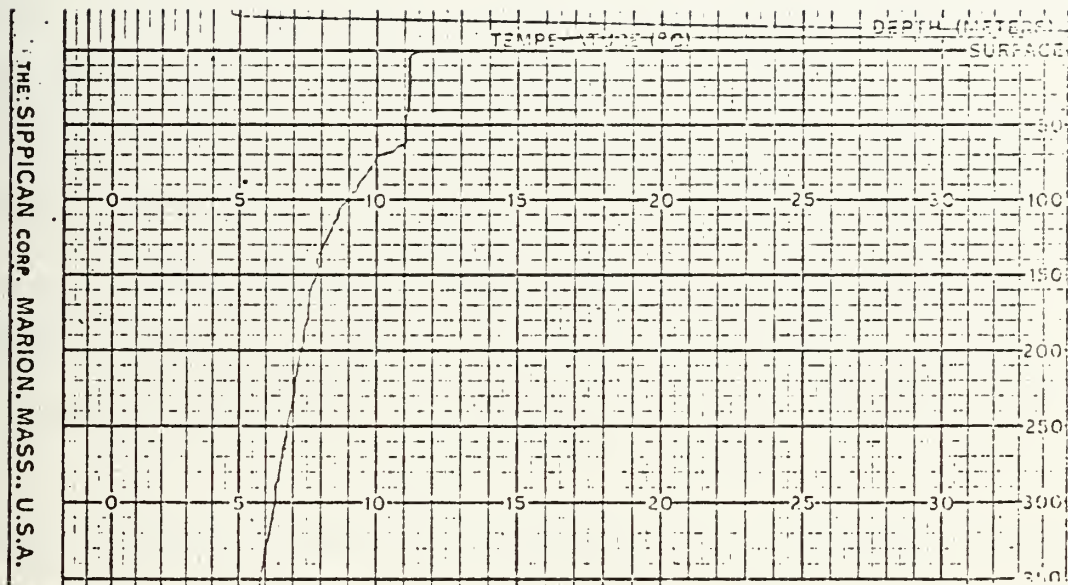


Figure 32. XBT trace depicting an "excellent" new and old mixed layer

overlying the old winter mixed layer, h_2 . New mixed layers do not depend solely on seasonal or synoptic changes.

Numerous cases of diurnal mixed layers were noted wherein the cooling of the surface at night caused the upper water column to become unstable and consequently, mixed, forming a new mixed layer. Meanwhile, during the day, the surface is heated, possibly producing a warm shallow layer over the old mixed layer, i.e., a new thermocline is formed.

New mixed layers may also be formed under a large number of other conditions. A storm, for example, will most likely cause a new mixed layer to form which will quite possibly be deeper than the old one. In this case, the new mixed layer supplants the old one, and becomes the old mixed layer, too.

Eventhough the old mixed layers are of importance to Navy applications, for their role in surface acoustic ducting, the new mixed layers are the layers of importance in mixed layer modeling, i.e., that is the layer predicted and modified by some bulk (layered) models in use today. Thus, one must find a suitable method for defining both of these significant features, as well as sea surface temperature, depicted in an XBT profile.

The first attempt to obtain mixed layer depths from the temperature depth profiles was made by computer comparison of three sequential points on the trace for a 0.2C change. (The value 0.2C was chosen for that is the accuracy of the

new XBTs; more precisely, 0.12C-0.31C [Heinmiller, 1982]. It is the value presently in use in producing the TOPS/TOPS-EOTS contoured mixed layer depth product.) This technique proved to be satisfactory except in cases of a surface thermocline, a very weak new mixed layer, no mixed layer, and an old mixed layer with a noticeable gradient (though still possessing the characteristic 'knee'). A similar technique was used by Thompson (1975) with the additional technique of starting his sequential comparison at three meters depth to avoid the surface thermocline problem. With either procedure one would expect to obtain a depth, no matter whether a mixed layer existed or not. (The depth for the 0.2C change obtained may be in the middle of a gradient.) Such was not the case, however, due to the digitization scheme used by FNOG wherein only depths of inflection points were listed. Comparison of the surface temperature with the temperature of the first inflection point, the point at the base of the shallow surface thermocline, may yield a greater than 0.2C change. This would in turn lead to 0.0m being denoted the mixed layer depth when a very noticeable mixed layer might be apparent below the shallow thermocline or possibly due to the response time of the XBT recorder.

These possible deficiencies made it necessary to return to the original traces and logs. Each trace was examined and redefined in terms of temperatures and depths of the features of interest, for example, surface temperature, the temperature

and depth of the base of the surface thermocline, the temperature and depth of each sequential possible mixed layer, and the temperature and depth of a deeper point chosen to define the seasonal thermocline. Final mixed layer depth values, as well as other values, were chosen by comparison of the computerized analysis, the traces, and the XBT logs. The computerized analysis was given the most weight, followed by results obtained from inspection of the traces. The XBT logs were given the least emphasis due to their variation with the experience, knowledge, and judgment of the observer and the not always optimal conditions under which they were recorded.

B. STATISTICAL CHARACTERIZATION

The several variables derived from the XBT profiles by the techniques previously mentioned were used as a basis for a statistical characterization of each cruise. Basic properties such as the mean, minimum, maximum, median, and standard deviation were examined. They are summarized in Table III. Two types of correlations coefficients were calculated, as well as Student-t confidence intervals, regression equations, and histograms and maps of SST, bucket temperature, old mixed layer depth (OMLD), old mixed layer depth temperature (OMLDT), new mixed layer depth (NMLD) and new mixed layer depth temperature (NMLDT). Only a limited selection of statistical quantities will be presented to convey the character of the upper ocean during the various cruises.

The first variables to be discussed are the SST's for the three cruises and the bucket temperatures from the first cruise. A total of 105 XBT's were available from the CCSI grid for the statistical characterization. Both XBT SST and bucket temperature were recorded with a comparison revealing the XBT SST field was overall slightly warmer than the bucket temperature field, i.e., 0.4C. (Fig. 33, Table III) A regression equation or least squares linear equation of the bucket temperature with respect to the XBT SST was calculated to be: $Y = .678 + .926(X1)$ where $X1 = \text{XBT SST}$. The R squared value, a measure of how well the regression equation fits the data, was 79.6%. (100% is a perfect fit. The R squared value is defined by $(100)(\text{sum of squares due to regression} / \text{total sum of squares.})$)

The two correlation coefficients computed were the Pearson product moment coefficient and the autocorrelation function with respect to distance. The former calculated for XBT SST's versus bucket temperatures, resulted in a large correlation coefficient, .892., though not 'large enough' considering the fact that the values should be exactly the same (except for measurement noise). The spatial autocorrelation function was computed using binned XBT pairs. Out of 210 km, the radial resolution for XBT pairs within a bin was 15 km. Beyond 210 km, it was increased to 25 km. XBT SST for CCSI (Fig. 34) had a correlation distance of approximately 30 km, using a 0.2 correlation as a reference. The correlation distance for the bucket temperature was slightly less, i.e., 27 km. (Fig. 35)

MIDDLE OF INTERVAL	NUMBER OF OBSERVATIONS	
10.4	1	*
10.6	2	**
10.8	2	**
11.0	17	*****
11.2	22	*****
11.4	23	*****
11.6	24	*****
11.8	6	*****
12.0	8	*****

MIDDLE OF INTERVAL	NUMBER OF OBSERVATIONS	
10.8	1	*
11.0	10	*****
11.2	22	*****
11.4	14	*****
11.6	23	*****
11.8	13	*****
12.0	11	*****
12.2	0	
12.4	1	*

MIDDLE OF INTERVAL	NUMBER OF OBSERVATIONS	
13.0	1	*
13.5	1	*
14.0	4	****
14.5	5	*****
15.0	6	*****
15.5	27	*****
16.0	20	*****
16.5	14	*****
17.0	14	*****
17.5	4	****
18.0	1	*

MIDDLE OF INTERVAL	NUMBER OF OBSERVATIONS	
14.0	2	**
14.4	3	***
14.8	4	****
15.2	3	***
15.6	4	****
16.0	20	*****
16.4	32	*****
16.8	31	*****
17.2	2	**

Figure 33. Histograms of CCSI bucket and SST, CCSII SST, and CCSIII SST (Temperatures in degrees Celsius)

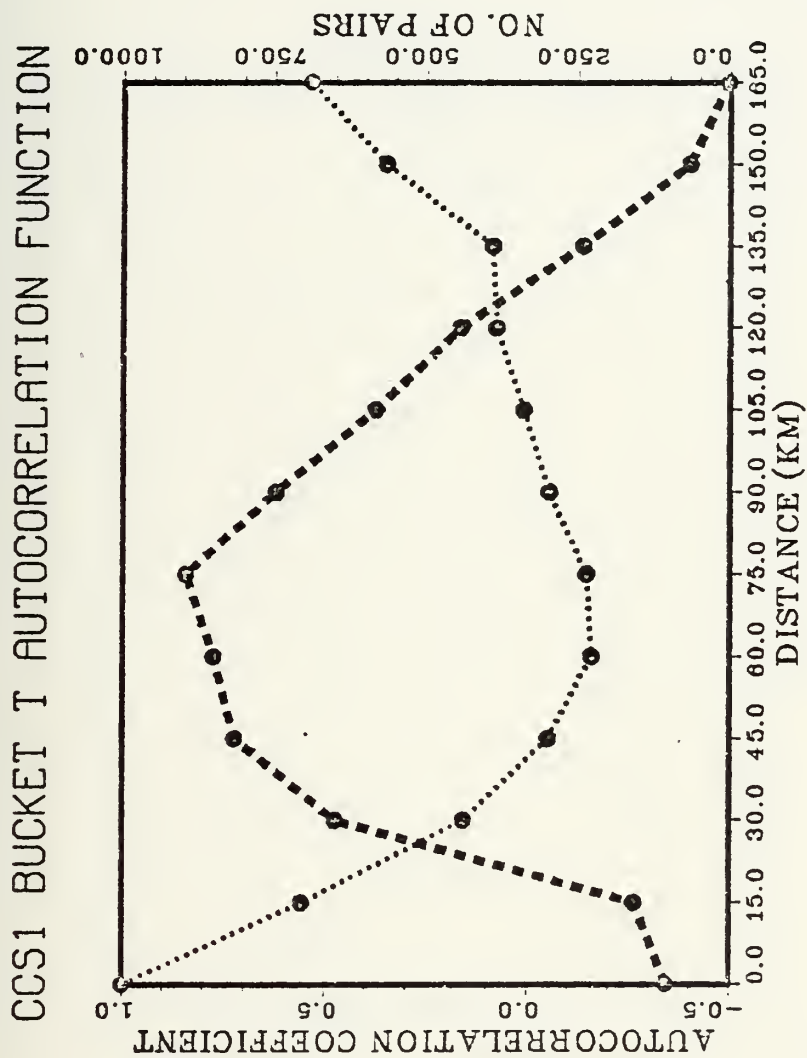


Figure 34. Autocorrelations function for CCS1 bucket temperatures with respect to distance; results depicted are for detrended data; also indicated are the number of data pairs

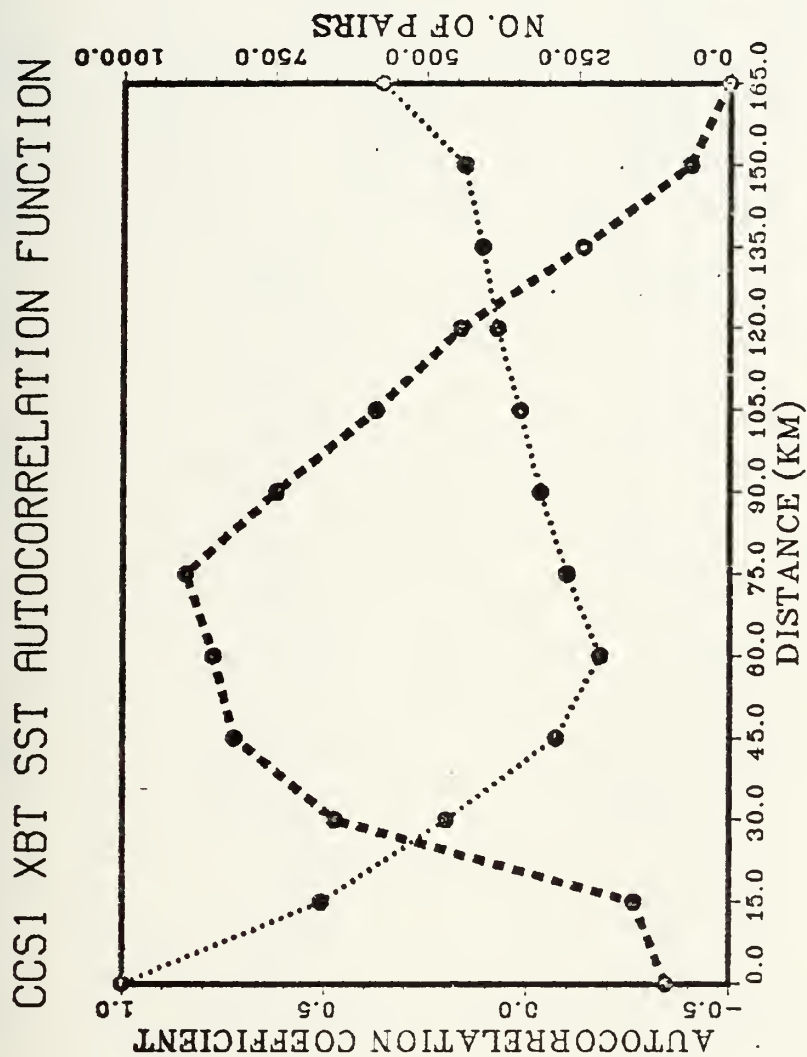


Figure 35. Autocorrelation function for CCSI XBT SST with respect to distance: results depicted are for detrended data and 'raw' data (with trend); also indicated are the number of data pairs

TABLE III
BASIC STATISTICS

	CCSI		CCSII		CCSIII	
	SST	Bkt	SST		SST	
Mean	11.5	11.3	15.9		16.3	
Stddev	.302	.314	.91		.703	
Min	10.9	10.4	12.9		13.9	
Max	12.4	12.0	18.0		17.1	
Median	11.5	11.3	15.8		16.5	
T 90%	(11.4,11.5)		(15.7,16.1)		(16.1,16.4)	
C.I.*						
	NMLDT		NMLDT		NMLDT	
Mean	11.3		15.4		15.9	
Stddev	.324		.822		.744	
Min	10.8		12.3		11.9	
Max	12.2		16.7		16.9	
Median	11.3		15.6		16.2	
T 90%	(11.3,11.4)		(15.3,15.6)		(15.8,16.1)	
C.I.*						
	NMLD		NMLD		NMLD	
Mean	39.1		15.1		16.3	
Stddev	25.5		8.3		8.1	
Min	1.0		4.0		5.0	
Max	82.0		55.0		50.0	
Median	33.0		13.0		15.0	
T 90%	(34.9,43.4)		(13.6,16.6)		(14.9,17.7)	
C.I.*						
	OMLDT		OMLDT		OMLDT	
Mean	11.2		14.7		15.5	
Stddev	.287		.927		.801	
Min	10.5		11.8		11.9	
Max	11.7		16.4		16.6	
Median	11.2		14.8		15.7	
T 90%	(11.1,11.2)		(14.6,14.9)		(15.4,15.6)	
C.I.*						
	OMLD		OMLD		OMLD	
Mean	64.8		37.8		29.5	
Stddev	12.0		13.4		12.2	
Min	27.0		6.0		8.0	
Max	95.0		69.0		65.0	
Median	63.5		38.0		28.0	
T 90%	(62.8,66.7)		(35.5,40.1)		(27.5,31.6)	
C.I.*						

Unites in table: all temperatures: degrees Celsius
all depths: meters

* T 90% C.I.: T Interval With 90% Confidence

During the latter two cruises, bucket temperatures were not recorded routinely. The CCSII data set consisted of 97 XBT's. As was to be expected, the SST values were much higher than those recorded for the March cruise. In fact, the minimum CCSII temperature, 12.9C, exceeded the maximum CCSI, 12.4C. The range of temperatures for CCSII, and thus the standard deviation in this case was quite large. A reason for the significant range, 12.9 - 18.0C, was the presence of cold eddies and cool anomalies near the peak of summertime warming.

The autocorrelation functions for SST for CCSII were plotted with and without a linear trend removed, Fig. 36. This was done to get some idea of the existence and effects of a trend in the data. Also shown is a 95% confidence region computed by $\pm \sqrt{2}/N$ where N is the number of pairs in the bin. (Using this N instead of the total N results in a more conservative confidence region.) Results indicate a slight increase of the correlation distance compared to the March cruise, i.e., 32 km for the detrended data and 38 km without the trend removed.

The mean SST for CCSIII was still higher, 16.2C, as might be expected for later in August. The range, however, fit within that of the second cruise. This may be related to the fact that CCSIII did not cover as large a region as CCSII. The correlation distance for this cruise was 40 km for the detrended data and 43 km without the trend removed. (Fig. 37)

SST2 AUTOCORRELATION FCNS

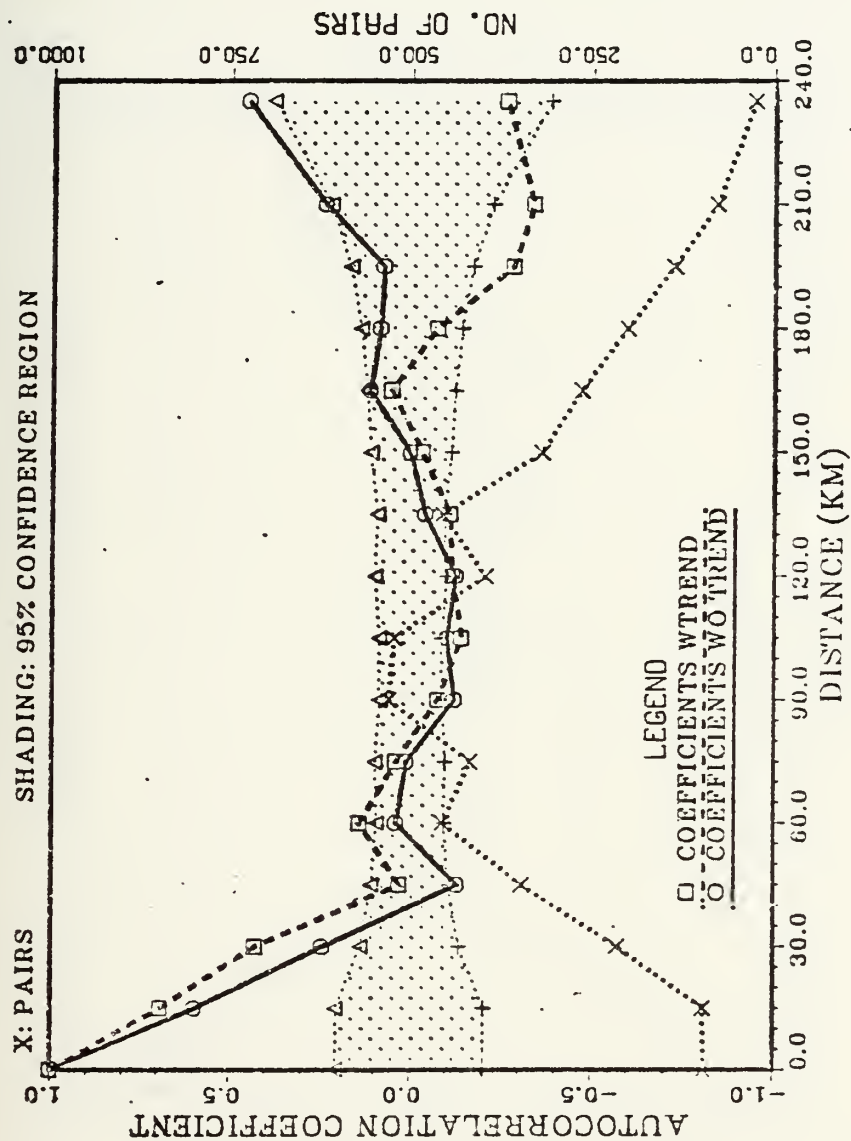


Figure 36. Autocorrelation function For CCSII XBT SST with respect to distance; Results depicted are for detrended data and 'raw' data; Also indicated are the number of data pairs and the 95% confidence limits

SST3 AUTOCORRELATION FCNS

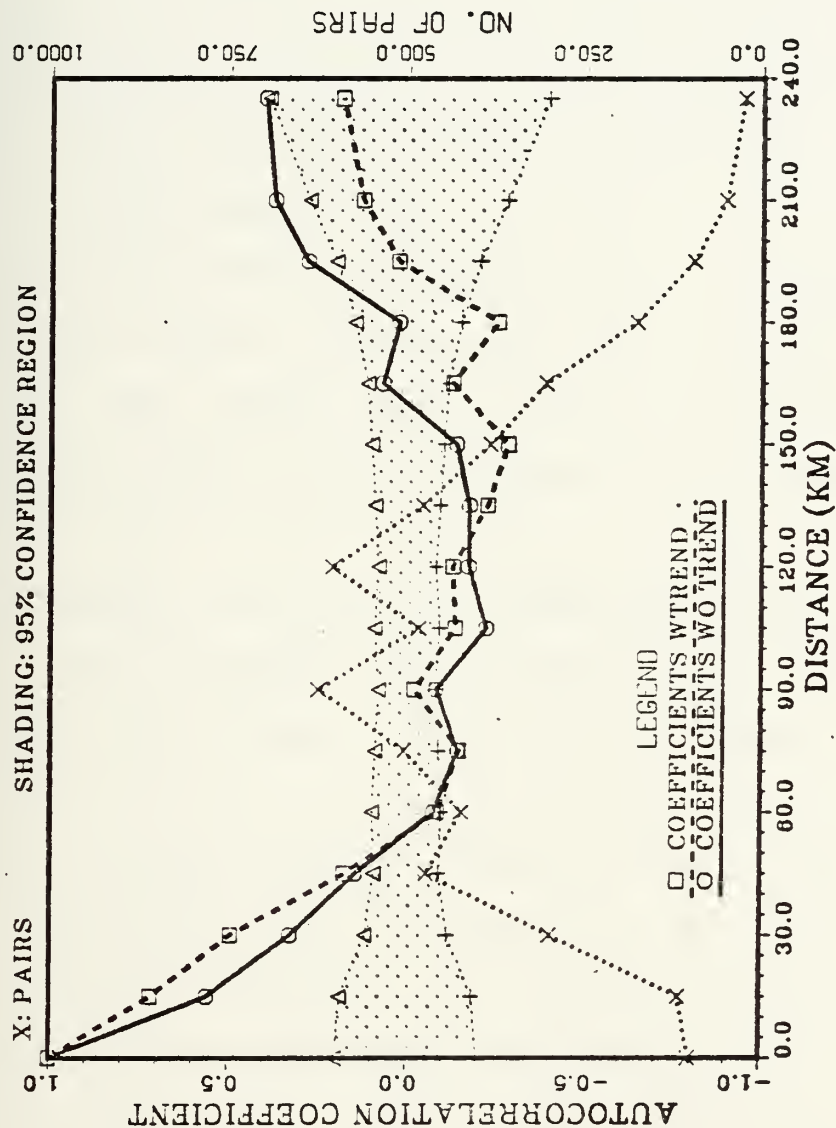


Figure 37. Autocorrelation function for CCSIII XBT SST. with respect to distance; Results depicted are for detrended data and 'raw' data; Also indicated are the number of data pairs and the 95% confidence limits

This might indicate a more homogeneous area as compared to the larger grid transited during CCSII.

The new mixed layers for the March cruise ranged from 0.0 m (when no new mixed layer was observed) to 82 m. (Table III) The largest Pearson products moment correlation obtained was for the NMLD's and OMLD's. This resulted due to a number of cases when the NMLD was identical to the OMLD, i.e., in cases of intense turbulence.

For CCSII, 84 XBT's possessed a NMLD. The NMLD's were, however, quite small, approximately half of those noted in CCSI, (Fig. 38). CCSIII had 94 instances of NMLD's. The distribution in the histogram appears to be Raleigh in nature.

Histograms of the OMLD's for the cruises are shown in Fig. 39. Most noticeable is the shift toward shallower mixed layers with time. In fact, the mean depth for the March cruise is a factor of two greater than the CCSIII mean OMLD. The Pearson product moment correlation coefficients for the OMLD in association with the majority of the other variables showed no dominant results. The largest coefficient obtained was with respect to the NMLD; the probable reason for this was already discussed. For CCSI, the correlation distance was merely 15 km. (Fig. 40) For CCSII, both the data with and without the trend removed, have a correlation distance of only approximately 14 km. (Fig. 41) CCSIII possessed old mixed layers that were more highly correlated than those

5 MISSING OBSERVATIONS

MIDDLE OF INTERVAL	NUMBER OF OBSERVATIONS	
0.	11	*****
10.	12	*****
20.	10	*****
30.	18	*****
40.	6	*****
50.	10	*****
60.	9	*****
70.	15	*****
80.	9	*****

13 MISSING OBSERVATIONS

MIDDLE OF INTERVAL	NUMBER OF OBSERVATIONS	
0.	10	*****
10.	31	*****
15.	12	*****
20.	20	*****
25.	5	*****
30.	4	*****
35.	1	*
40.	0	
45.	0	
50.	1	*

7 MISSING OBSERVATIONS

MIDDLE OF INTERVAL	NUMBER OF OBSERVATIONS	
0.	9	*****
10.	28	*****
15.	19	*****
20.	18	*****
25.	12	*****
30.	5	*****
35.	1	*
40.	1	*
45.	0	
50.	1	*

Figure 38. Histograms of NMLD (meters) for CCSI, CCSII, and CCSIII.

5 MISSING OBSERVATIONS

MIDDLE OF INTERVAL	NUMBER OF OBSERVATIONS	
25.	1	*
30.	1	*
35.	1	*
40.	1	*
45.	2	**
50.	8	*****
55.	7	*****
60.	25	*****
65.	14	*****
70.	15	*****
75.	8	*****
80.	13	*****
85.	1	*
90.	2	**
95.	1	*

5 MISSING OBSERVATIONS

MIDDLE OF INTERVAL	NUMBER OF OBSERVATIONS	
5.	1	*
10.	3	**
15.	4	****
20.	2	**
25.	5	*****
30.	21	*****
35.	9	*****
40.	13	*****
45.	10	*****
50.	14	*****
55.	3	***
60.	5	*****
65.	1	*
70.	1	*

2 MISSING OBSERVATIONS

MIDDLE OF INTERVAL	NUMBER OF OBSERVATIONS	
10.	6	*****
15.	4	****
20.	21	*****
25.	18	*****
30.	19	*****
35.	7	*****
40.	9	*****
45.	5	*****
50.	5	*****
55.	0	
60.	4	****
65.	1	*

Figure 39. Histograms Of OMLD (meters) for CCSI, CCSII, and CCSIII.

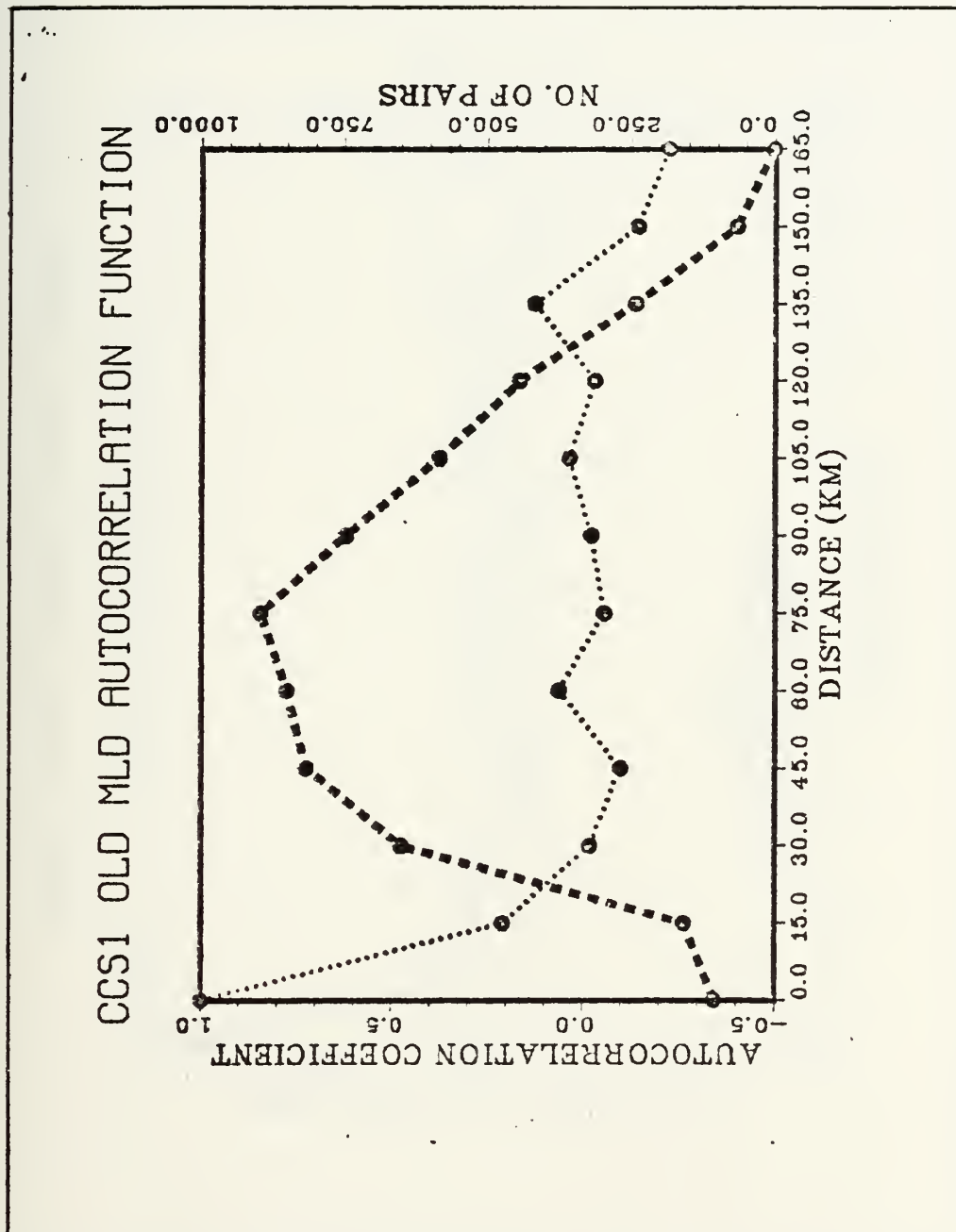


Figure 40. Autocorrelation function for CCS1 old mixed layer depth

MLD2 AUTOCORRELATION FCNS

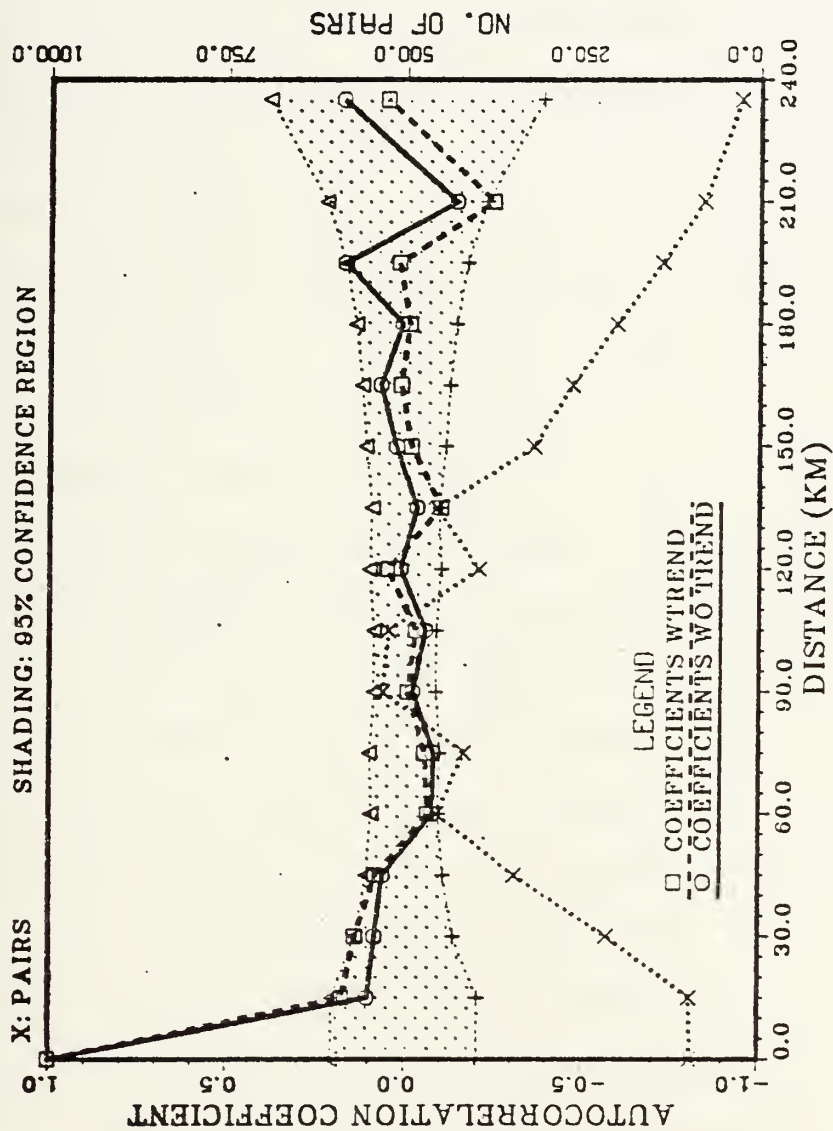


Figure 41. Autocorrelation function for CCSII old mixed layer depth

previously examined. (Fig. 42) The correlation distance for the detrended data was approximately 35 km; without the trend removed the correlation distance was approximately 50 km. The increase in the correlation distance from CCSII to CCSIII may be due to the fact that the former cruise covered a wider and more diversified domain than did the latter.

Contours of OMLD are included for CCSII and CCSIII to give an idea of the variability of mixed layers (a quasi-synoptic depiction), and to bring to light a common problem encountered in trying to contour 'real' data. The data must be placed on a regularly spaced grid prior to using contouring graphics packages. One would think the answer to the problem would be to merely interpolate the data to the new grid. Problems arise, however, from data set to data set depending on the noise or gradients in the data. Certain schemes seem to work well for some sets and not to work for others. The enclosed computer plotted contoured fields are the result of interpolation by trying to fit a five degree polynomial to the data. (Fig. 43) The results do not have much worth as seen when compared with the hand contours. (Fig. 44) Only the locations of some of the minimum/maximum centers are retained. In the future, the technique of optimal interpolation should be applied to the data for improved interpolated values and consequently, more appropriately smoothed contoured fields.

MLD3 AUTOCORRELATION FCNS

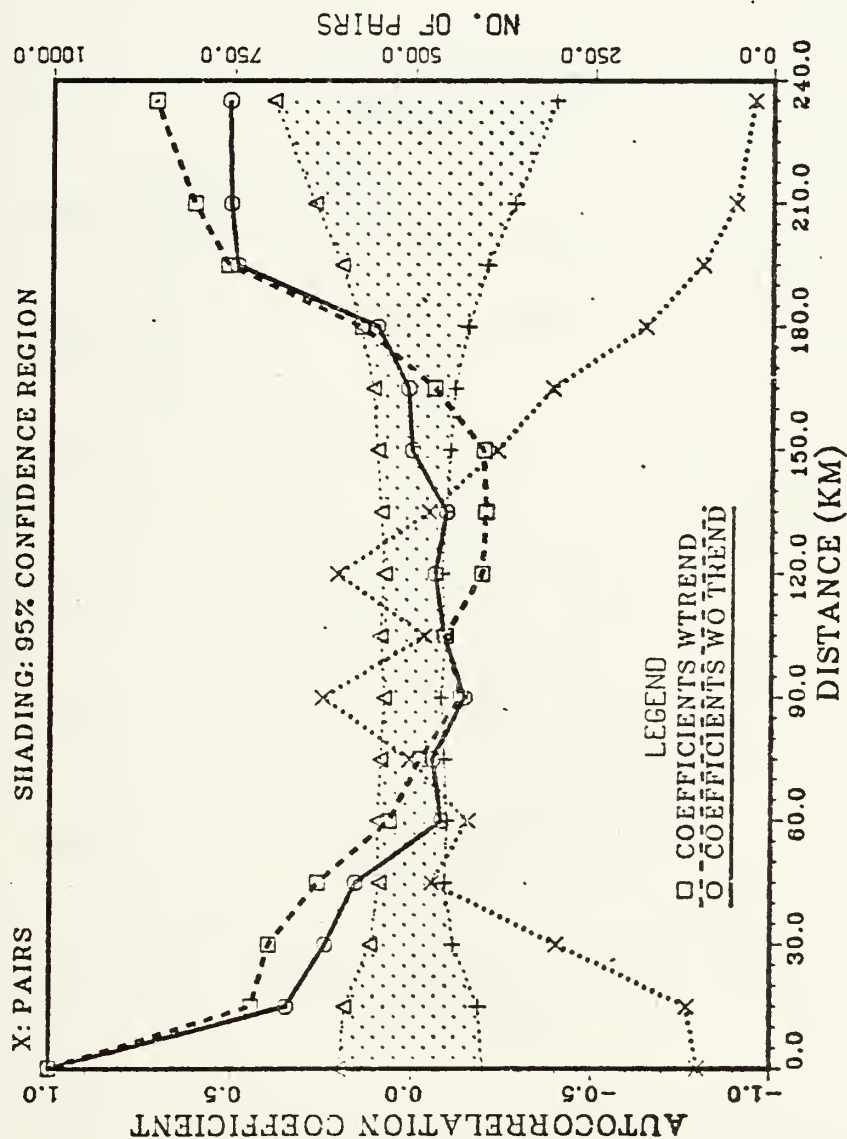


Figure 42. Autocorrelation function for CCSIII old mixed layer depth

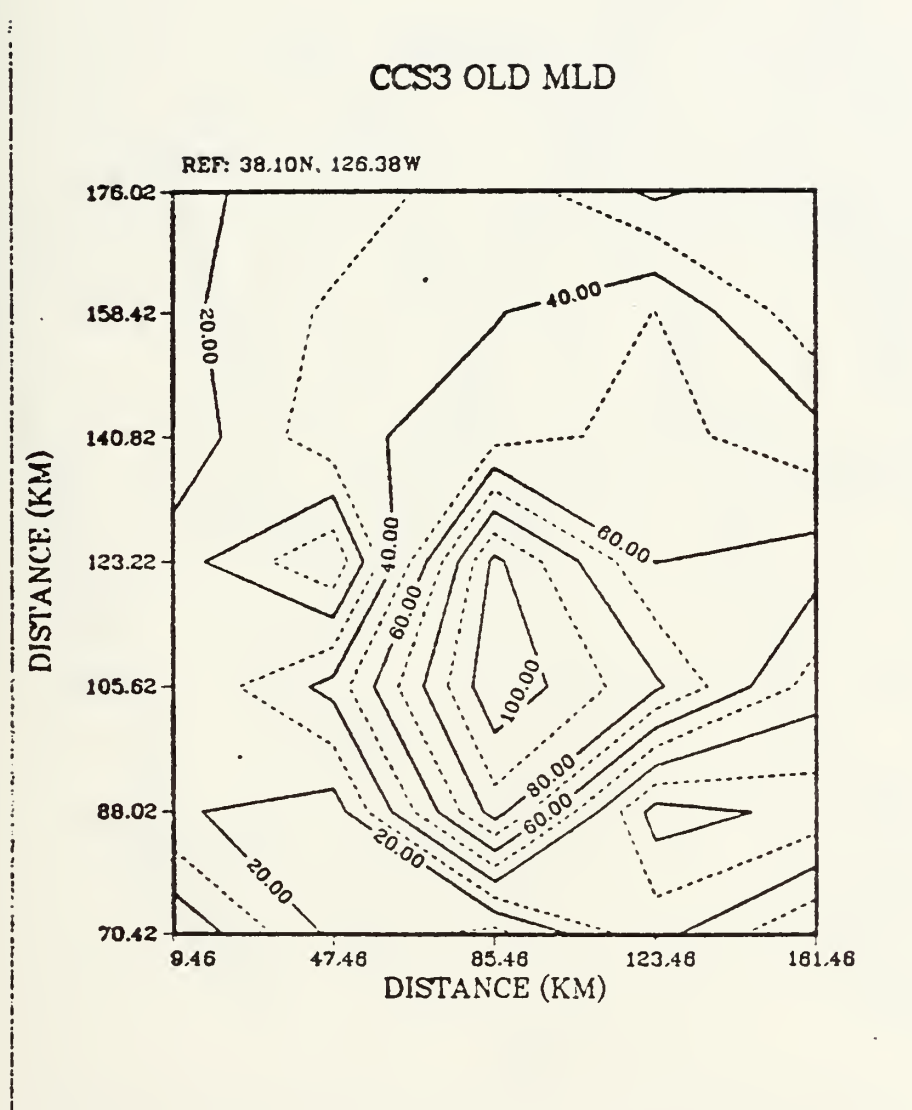


Figure 43. Computer contoured old mixed layer depths from CCSIII data were interpolated to a regular rotated grid and contoured; rotation origin: 37.33N, 126.25W; subplot origin: 38.10N, 126.38W

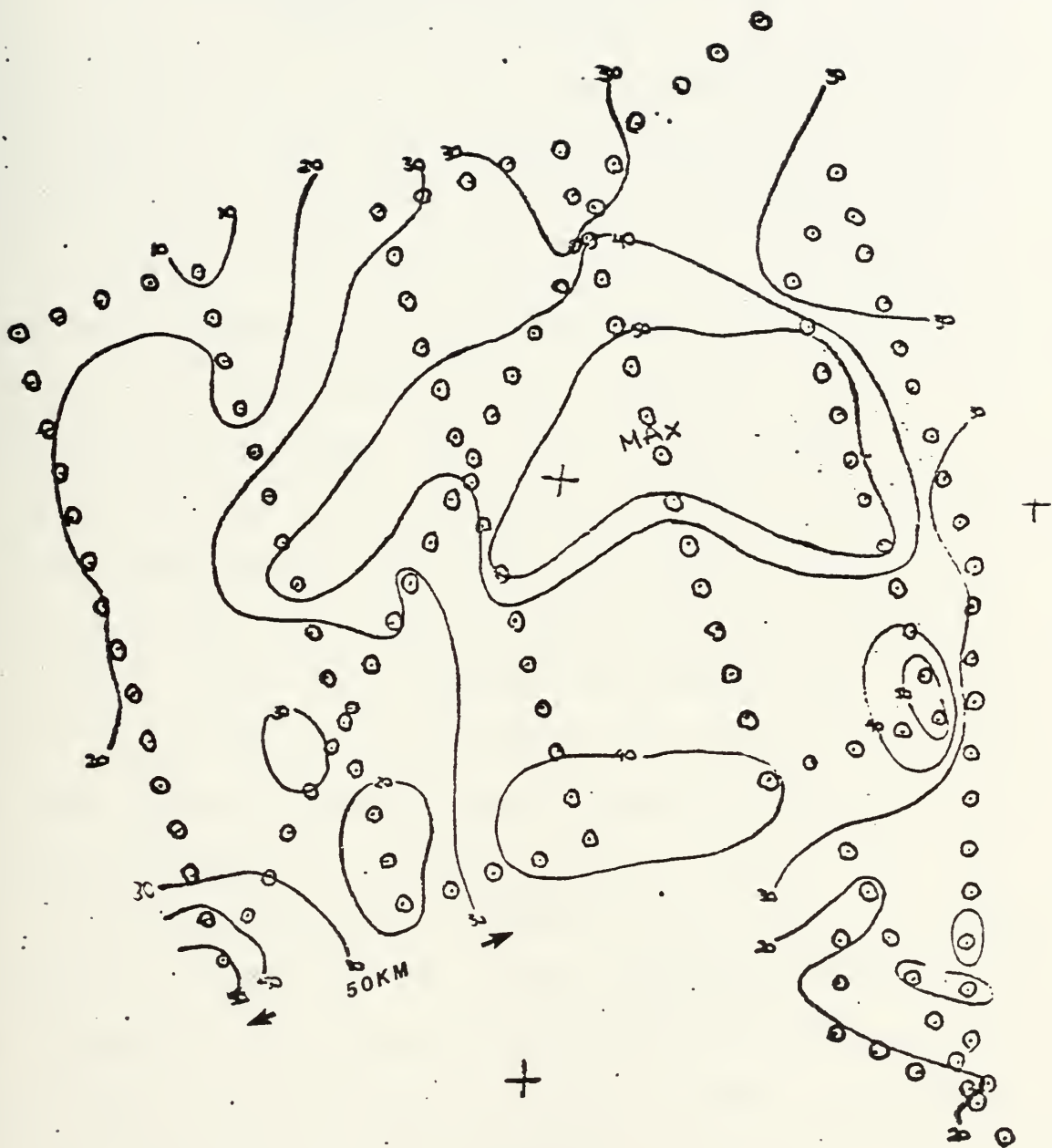


Figure 44. Hand contoured old mixed layer depths
(meters) from CCSIII

IV. ANALYSIS OF OBSERVED AND SIMULATED TEMPERATURE STRUCTURE

The first run was of the Garwood model initialized with the TOPS predicted profile for 1 August. The initial mixed layer depth was set at 20m, and the initial SST chosen was 17.7C (the SST of the TOPS analysis profile). The 24 daily profiles were averaged so as to produce one 'representative' profile per day. The average profiles along with their standard deviations compose Figs. 45-58. The standard deviation was nonzero only in the region at and/or above the base of the mixed layer, because the Garwood model does not alter regions below the furthest extent of the mixed layer base. For the 13-day cruise period, the Garwood model cooled the mixed layer by approximately two thirds of a degree, and deepened the mixed layer to approximately 37m. A substantial amount of entrainment occurred from 2 to 3 August, with the simultaneous increase in wind speed (7.8 m/s), and decrease in the SST at 00Z. Thus, there was increased forced convective activity due to increased wind stirring and increased free convection due to surface cooling. Significant mixing also occurred over the time spans; 7 to 8, 9 to 10, 12 to 13 August with some entrainment also occurring from 11 to 12 and 10 to 11 August, but not as pronounced as that during the previously stated times. Not much occurred during the other time spans.

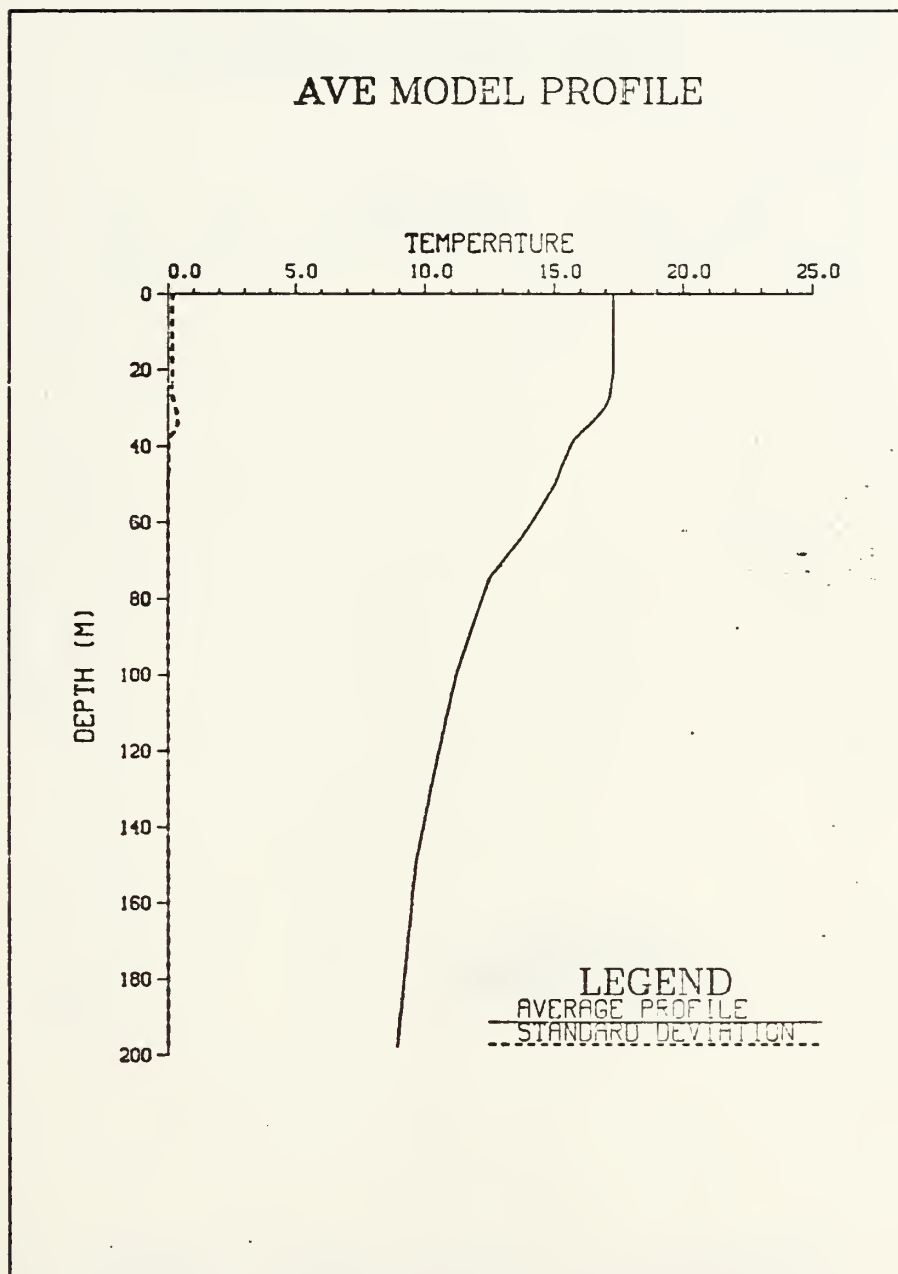


Figure 45. Overall average profile from Garwood model. (Temperature in degrees Celsius)

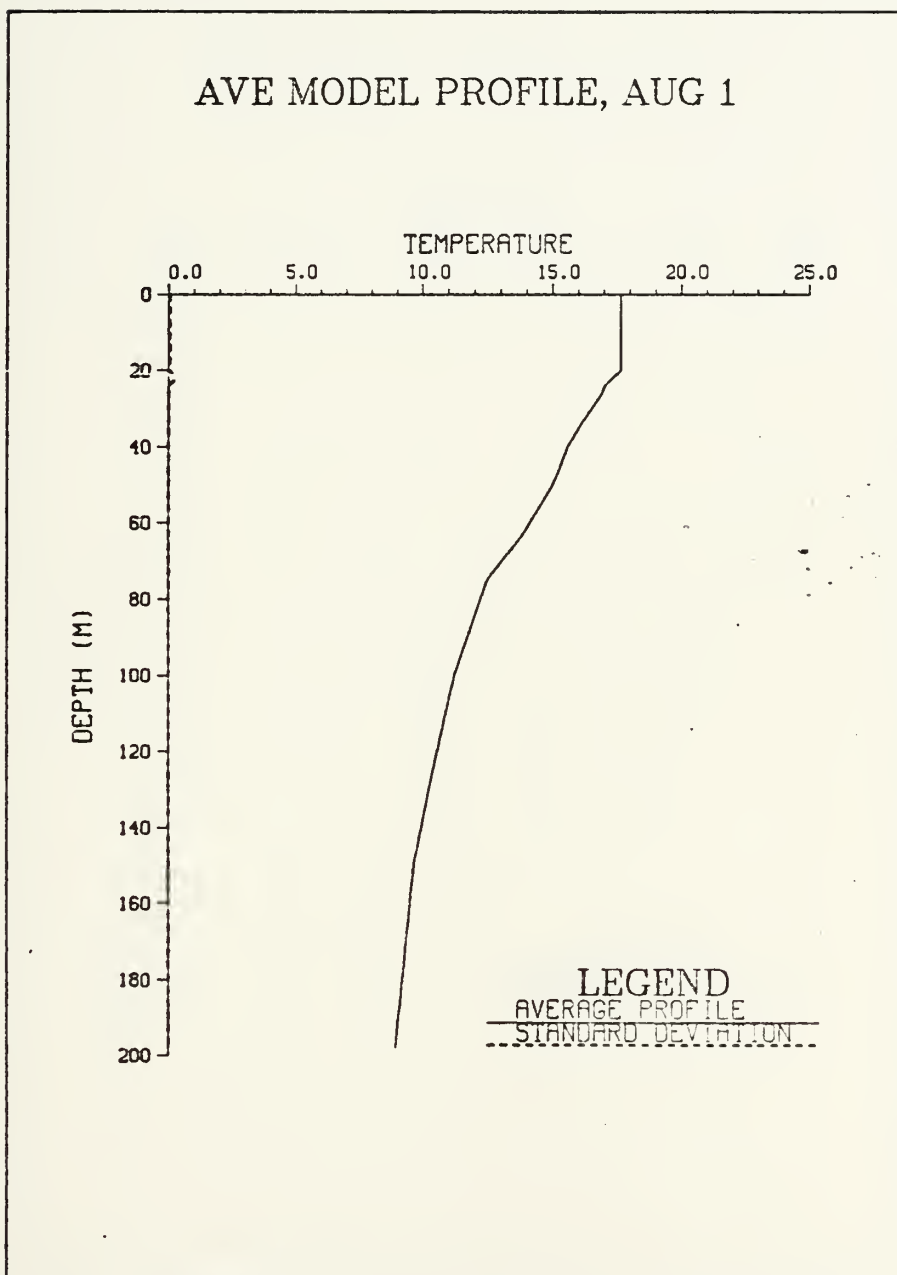


Figure 46. Average 1 August profile from Garwood model. (Temperature in degrees Celsius) Initialized with FNOC analyzed profile

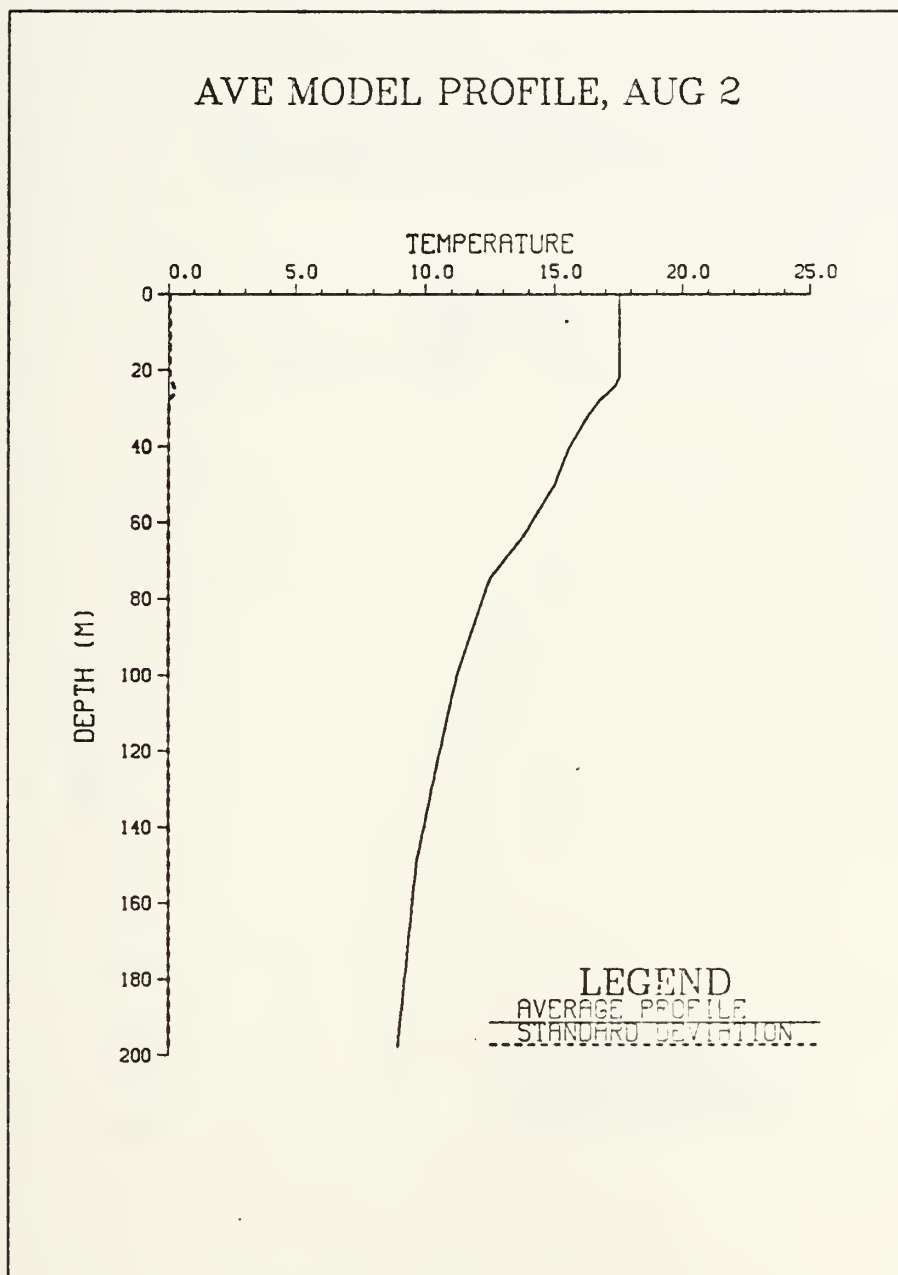


Figure 47. Average 2 August profile from Garwood model. Initialized with FNOC analyzed profile (Temperature in degrees Celsius)

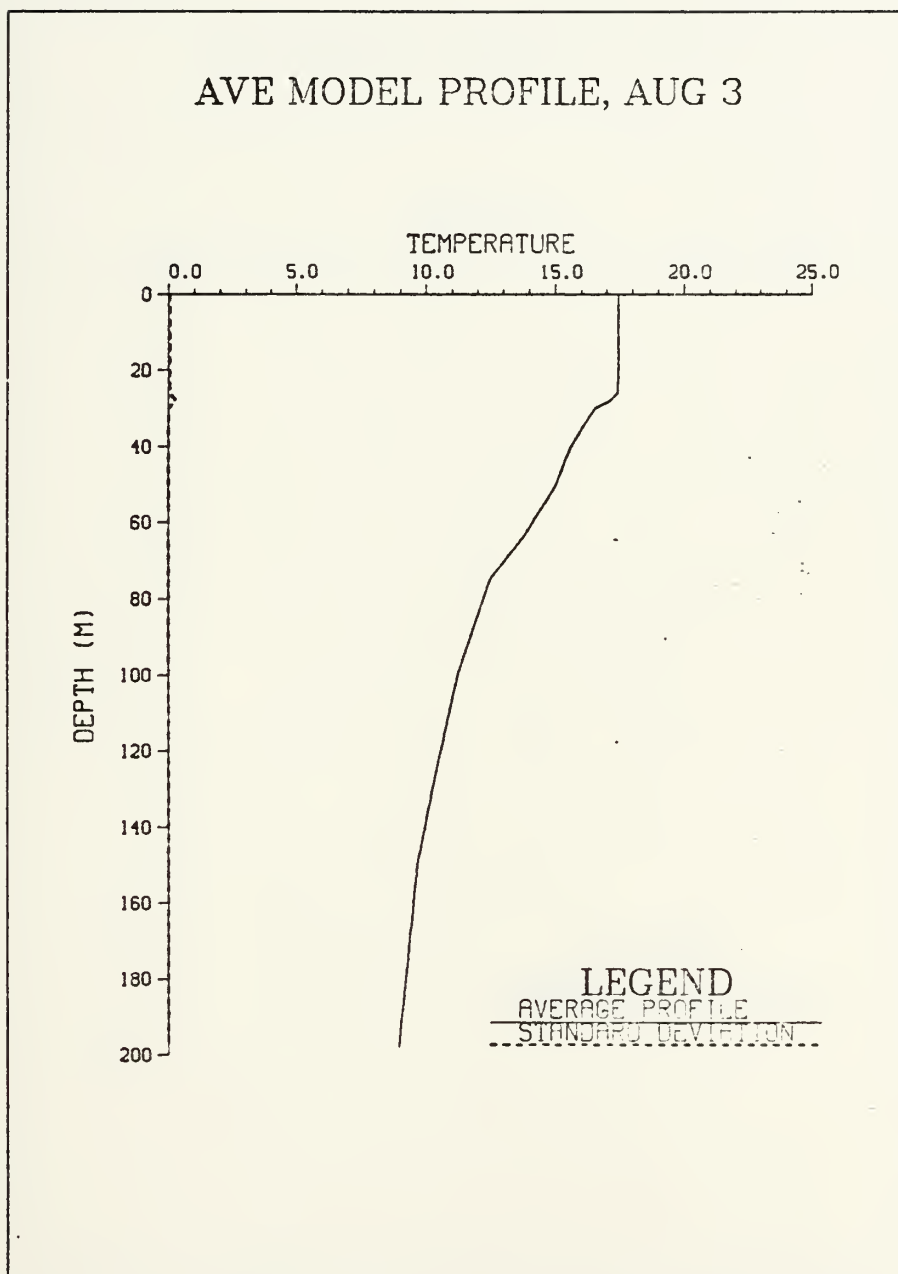


Figure 48. Average 3 August profile from Garwood model. Initialized with FNOC analyzed profile (Temperature in degrees Celsius)

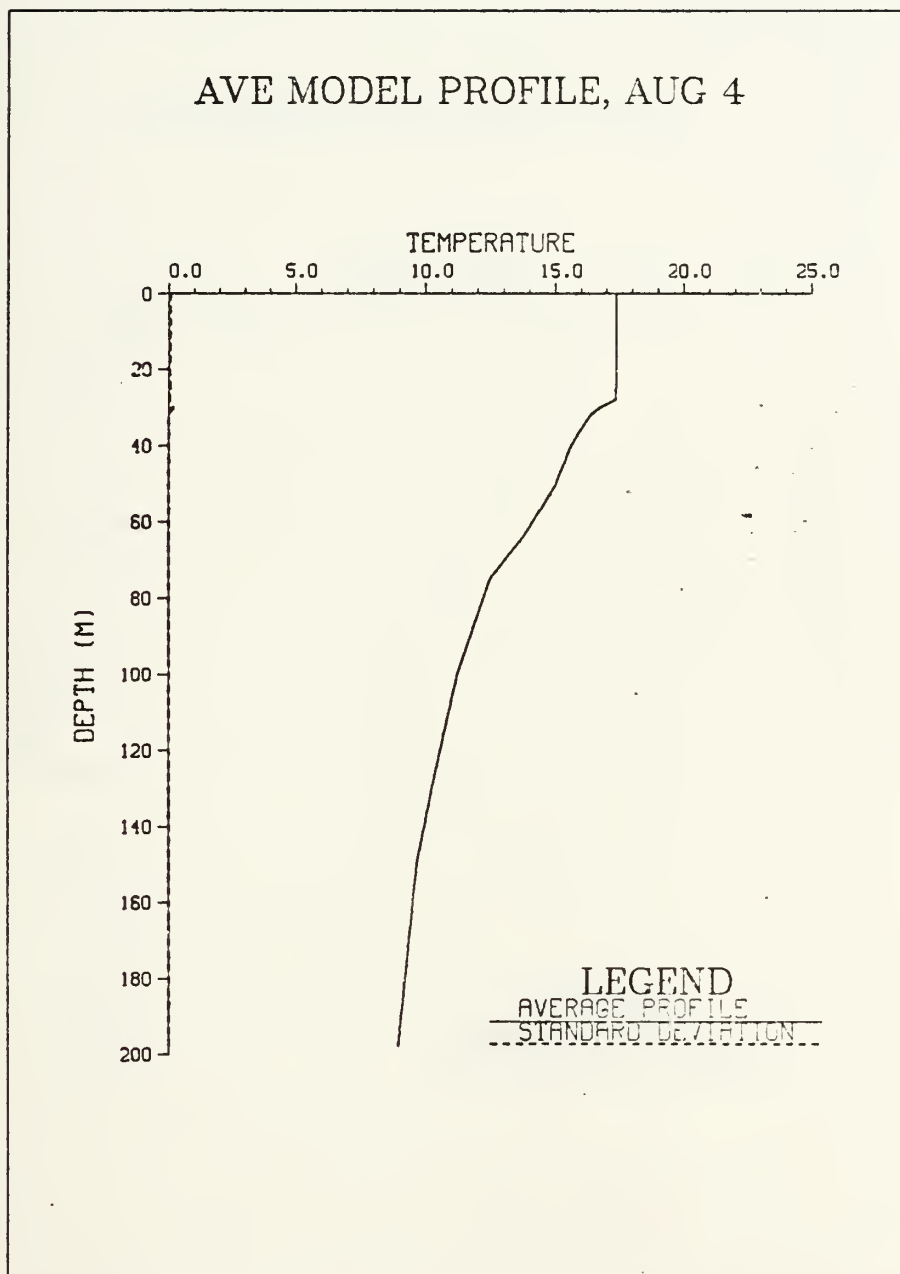


Figure 49. Average 4 August profile from Garwood model. Initialized with FNOG analyzed profile (Temperature in degrees Celsius)

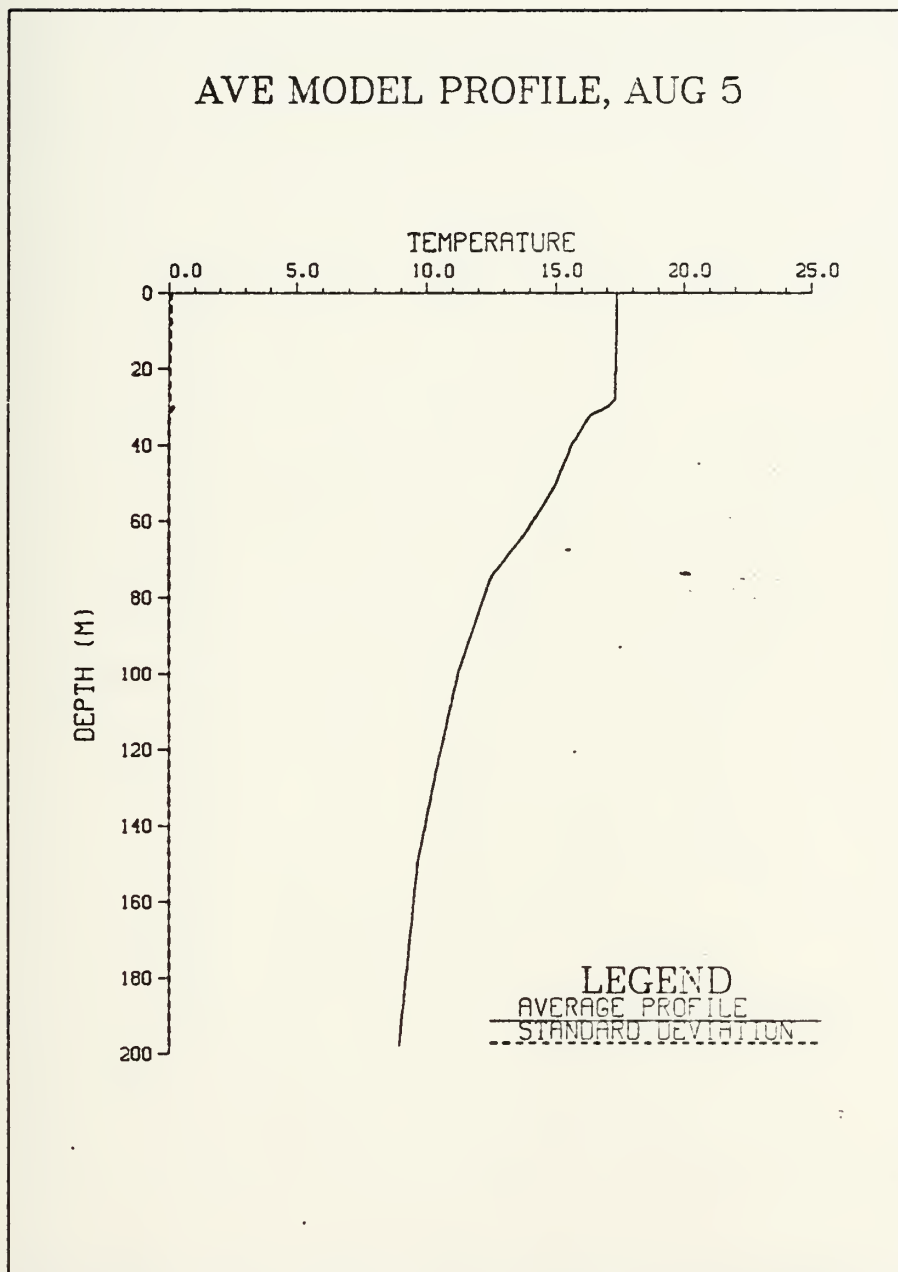


Figure 50. Average 5 August profile from Garwood model. Initialized with FNOC analyzed profile (Temperature in degrees Celsius)

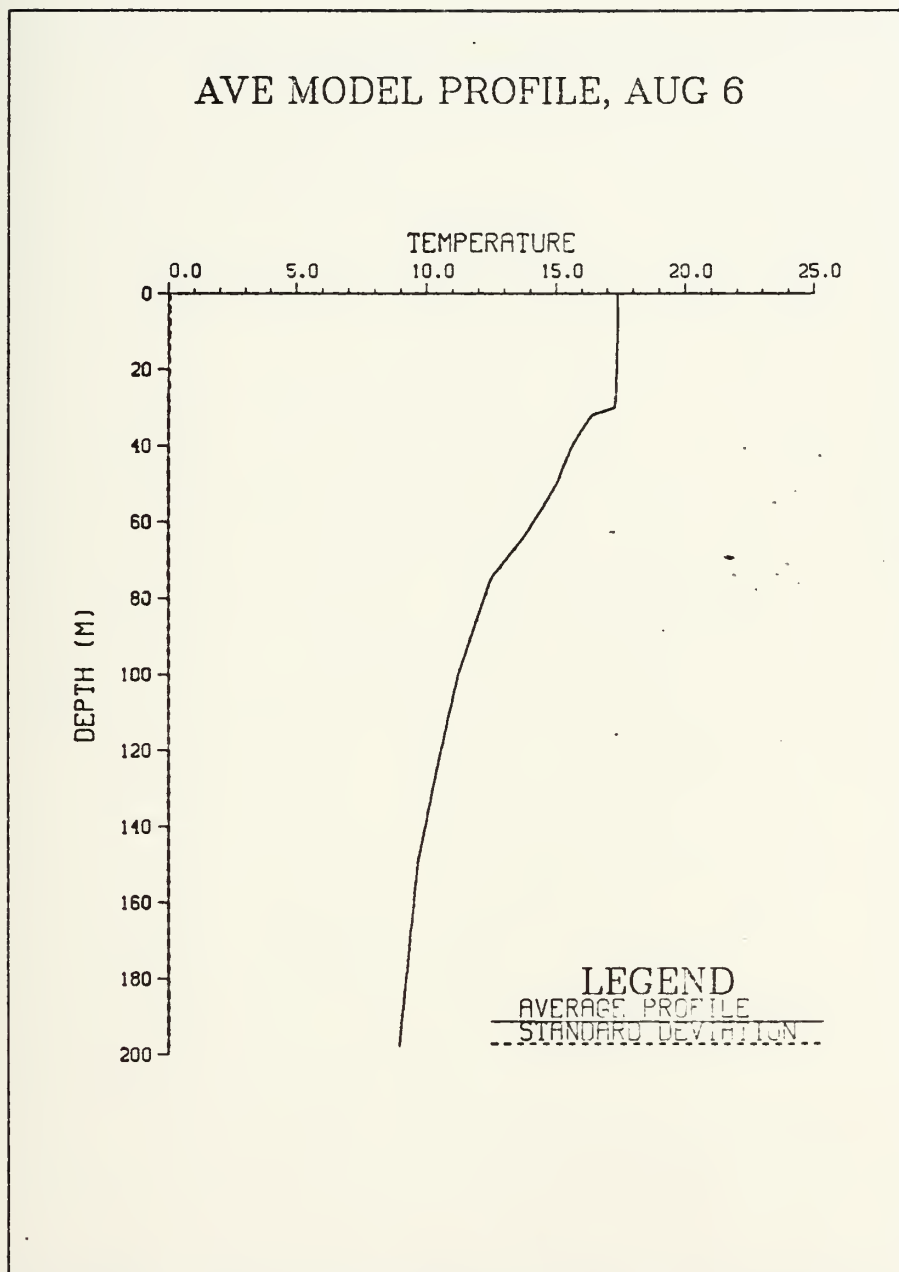


Figure 51. Average 6 August profile from Garwood model. Initialized with FNOC analyzed profile (Temperature in degrees Celsius)

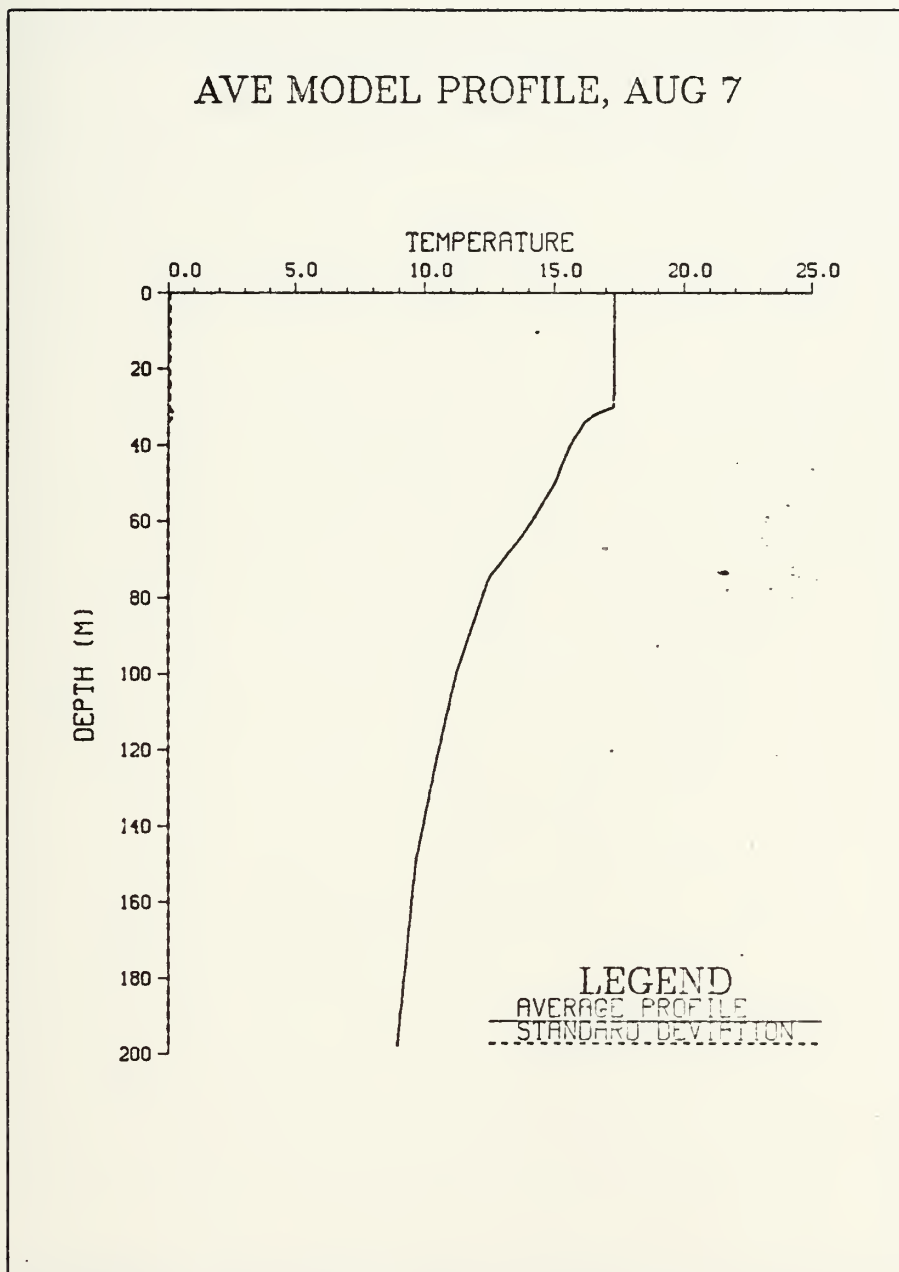


Figure 52. Average 7 August profile from Garwood model. Initialized with FNOC analyzed profile (Temperature in degrees Celsius)

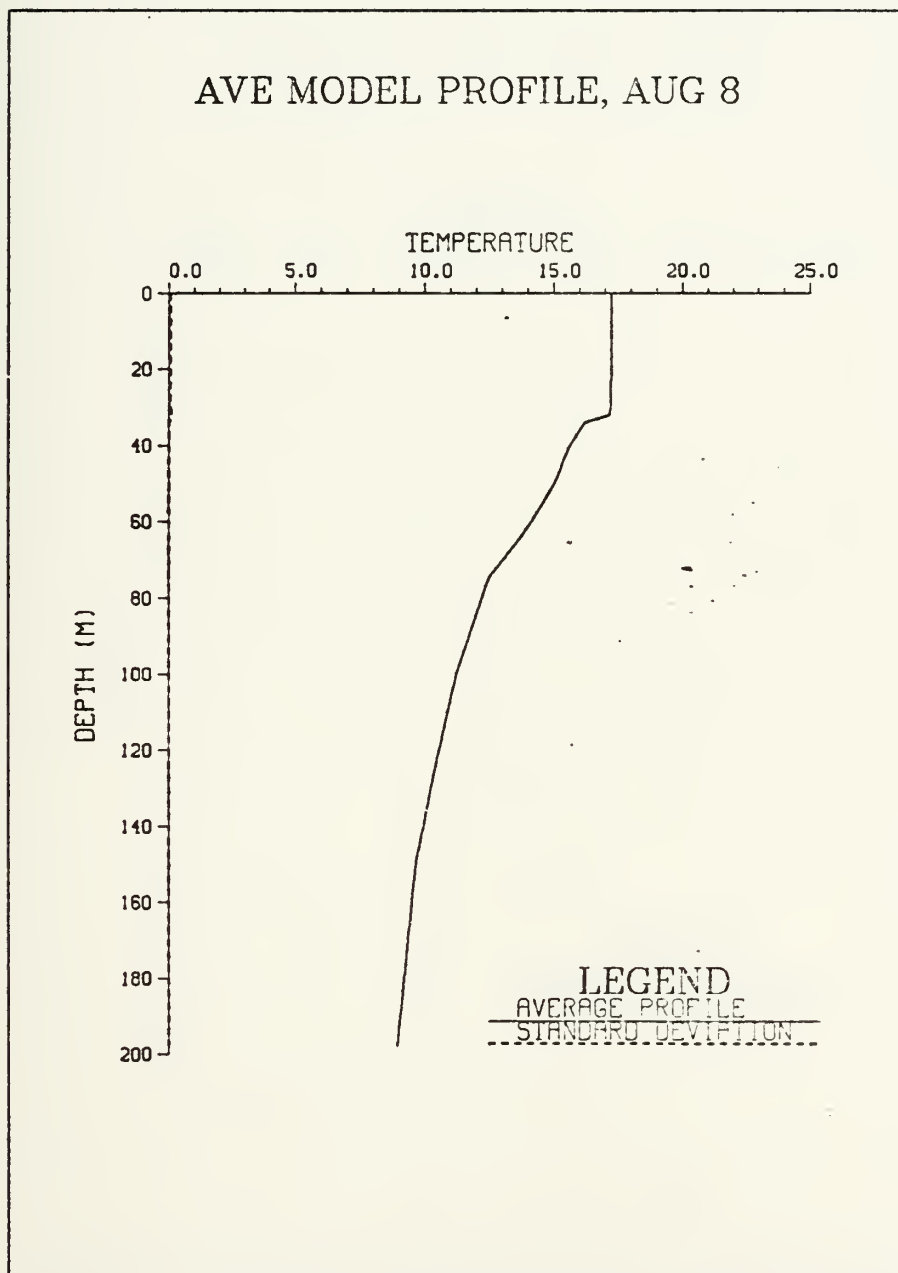


Figure 53. Average 8 August profile from Garwood model. Initialized with FNOC analyzed profile (Temperature in degrees Celsius)

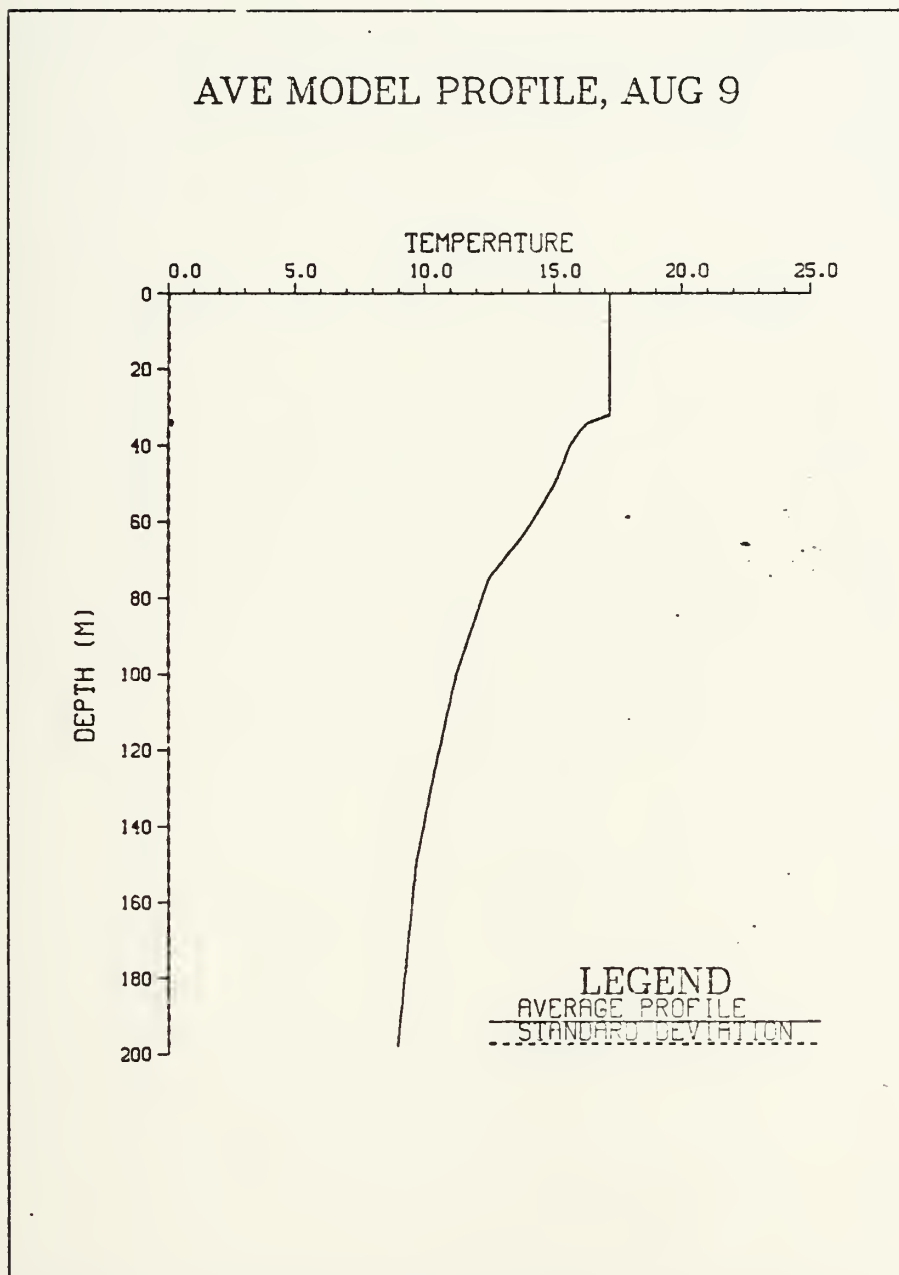


Figure 54. Average 9 August profile from Garwood model. Initialized with FNOC analyzed profile (Temperature in degrees Celsius)

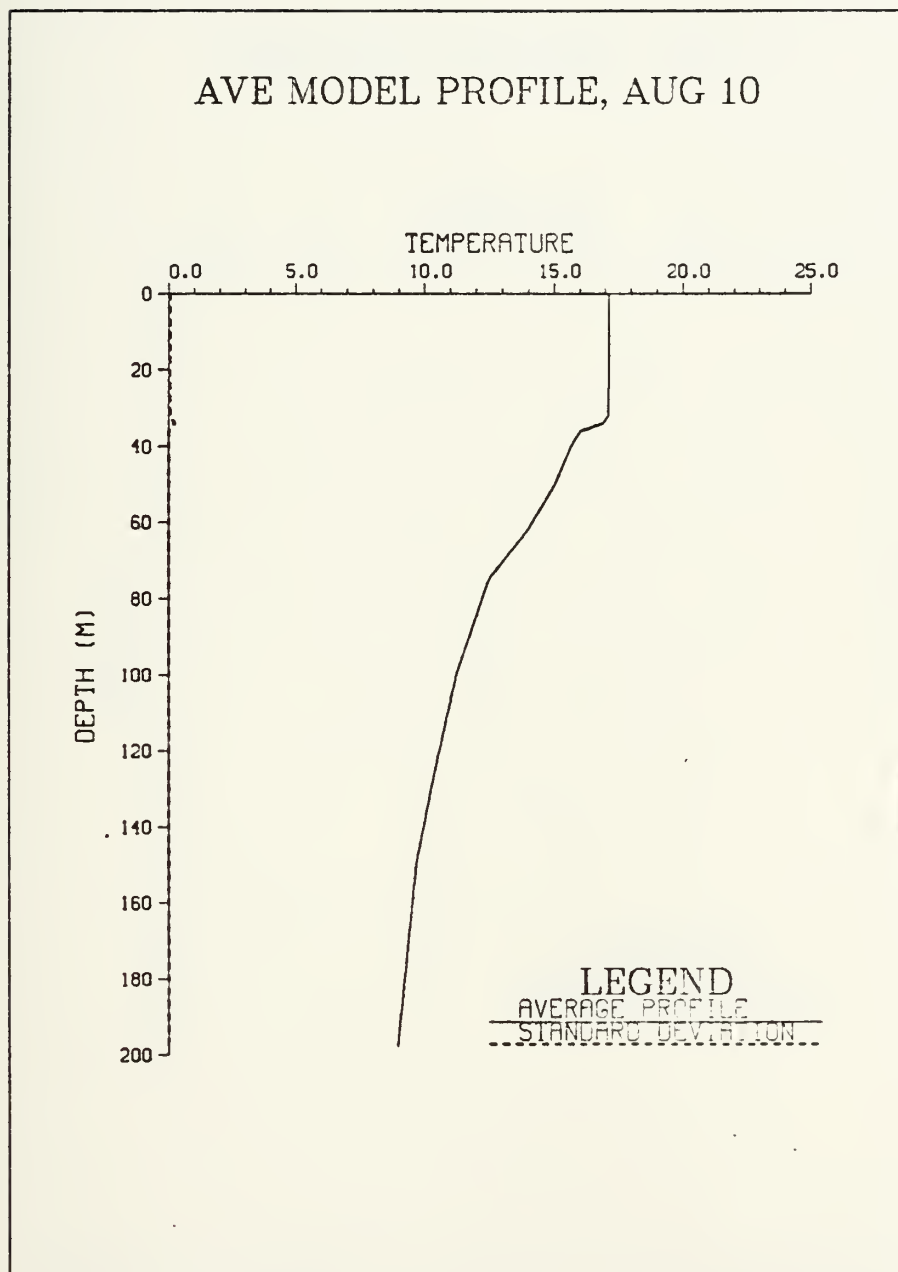


Figure 55. Average 10 August profile from Garwood model. Initialized with FNOC analyzed profile (Temperature in degrees Celsius)

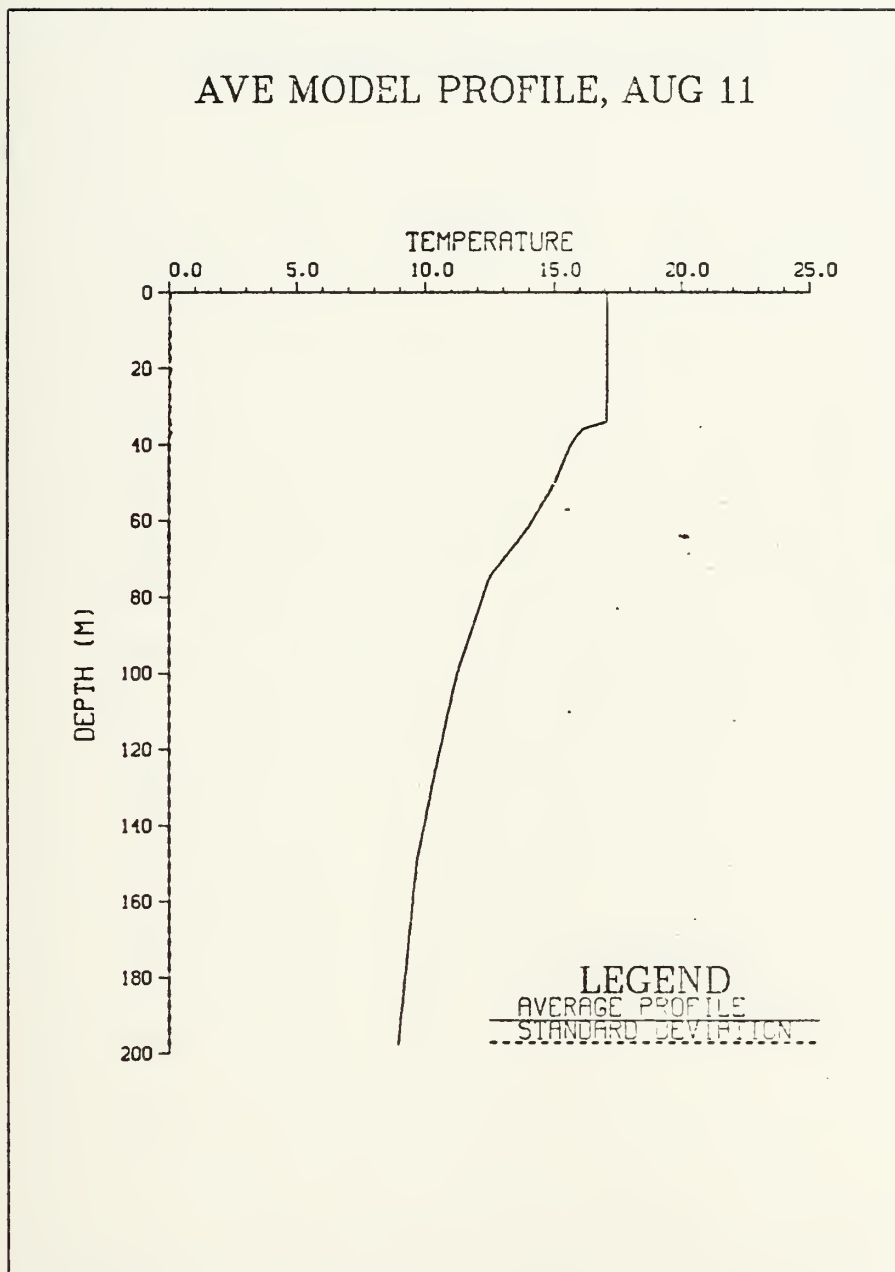


Figure 56. Average 11 August profile from Garwood model. Initialized with FNOC analyzed profile (Temperature in degrees Celsius)

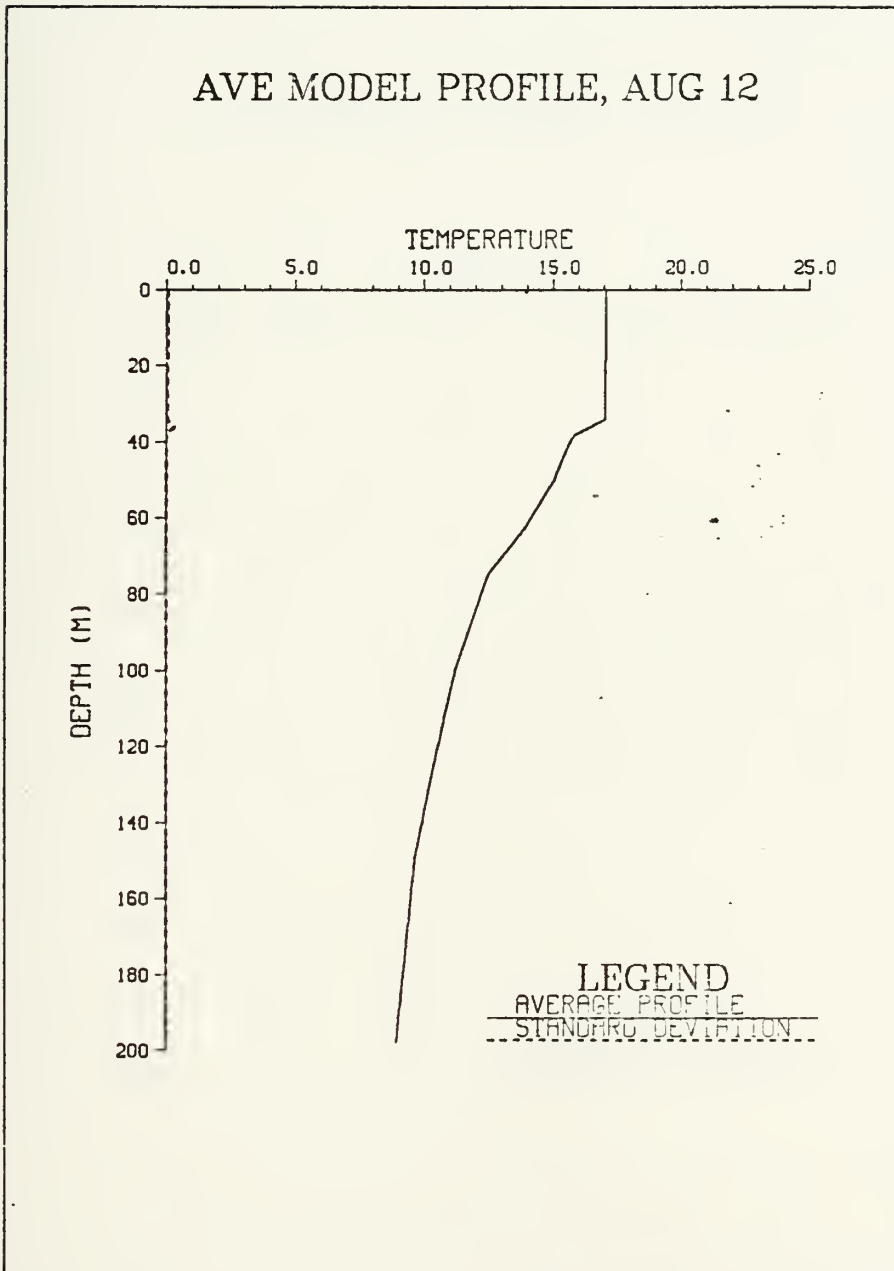


Figure 57. Average 12 August profile from Garwood model. Initialized with FNOC analyzed profile (Temperature in degrees Celsius)

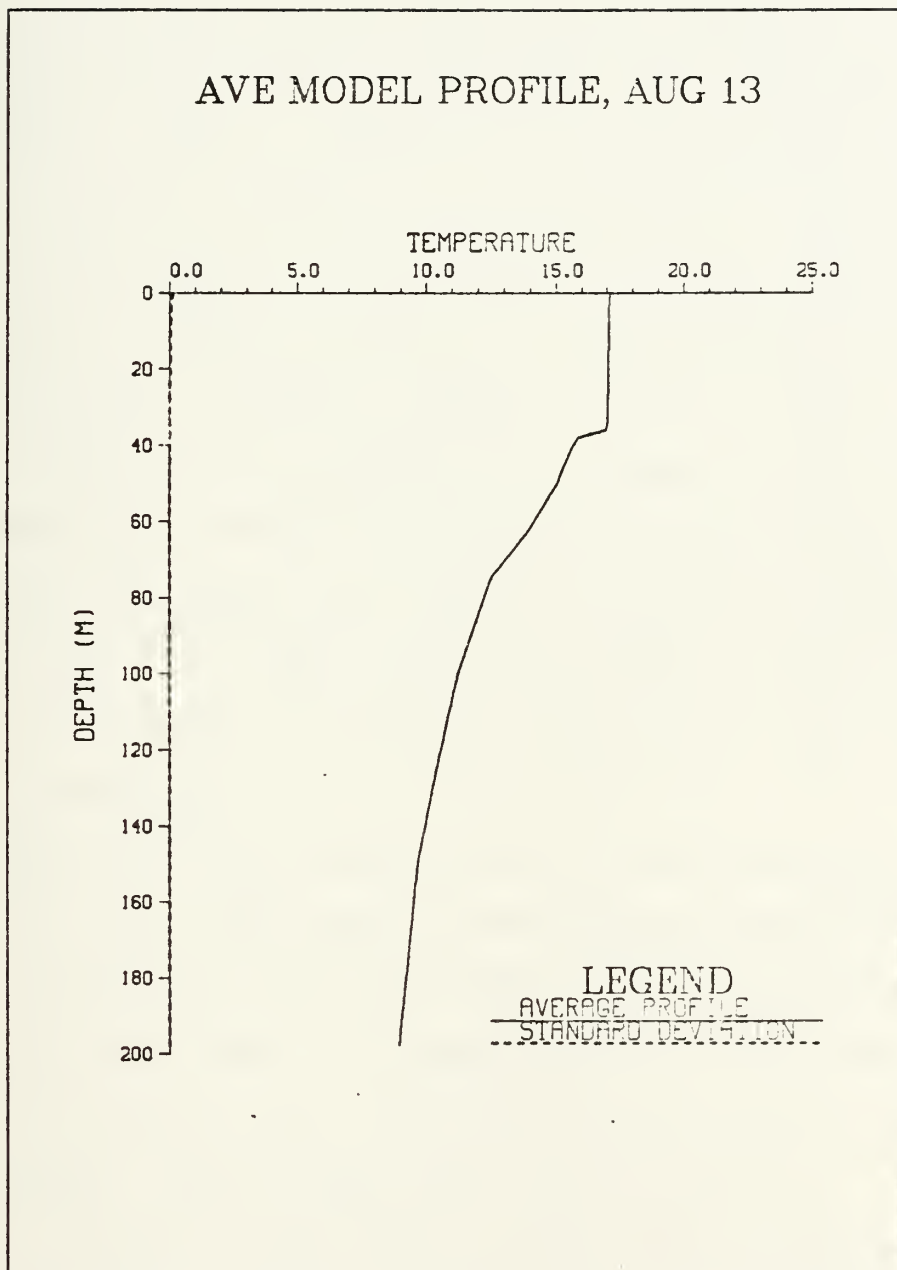


Figure 58. Average 13 August profile from Garwood model. Initialized with FNOC analyzed profile (Temperature in degrees Celsius)

The time-depth contours of temperature in Fig. 59 are another way of indicating the deepening and shoaling of the mixed layer depth. It is quite obvious that the depths below the mixed layer are not affected by the model.

The TOPS profiles, on the otherhand, are affected at all levels (down to 500m). The profiles are more complex and harder to interpret, because of the variations occurring over the entire profile. The process of energy addition/subtraction to the mixed layer is no longer as obvious as with a bulk model. Overall, changes over the 13 days, however, clearly show a substantial increase in the mixed layer temperature; the SST increased approximately one degree, while the mixed layer depth increased to approximately 40m. (Figs. 60, 61) (TOPS and TEOTS profiles for the other days may be found on the composite figures to be discussed in the last section.)

A comparison of the contours for the TOPS predicted profiles (Fig. 62) with those of the Garwood model gives further indications of the difference in results of the diffusion and the 'slab' or integral models. For these contours to resemble those obtained from the Garwood model, the mixed layers would indeed have to be 'slab-like'. (The 'plateaus' located in the center of the contour field are due to repeated profiles, i.e., profiles for 6 and 7 August were not obtained from FNOC.)

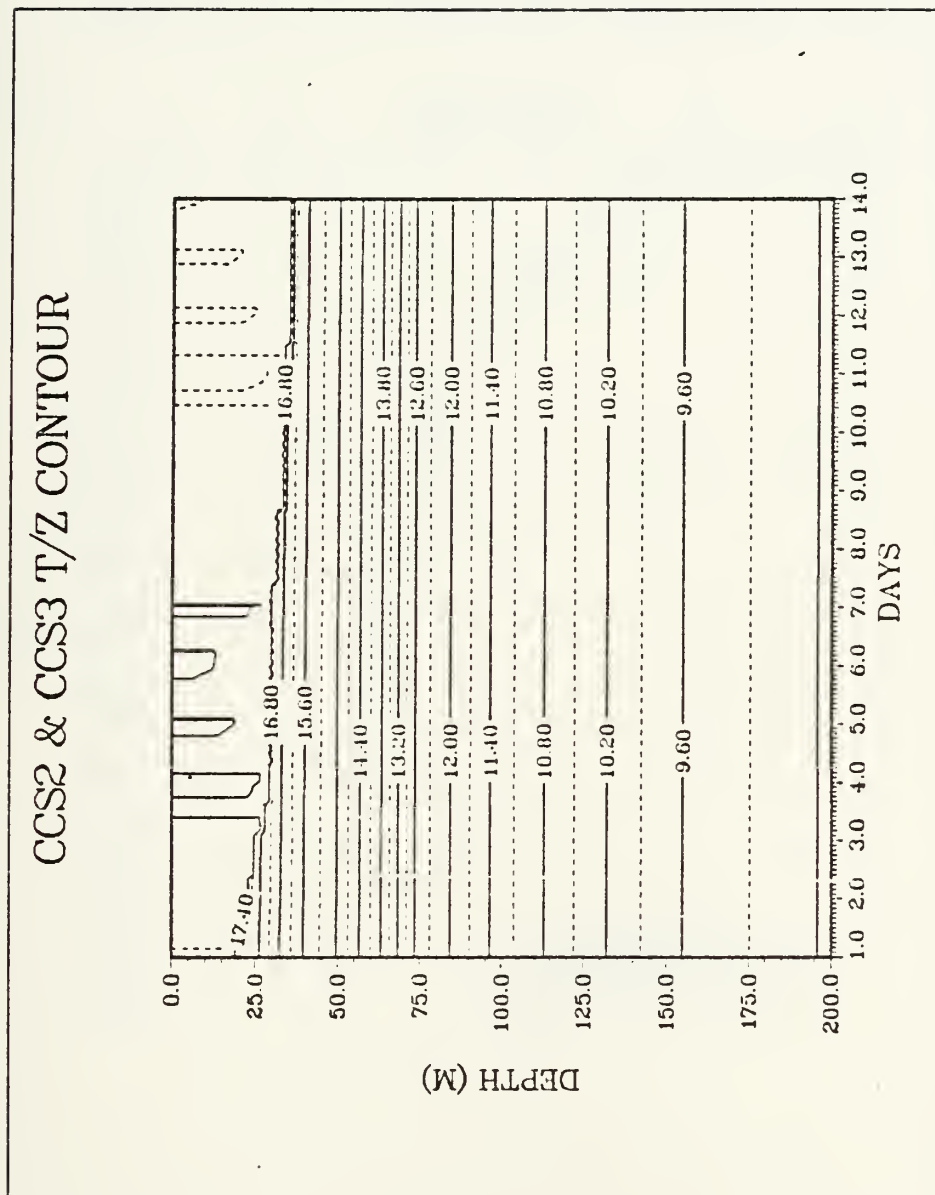


Figure 59. Contoured Garwood model simulated T/Z Field

FNOC TOPS&TEOTS PROFILES

39.1N, 127.7W:DATE-820801,00Z

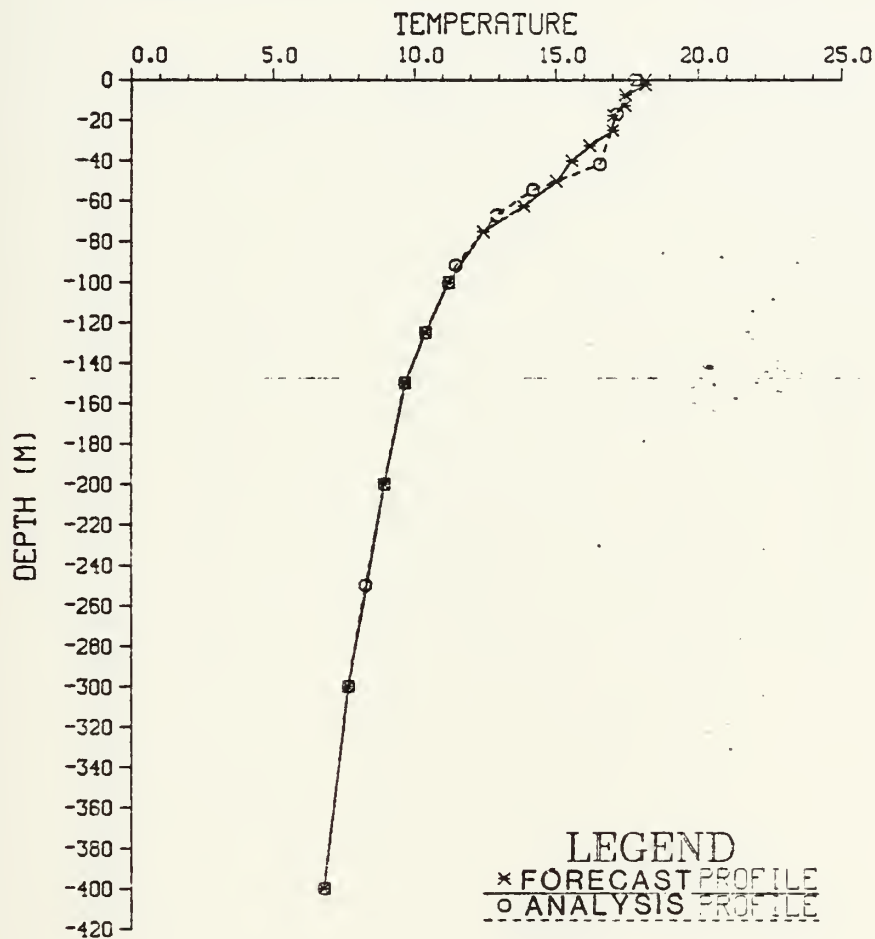


Figure 60. TOPS and TEOTS profiles for 1 August 1982. (Temperature in degrees Celsius)

FNOC TOPS&TEOTS PROFILES

39.1N, 127.7W:DATE-820813,00Z

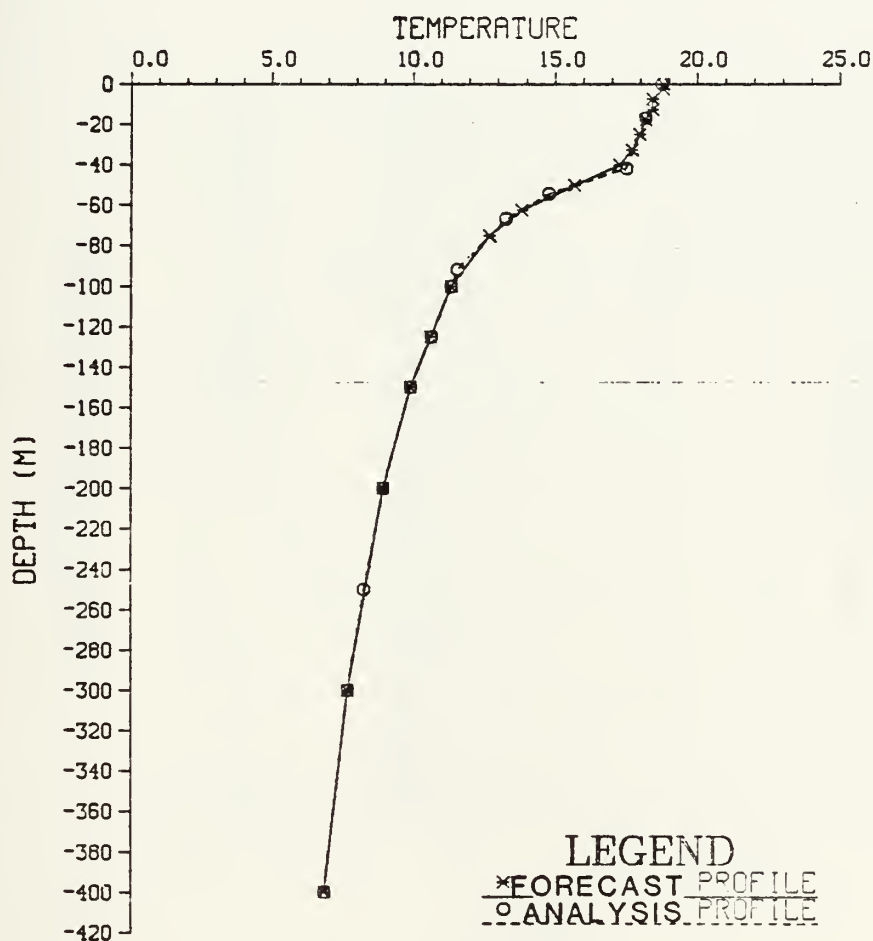


Figure 61. TOPS and TEOTS profiles for 13 August 1982 (Temperature in degrees Celsius)

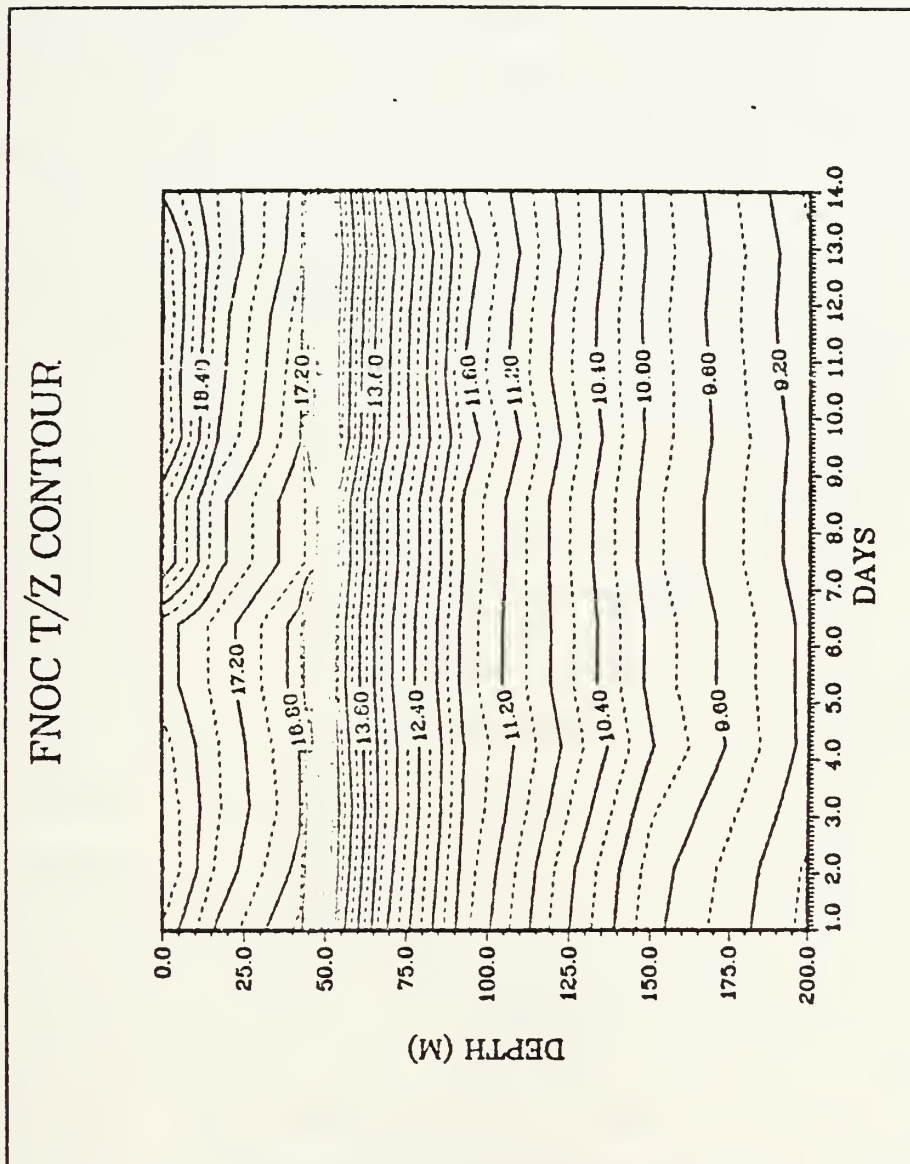


Figure 62. Contoured T/Z field composed of TOPS profiles

Both of these sets of profiles and contours were compared with those obtained from daily averaged XBT profiles. The variability of the upper water column as noted in the latter two sets of profiles was not as apparent in the series of averaged XBT profiles, as expected. The trend of the latter XBT's, averaged in space and time, had a tendency to wander quite a bit. For example, the SST from 1 August to 2 August jumped 1C with a corresponding increase of 0.3C at 400m. (Figs. 63, 64) Similar changes occurred for other profiles. For example, the 13 August profile indicated a -1.3C change in SST and a -0.7C change in the temperature at 400m since 12 August. (Figs. 65, 66) (Average XBT profiles for the other days may be found on the composite figures to be discussed in the last section.) Mixed layers and their temporal variations are not well represented by these profiles due to the spatial heterogeneity within the study domain. It takes a stretch of the imagination to identify a mixed layer in some of the profiles. Once identified, the mixed layers do not tend to exhibit the characteristics expected for mixed layer evolution, e.g., the deeper layers are not necessarily cooler. The characteristics seem to be more of a 'random' nature, i.e. they are affected by factors other than those of mixing and heating.

The use of average XBT profiles is somewhat of a controversial issue. One side holds that the averaging of XBT's has some worth in that it will cancel some of the spatial

AVE XBT PROFILE, AUG 1

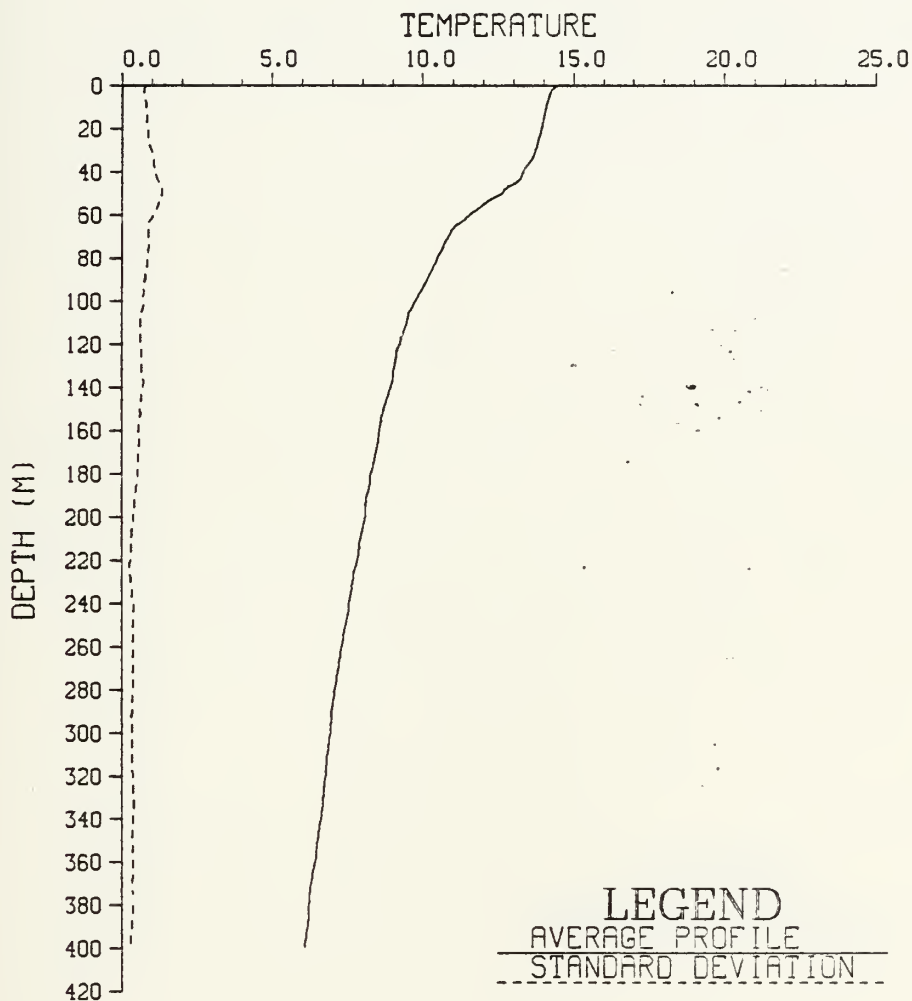


Figure 63. Average XBT and standard deviation plot for 1 August 1982. (Temperature in degrees Celsius)

AVE XBT PROFILE, AUG 2

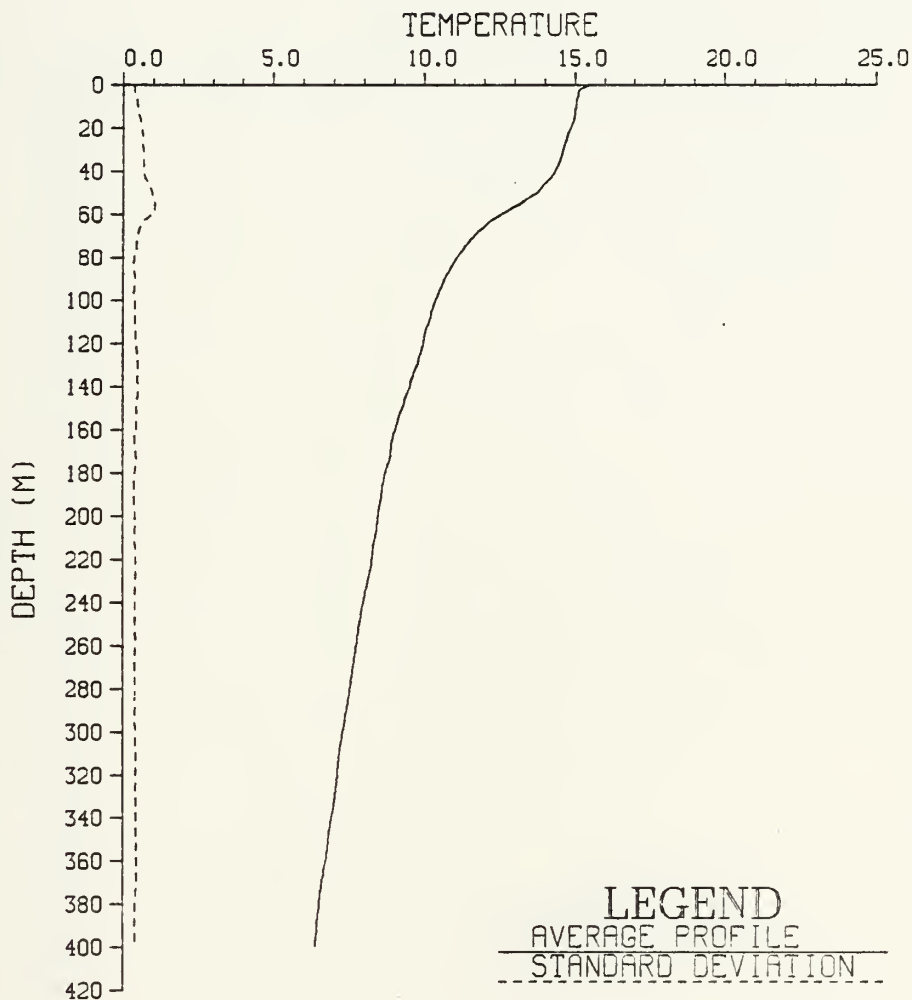


Figure 64. Average XBT and standard deviation plot for 2 August 1982. (Temperature in degrees Celsius)

AVE XBT PROFILE, AUG 12

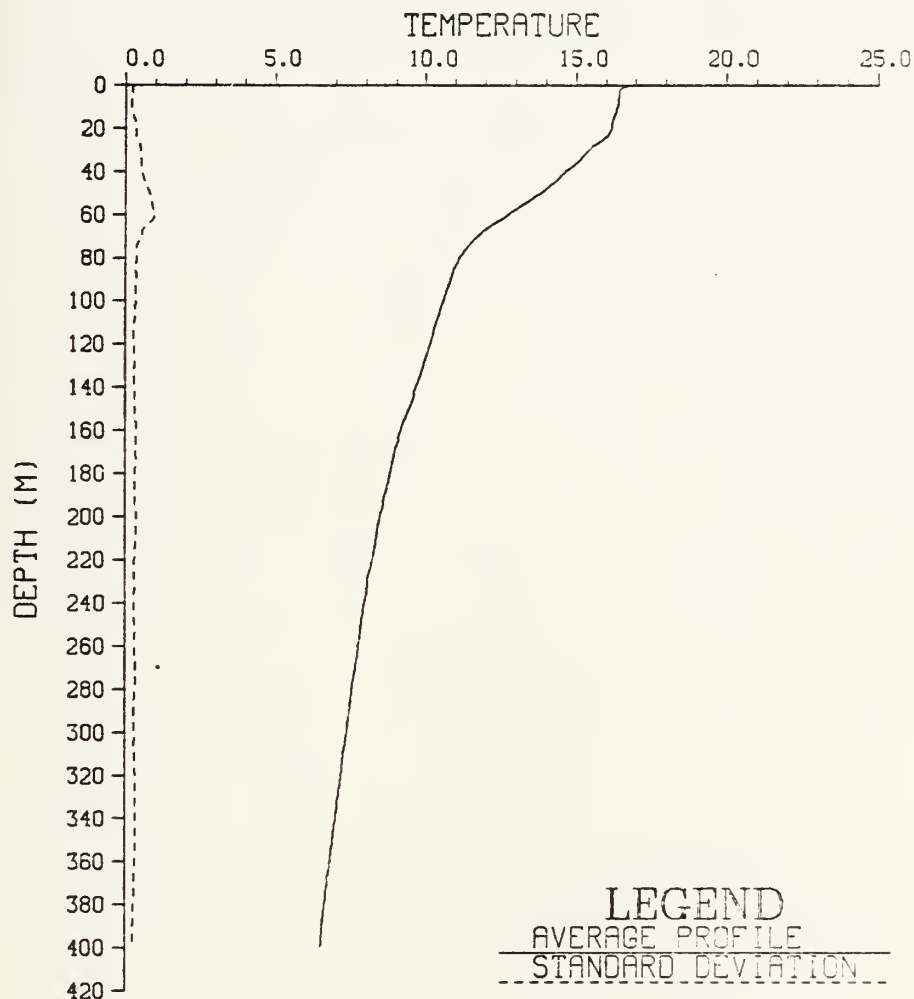


Figure 65. Average XBT and standard deviation plot for 12 August 1982. (Temperature in degrees Celsius)

AVE XBT PROFILE, AUG 13

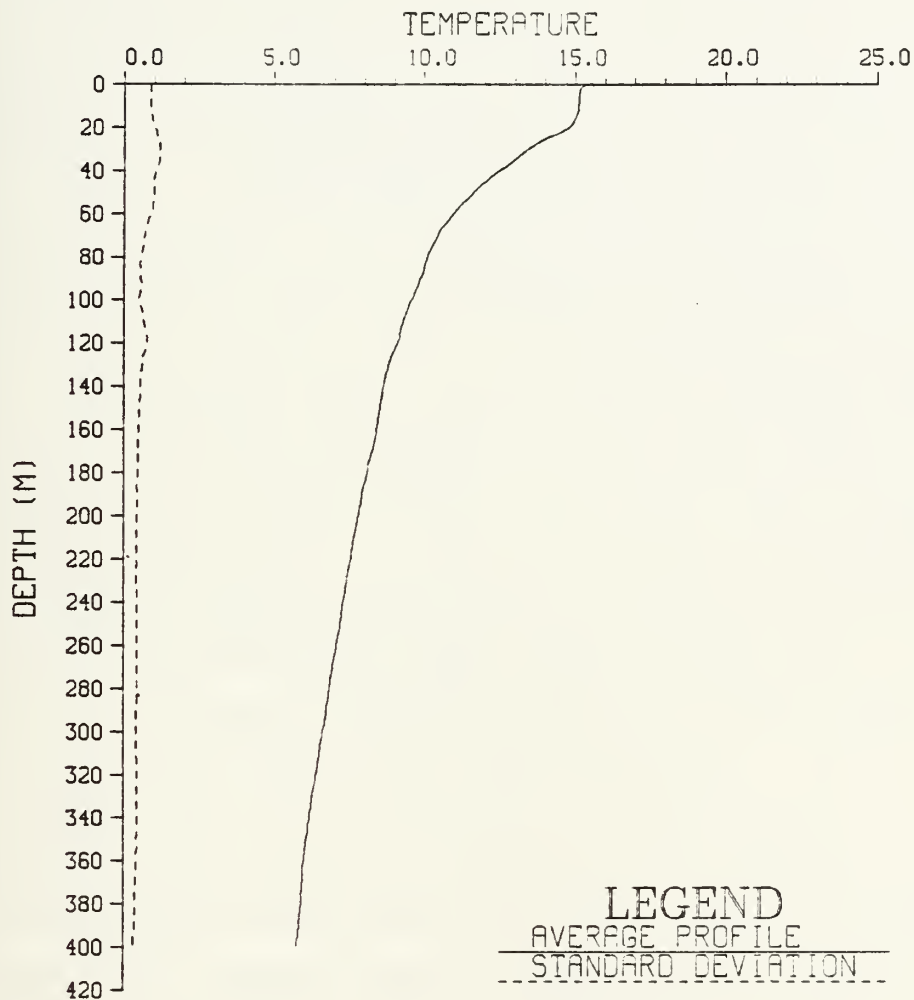


Figure 66. Average XBT and standard deviation plot for 13 August 1982. (Temperature in degrees Celsius)

and temporal effects. The other contends that the averaging of XBT's destroys the vertical structure, and, therefore, should not be the method by which one obtains a single daily profile with which to compare the model simulations. The latter believes that a median XBT (based on various criteria) would be a much better 'measuring stick' for model simulation success. Having gone through the abundant supply of XBT traces, comparing the averaged profiles with the series, the author is convinced of the latter viewpoint, though not contradicting that of the former. The corollary, then, is that the thermal structure is not robust over modest distances of a day's transit in a slow ship (ca. 3ms^{-1}). It is also suggested that greater care should be taken in grouping the XBT profiles in space-time for analysis. Indicated on the righthand panels in Figs. 67 and 68 are a series of hypothetical XBT traces for two cases: one containing XBT's with pronounced jumps at the mixed layer bases, and the other containing XBT's with gradually sloping mixed layers. The lefthand panel of each figure depicts the average XBT trace for the series, as well as a median XBT. (The average profile is the shallower of the two.) From these it can be seen that averaging distorts the vertical structure, making the mixed layer depth shallower, and the temperature at the base of the mixed layer colder.

Median XBT profiles were almost as hard to define as were the mixed layer depths, especially over a substantial

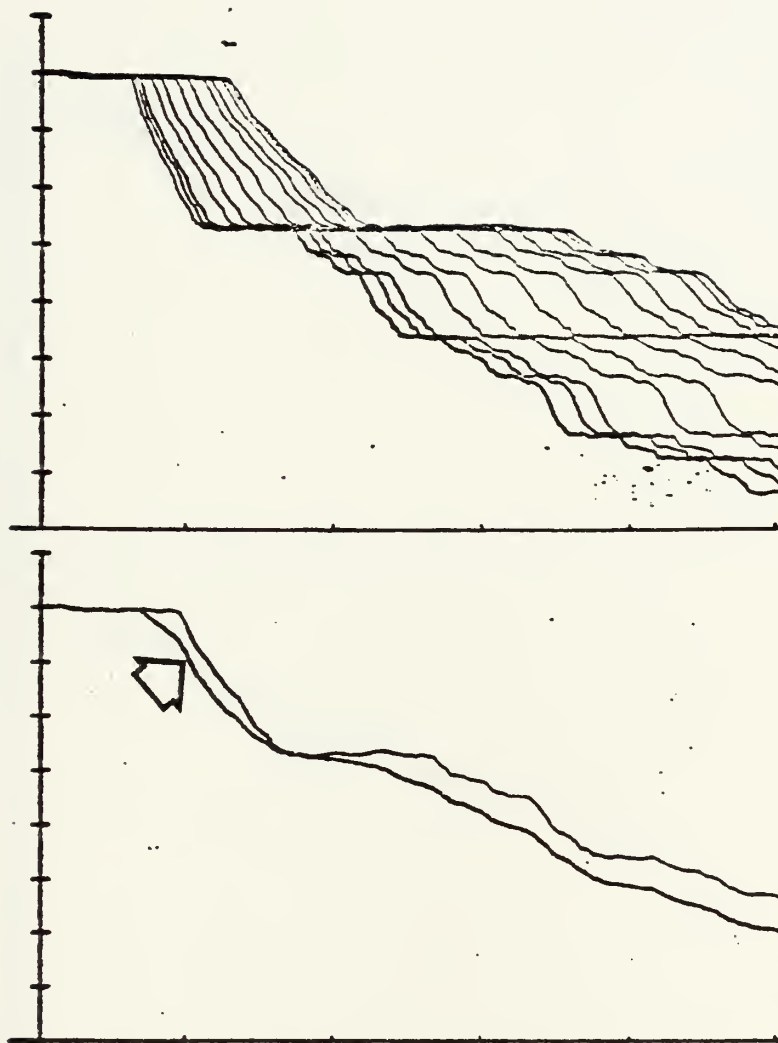


Figure 67. Averaging XBT's with steep thermoclines A) Right panel: XBT's to be averaged; B) Left panel: Average (indicated by arrow) and median XBT's

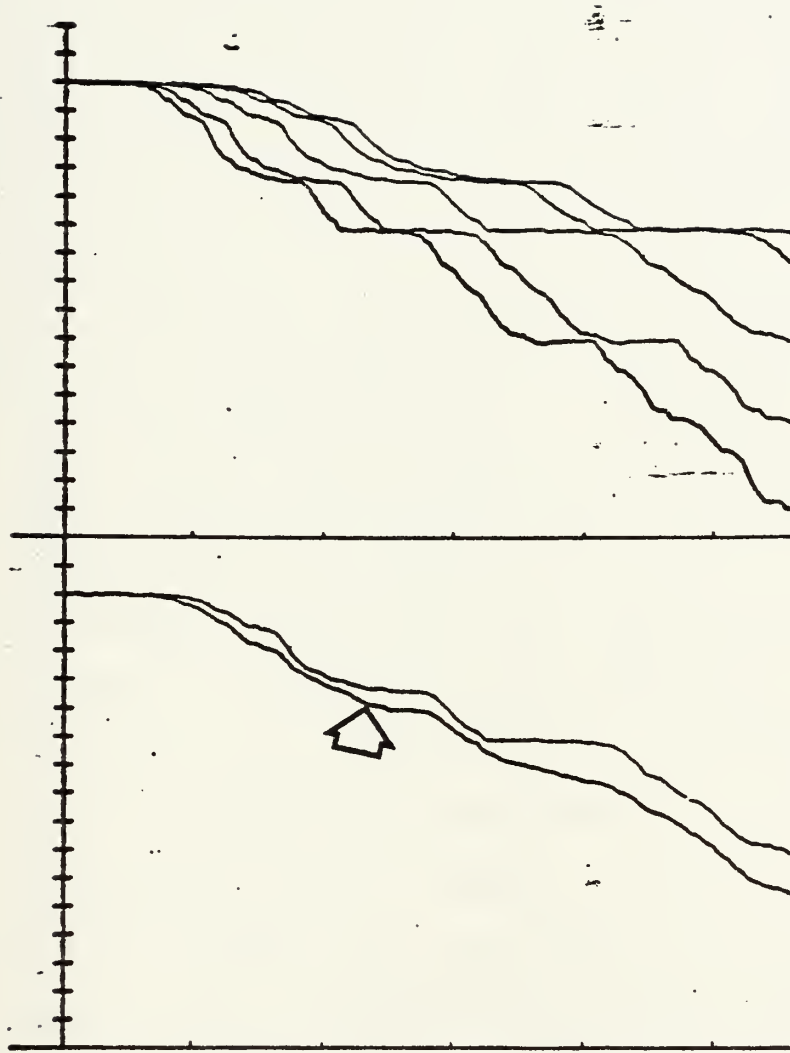


Figure 68. Averaging XBT's with less steep thermoclines A) Right panel: XBT's to be averaged; B) Left panel: Average (indicated by arrow) and median XBT's

time and distance. XBT traces for a day varied from having 'excellent bulklike' mixed layers to having no mixed layers. The SST's did not vary in any predictable pattern, i.e., SST's of XBT traces without mixed layers were in fact colder than the SST's of the traces with mixed layers. The transit of the ship across numerous fronts, jets, and eddies would be one explanation for these anomalies and ambiguities.

Instead of obtaining a daily median profile, profiles for the same time each day were used as the 'observed' reality. The time chosen was 1800Z or 1000 local time to allow for the largest sample of XBT's, and to avoid periods of major diurnal heating or cooling. Fig. 69 is the T/Z contour for the XBT's closest to 1800Z each day, approximately within 30 minutes. There were no XBT's available for the designated time on 5, 6, 7, or 8 August. Therefore, the profiles for 5, 6 August were made identical to that of 4 August. The profiles for 7, 8 August were made identical to the profile for 9 August. The 'wavelike' nature and the two events present in the average XBT T/Z contour field at 2, 12 August are also located in the 1800Z XBT T/Z contour field. Associated with these peaks or troughs, one might expect to find a change in the mixed layer due to fluctuations in the whole water column. Such in fact was the case for mixed layers of 2 and 12 August.

CA. 1800 XBT T/Z PROFILES

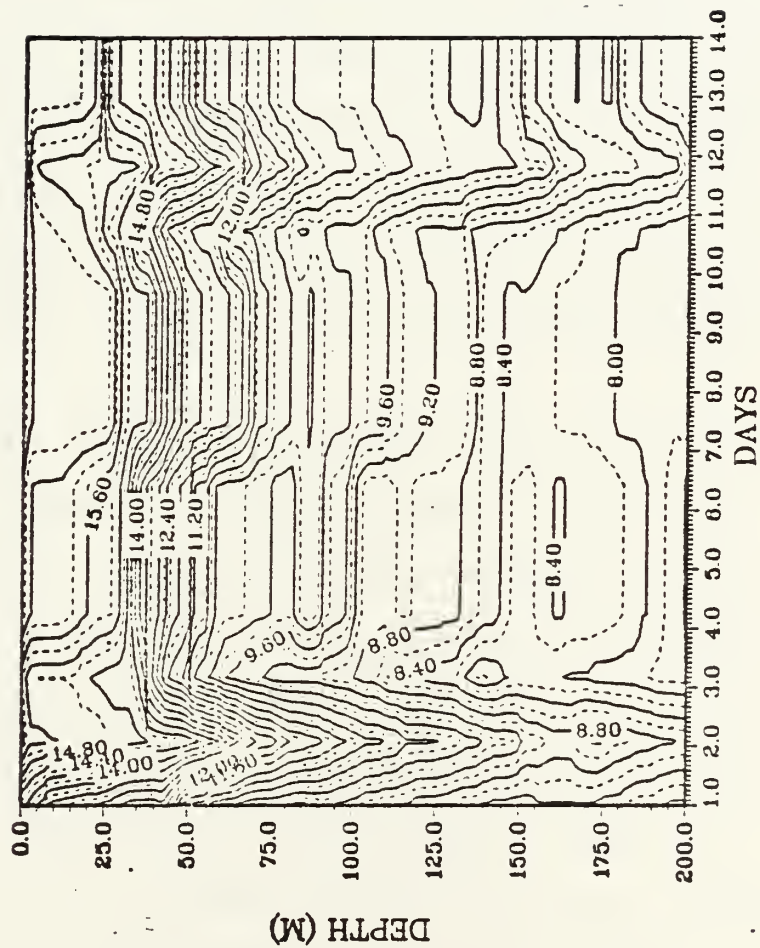


Figure 69. Contoured temperature/depth of 1800Z XBT's.

Returning to the results of the Garwood and TOPS model runs discussed thus far, one must keep in mind a number of important points. Recall that the Garwood model simulation shown was initialized with a profile from outside the study region and with inputs of varying degrees of accuracy. It was not known exactly how good the boundary conditions were, nor how sensitive that model would be to them. A sensitivity test was performed to decide whether the Garwood model was deepening the layer due to the 19.5m FNOC winds being too strong. This was done by decreasing the drag coefficient by 10%, equivalent to decreasing the FNOC winds to 95% of their original magnitude. As can be seen from profiles for 1 and 13 August 1982 (Figs. 70, 71), the effects are not very substantial.

In addition, it should be remembered that the TOPS model was initialized and run at a point outside of the cruise grid. It is not known what values TOPS received as initial or boundary conditions, only that it received its atmospheric forcing from the atmospheric primitive equation model and NOGAPS, and that eight XBT's were used in the TEOTS analysis. Finally a slightly warmer SST is expected for the FNOC gridpoint, because it is further offshore than the study domain. According to the previous fortnightly mean, however, the difference should only be about 1C.

To make simulations more consistent within the domain, a second run was performed using XBT 96 to initialize the Garwood model. This XBT, deployed on 4 August, was chosen

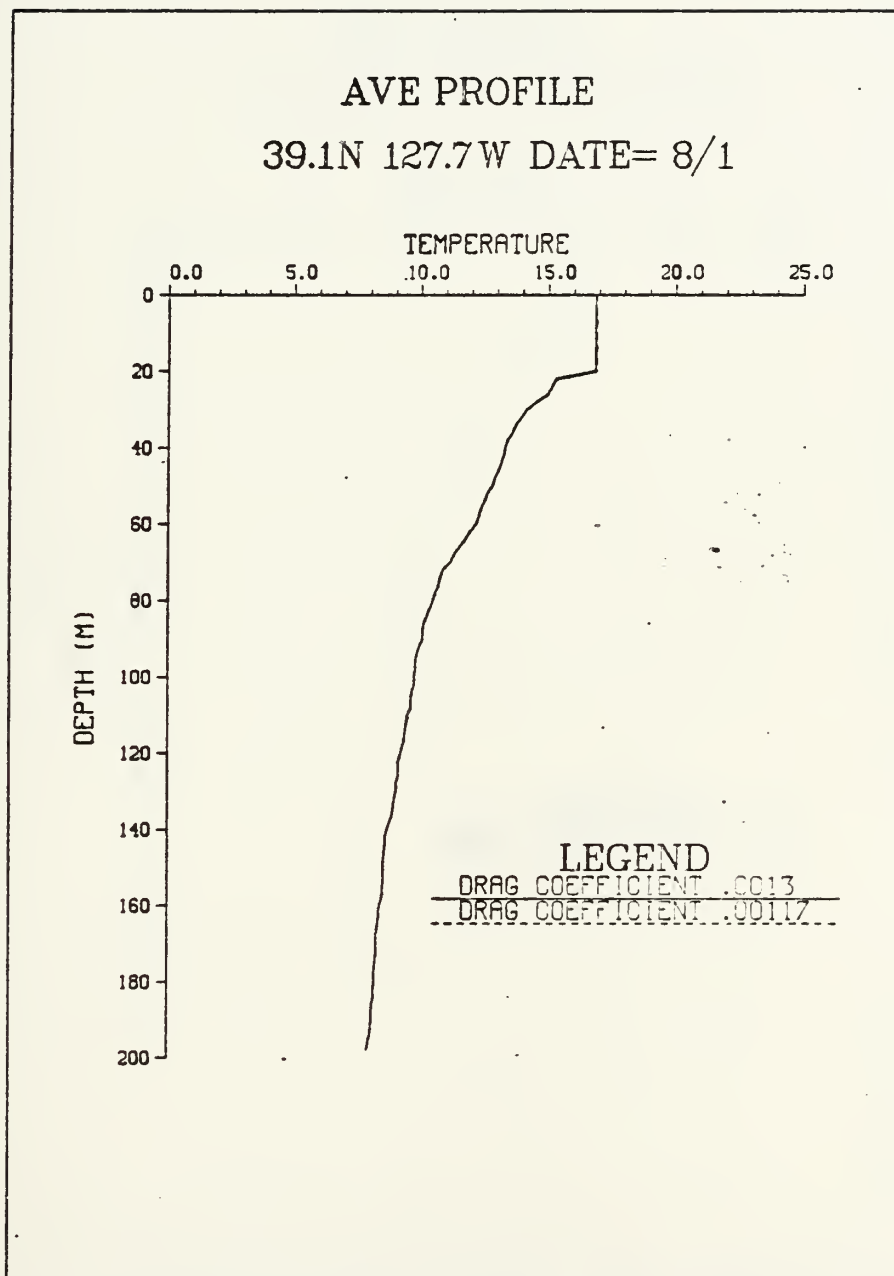


Figure 70. Daily average and average tuned Garwood profiles: 1 August (Temperature in degrees Celsius)

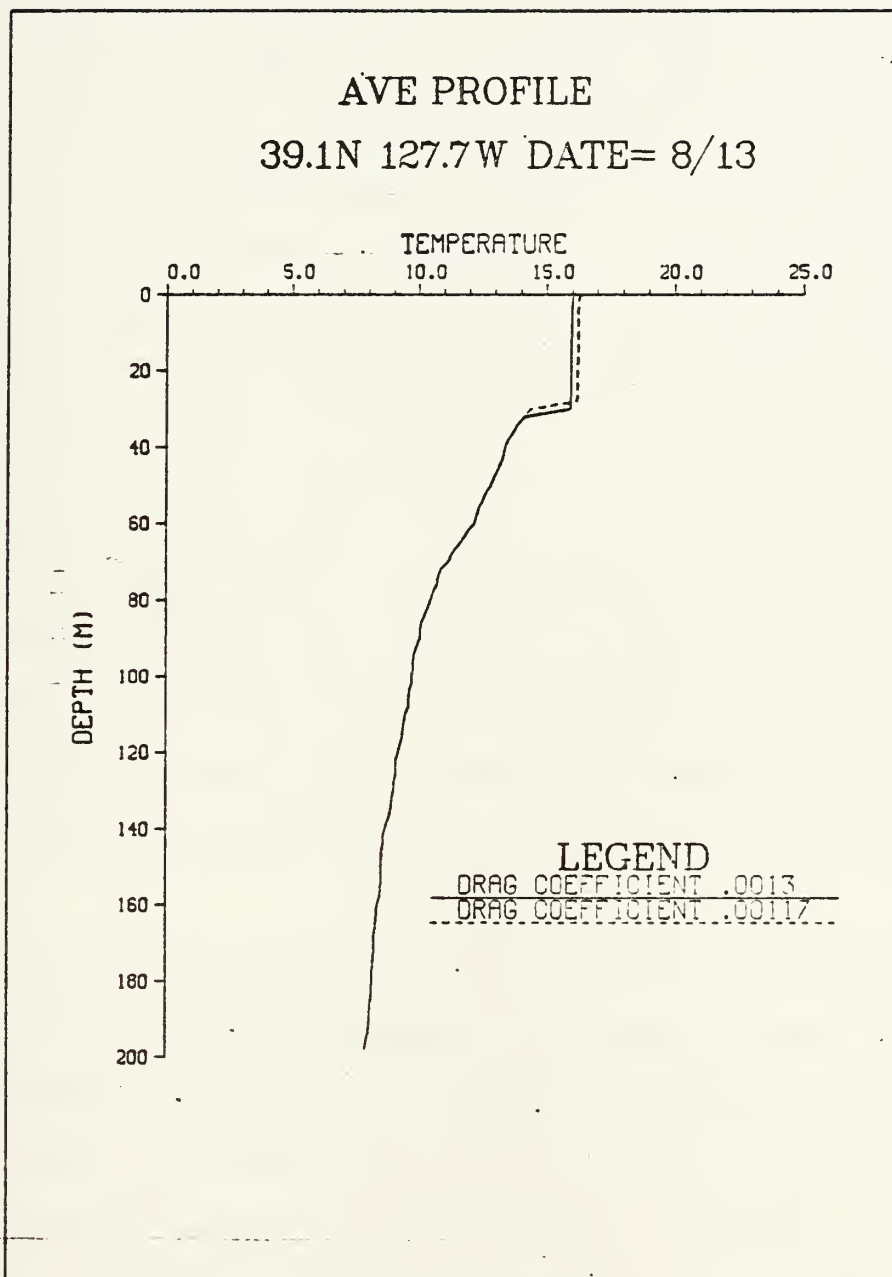


Figure 71. Daily average and average tuned Garwood profiles: 13 August. (Temperature in degrees Celsius)

because its location was resampled on 10 August with the launch of XBT 216. (Fig. 72) (It was hoped that by choosing XBT 96 to initialize the Garwood model, its mixed layer evolution could be compared and evaluated with the data obtained from XBT 216. The initial SST used was that of XBT 96. An initial mixed layer depth of 20m was "assumed".)

In addition, to avoid comparing simulations of two differently forced models, the Mellor level-2.5 model was obtained and modified to produce simulations using forcing identical to that used in the Garwood model. Profiles resulting from the model runs (Figs. 73-85) along with the applicable 1800Z XBT profiles, TOPS predicted profiles, and daily averaged profiles are examined. (Notes: A) repeated TOPS, 1800Z, and average XBT profiles during in-port period; B) TOPS profiles correspond to 1600 local time, i.e., afternoon heating exists; C) Mellor profiles are not daily averages.)

Based on the overall change in the profiles, Garwood and Mellor profiles cooled and deepened the mixed layer. The profiles seemed to be quite consistent with the observed data by 4 August and even more so by 10 August. The cooling trend in the XBT's seemed to be consistent with that apparent from XBT 96 to XBT 216. However, caution is required, because the role of the horizontal and vertical advection has not been assessed.

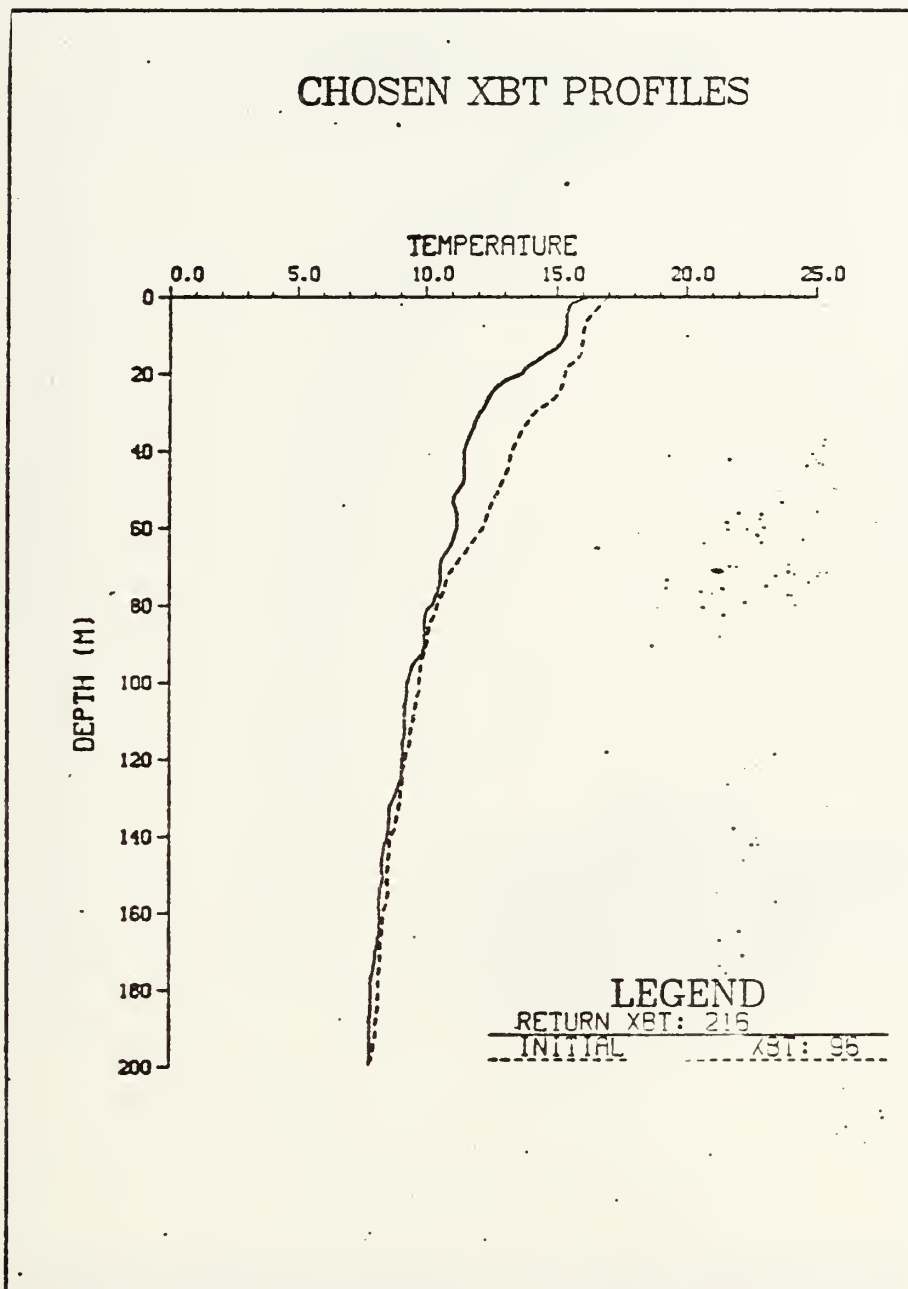


Figure 72. XBT's 96 and 216 (Temperature in degrees Celsius) launched at approximately the same location on 4 and 10 August, respectively

DAILY PROFILE, 8/1

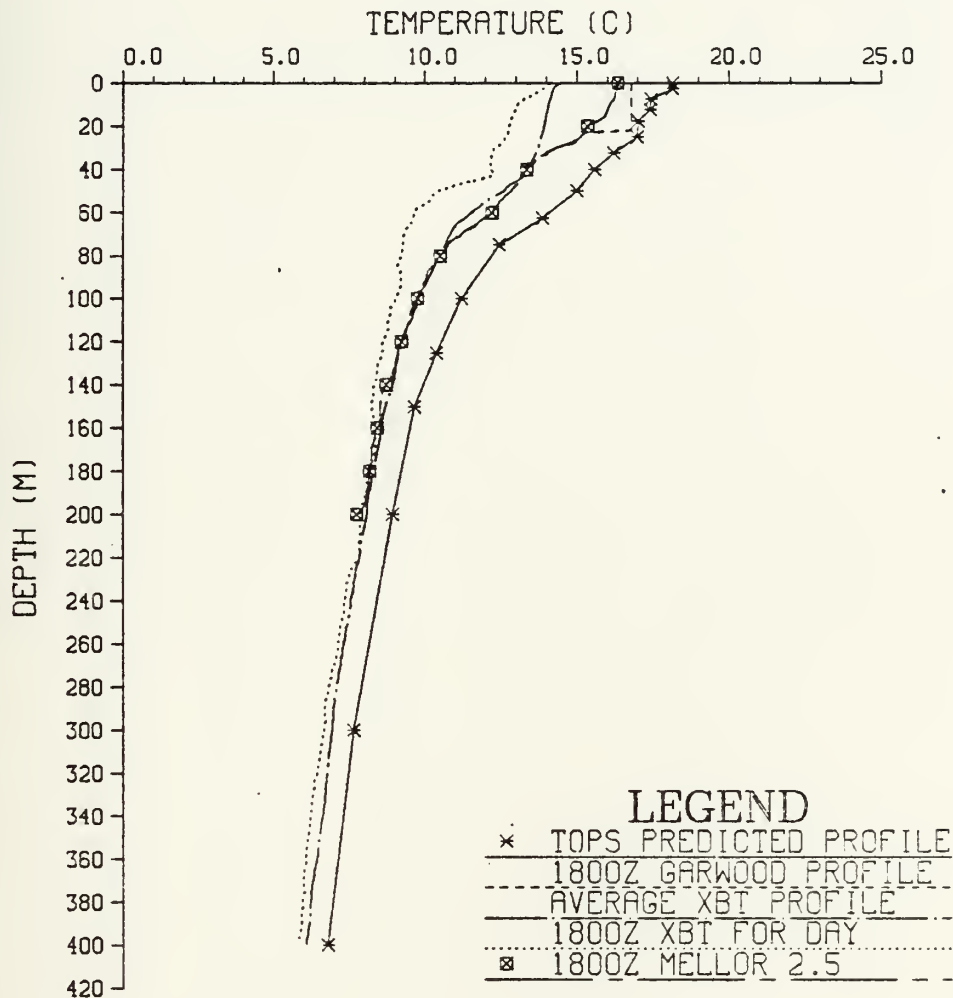


Figure 73. August 1 composite of simulated and observed profiles

DAILY PROFILE, 8/2

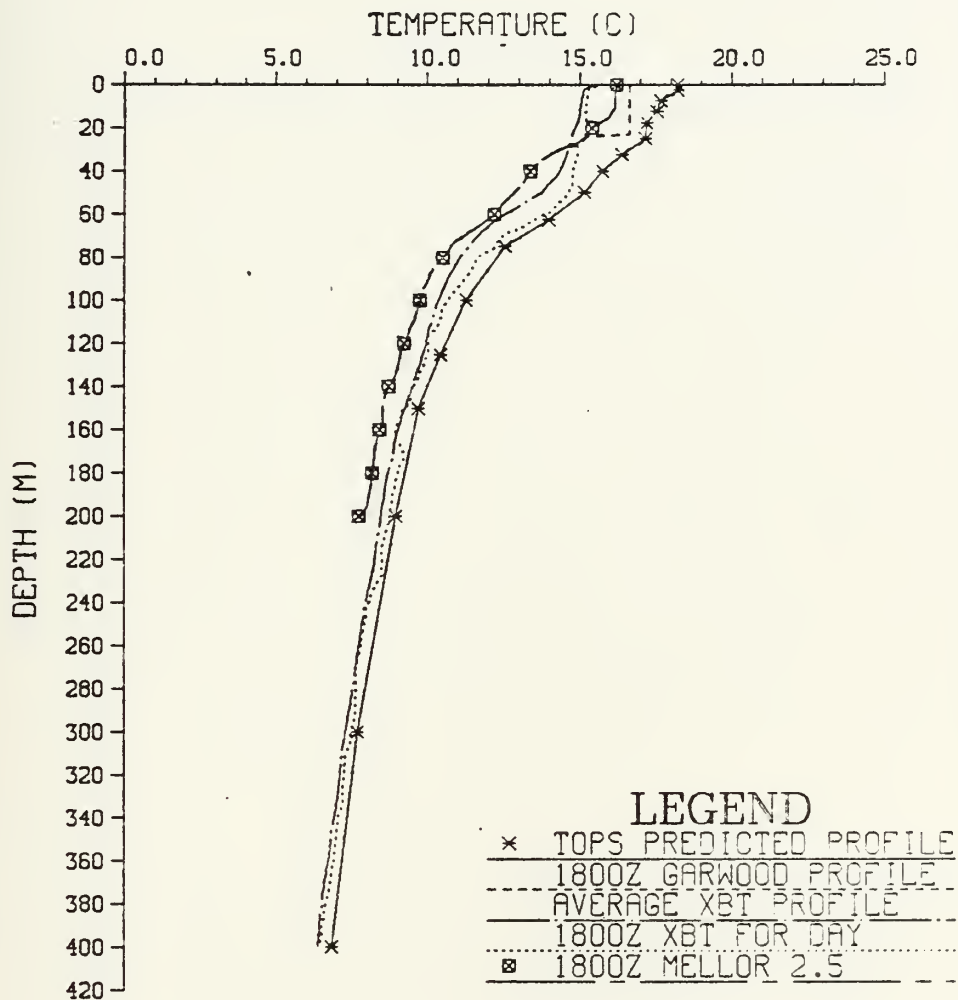


Figure 74. August 2 composite of simulated and observed profiles

DAILY PROFILE, 8/3

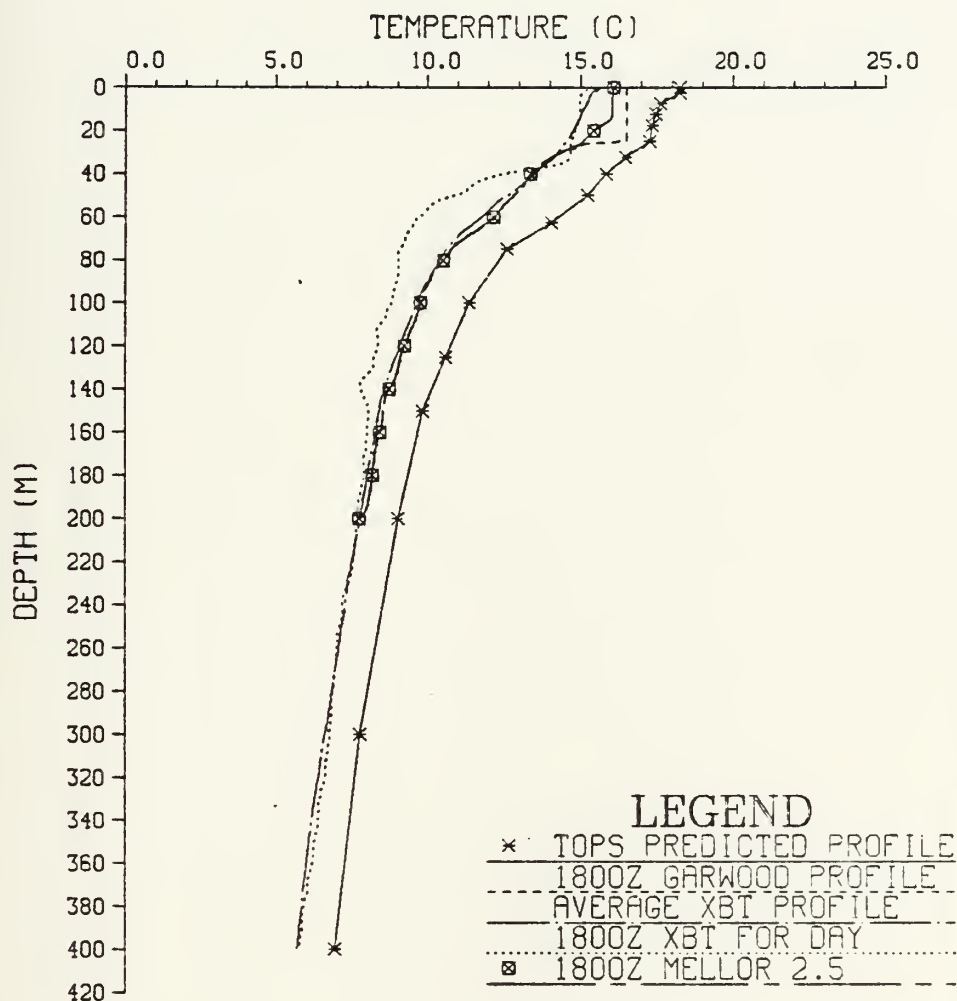


Figure 75. August 3 composite of simulated and observed profiles

DAILY PROFILE, 8/4

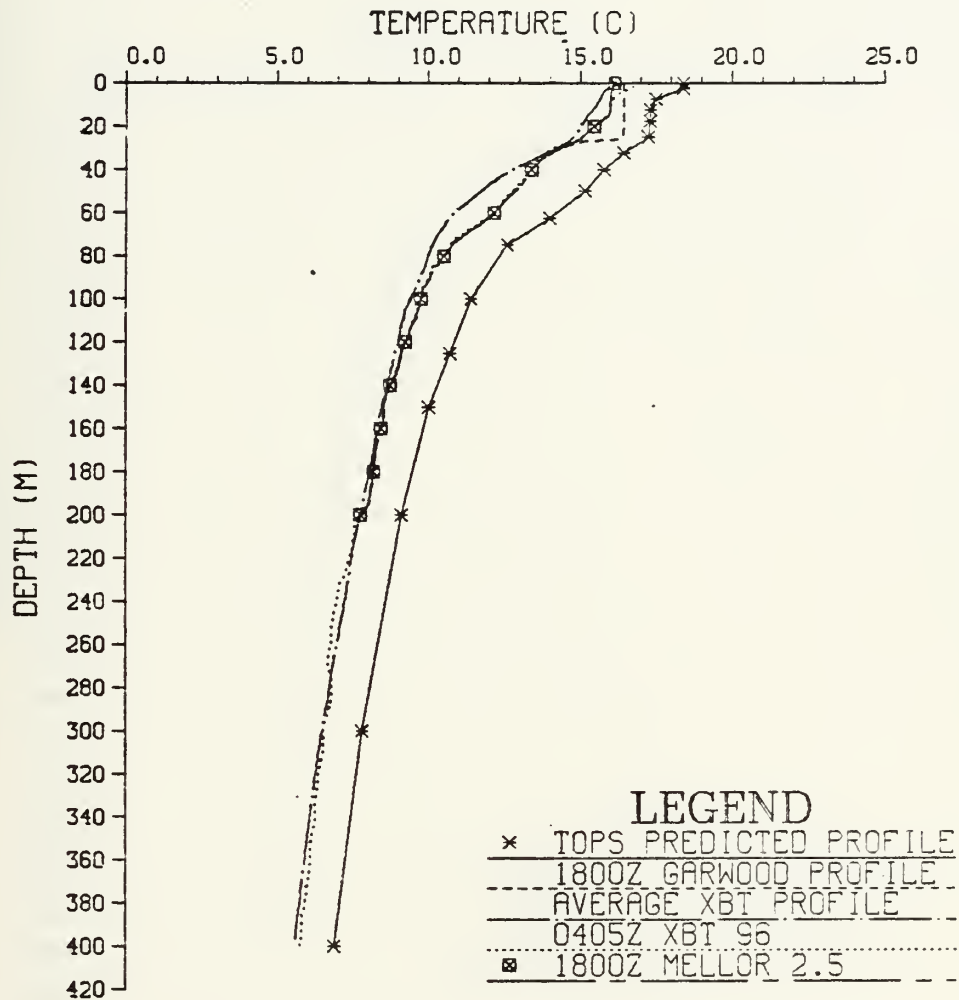


Figure 76. August 4 composite of simulated and observed profiles

DAILY PROFILE, 8/5

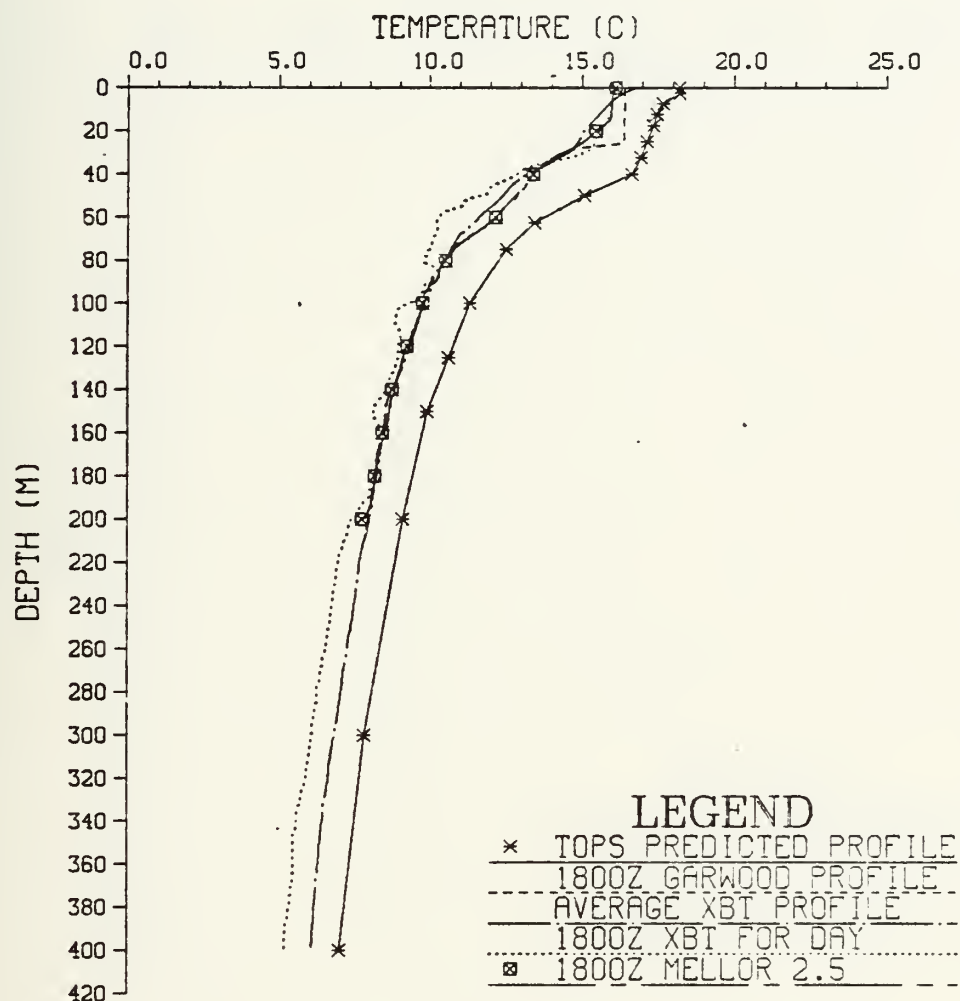


Figure 77. August 5 composite of simulated and observed profiles.

DAILY PROFILE, 8/6

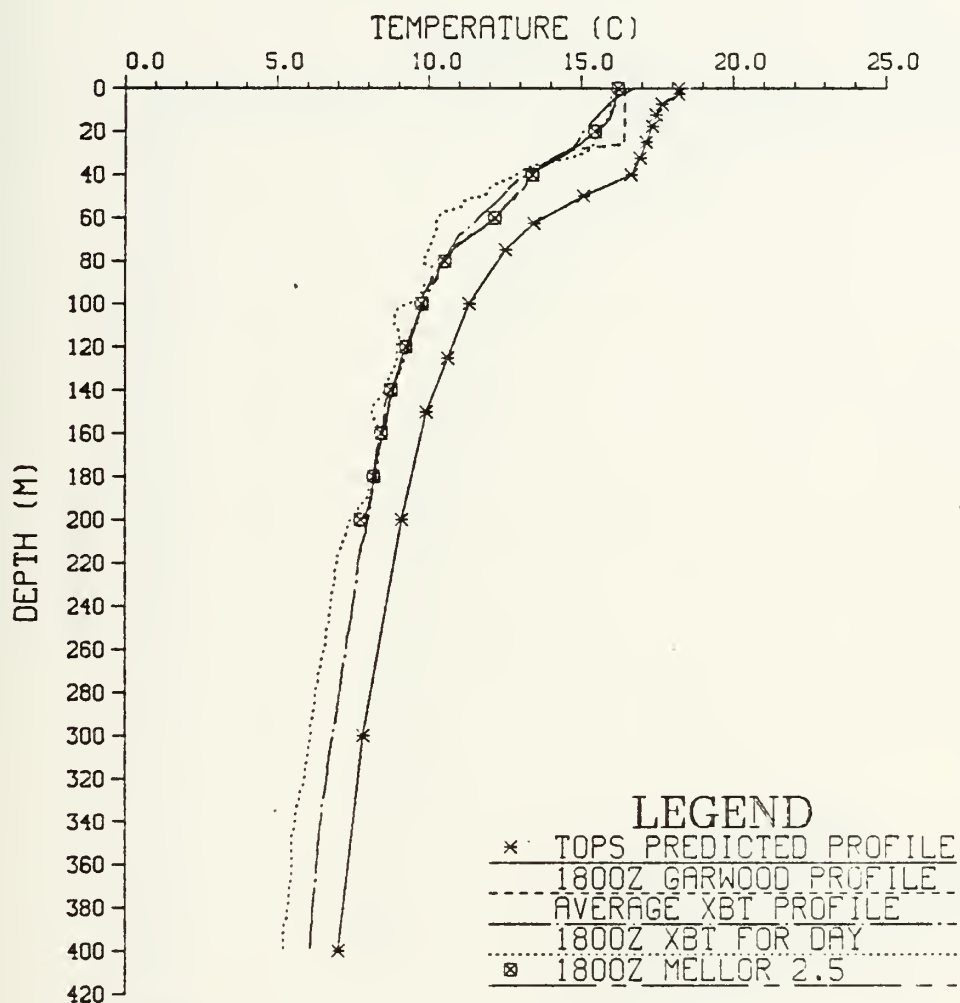


Figure 78. August 6 composite of simulated and observed profiles.

DAILY PROFILE, 8/7

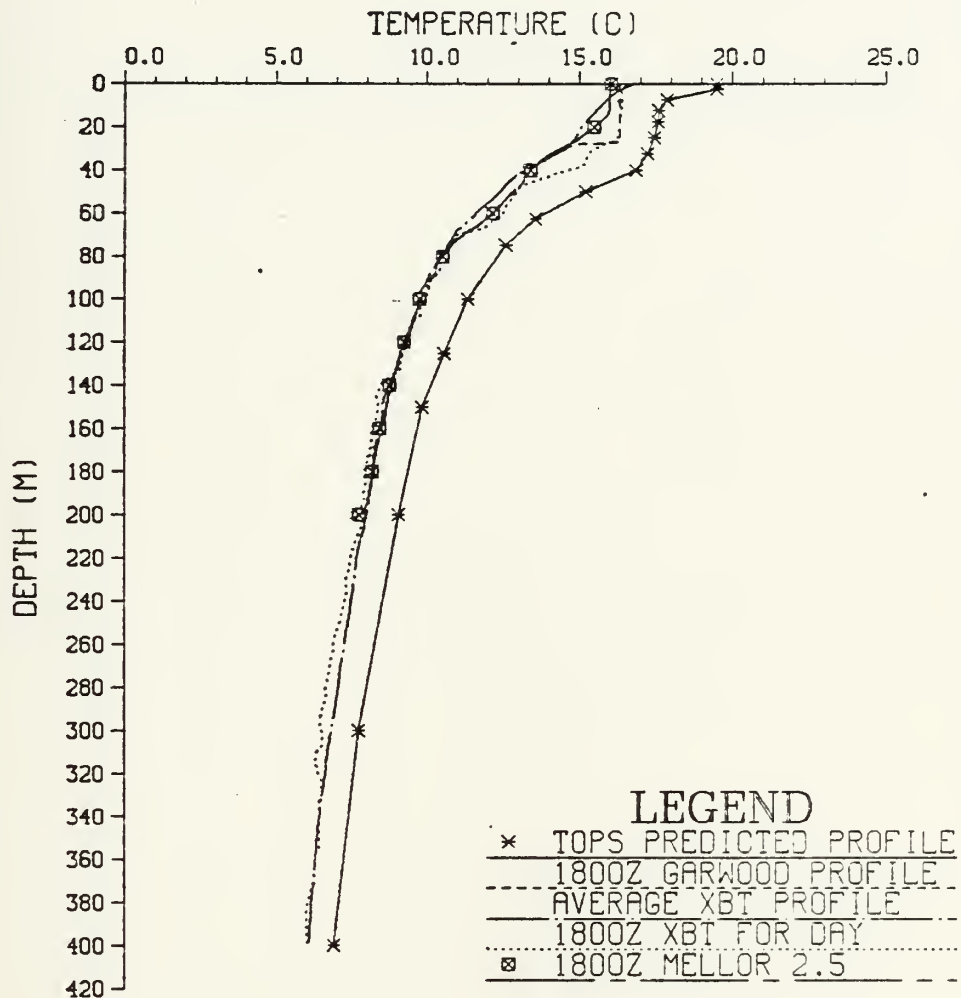


Figure 79. August 7 composite of simulated and observed profiles.

DAILY PROFILE, 8/8

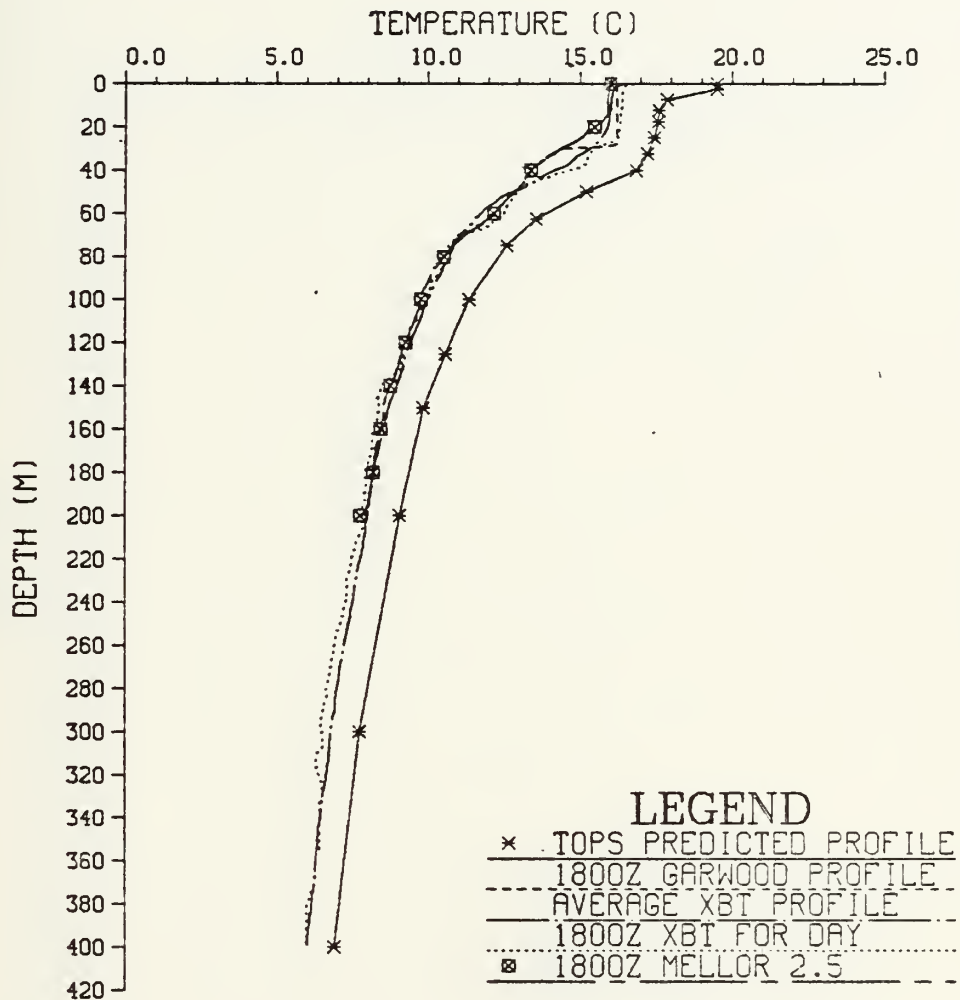


Figure 80. August 8 composite of simulated and observed profiles

DAILY PROFILE, 8/9

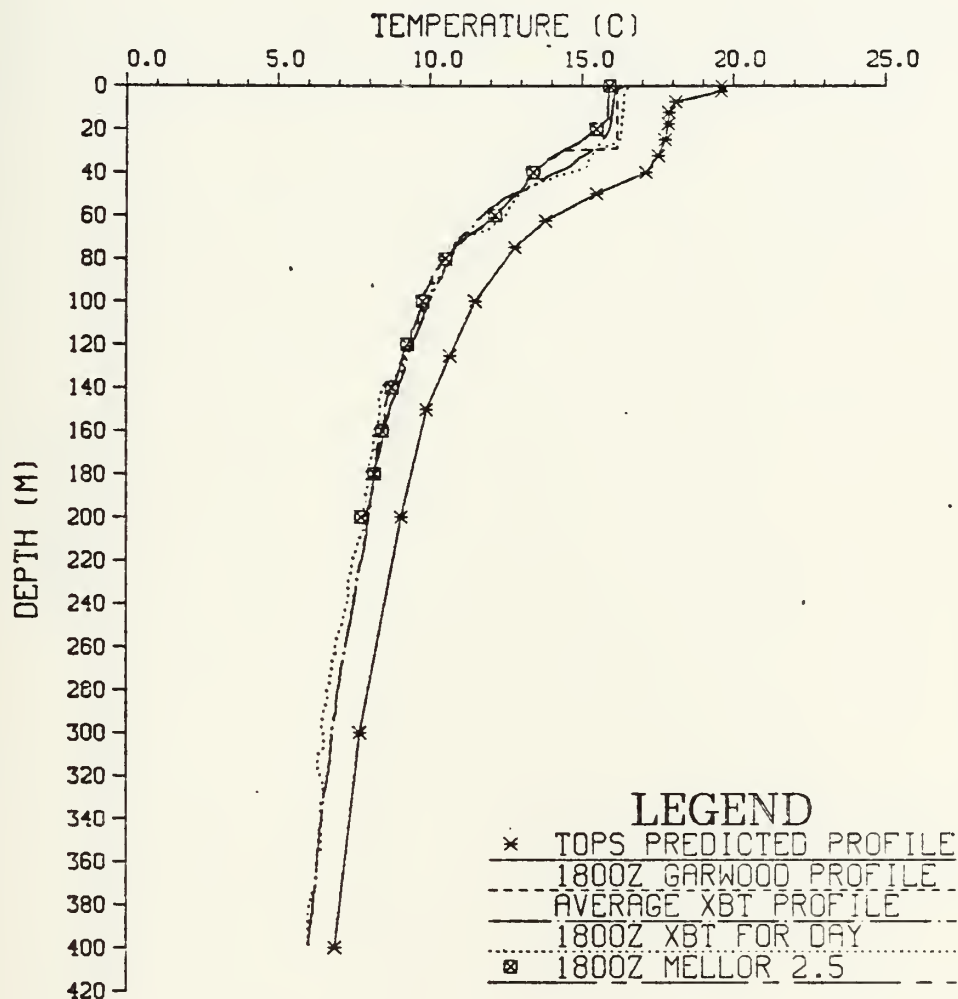


Figure 81. August 9 composite of simulated and observed profiles

DAILY PROFILE, 8/10

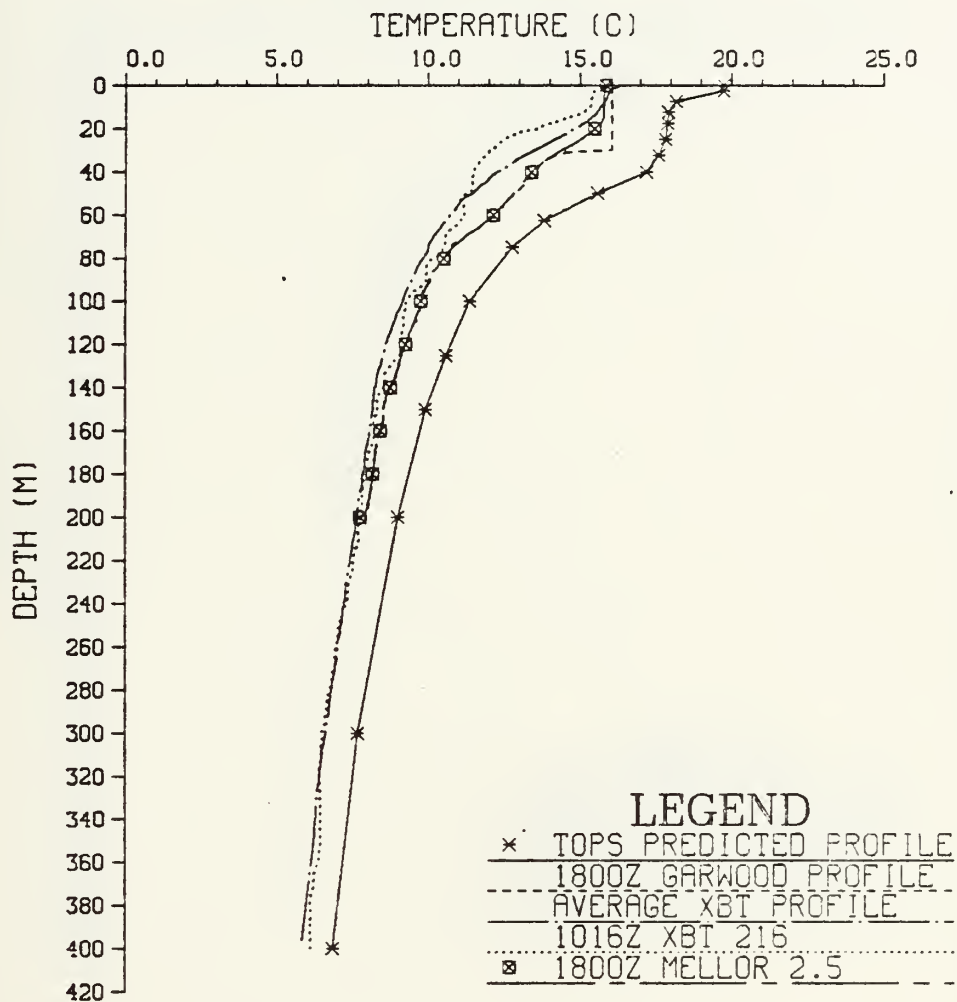


Figure 82. August 10 composite of simulated and observed profiles

DAILY PROFILE, 8/11

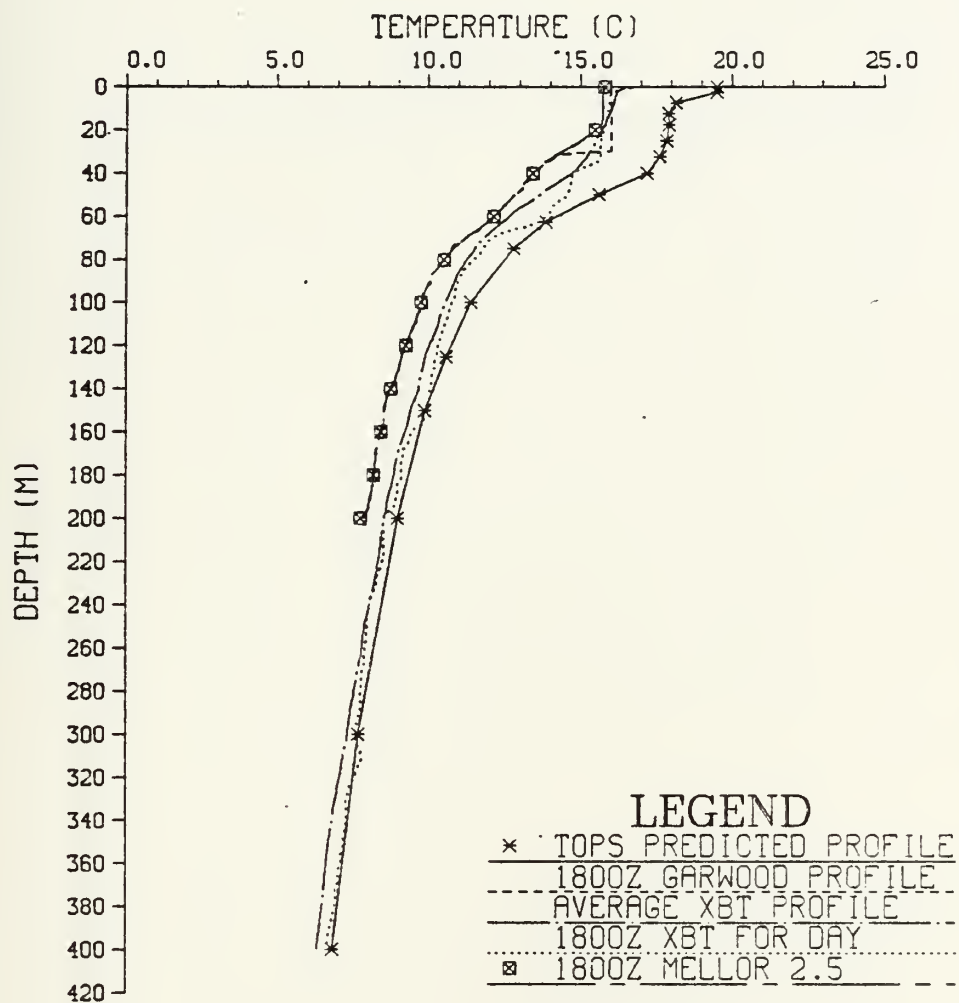


Figure 83. August 11 composite of simulated and observed profiles.

DAILY PROFILE, 8/12

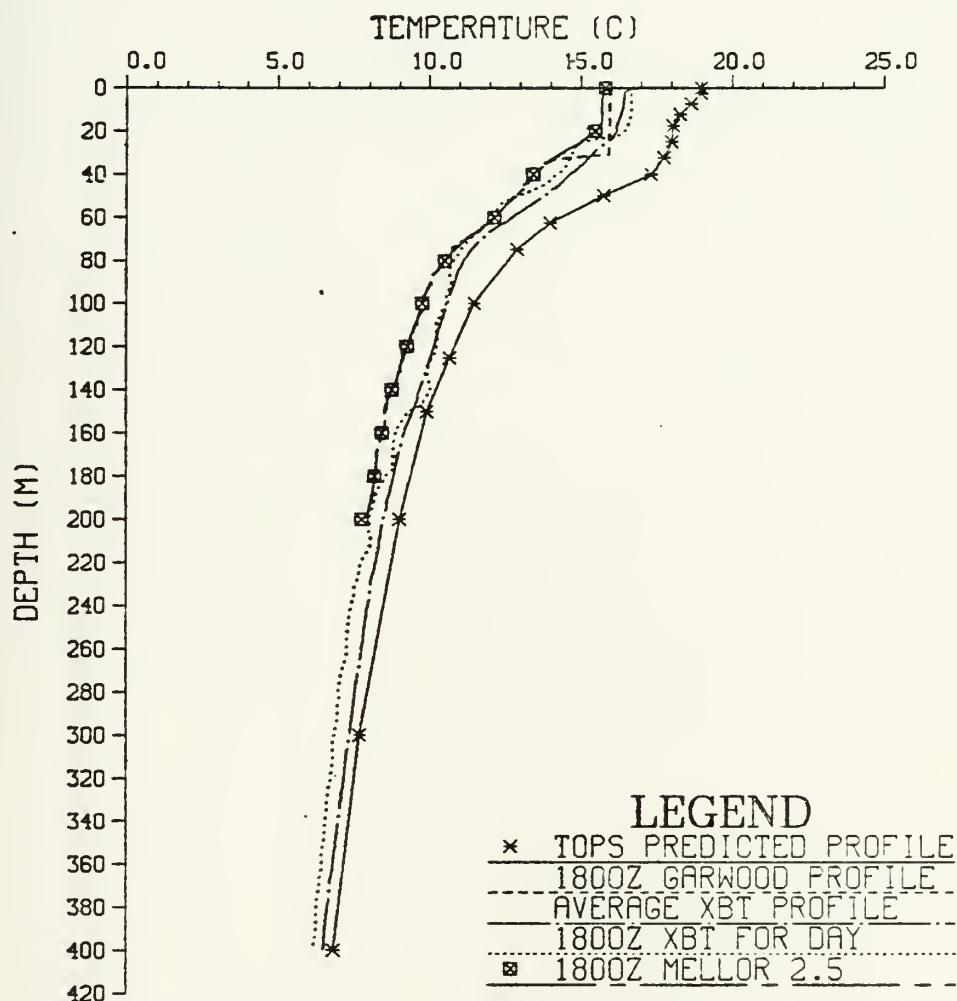


Figure 84. August 12 composite of simulated and observed profiles.

DAILY PROFILE, 8/13

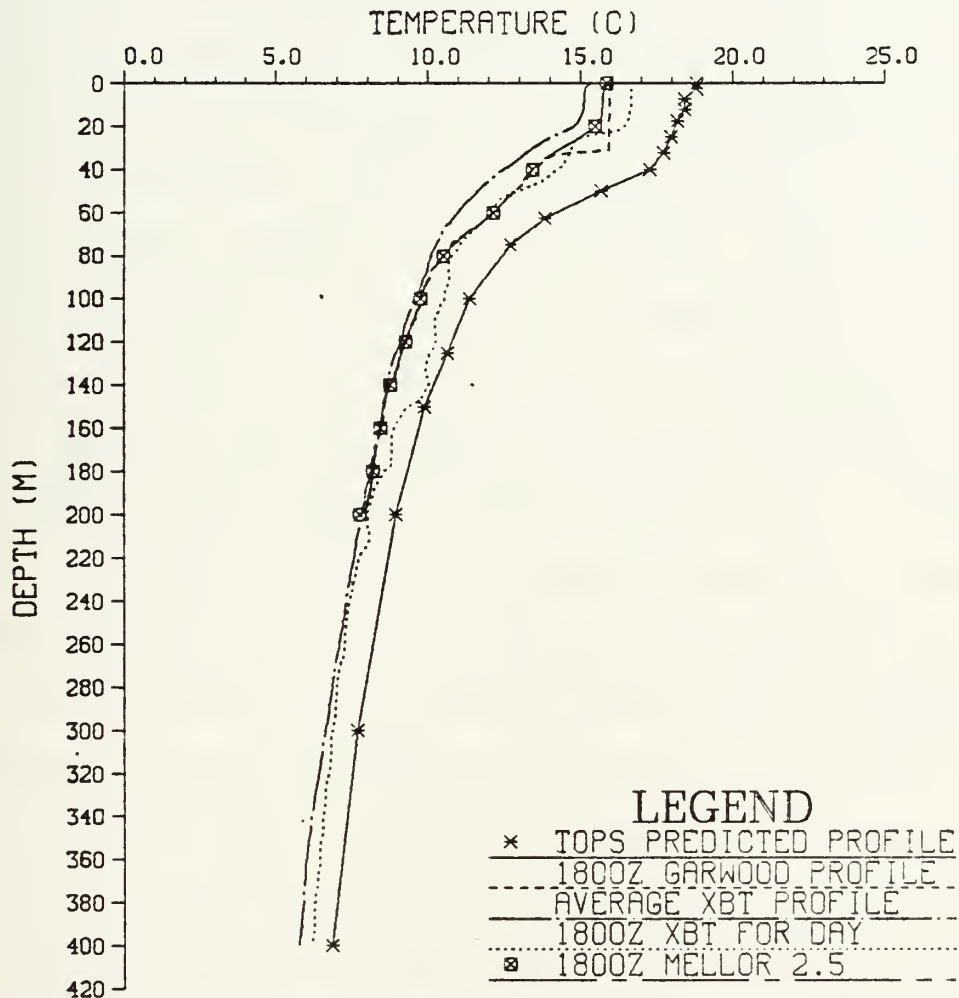


Figure 85. August 13 composite of simulated and observed profiles.

The TOPS profiles, though not expected to resolve the small scale variability of the boundary current region, on the otherhand, started out warmer than the other profiles and indicated additional warming with time. The fact that the gridpoint used was further offshore than the cruise region caused one to expect a slightly greater surface temperature for the FNOC profiles. That the forcing averaged 184 Watts/m² per day was, however, not anticipated. This heating is, however, believed to be part of a larger problem, viz., a heat bias in the atmospheric PE model. Heats biases of varying signs have been previously identified by Elsberry, et.al. (1979), Budd (1980), and Warn-Varnas, et.al. (1982) and shown to possess temporal and spatial scales of a month and tens of thousands of kilometers, respectively. Warn-Varnas, et.al. (1982), for example, found that a limited-area version of TOPS initialized and forced with FNOC fields revealed considerable skill during 60-day runs in comparison to persistence if a bias of about 150 ly/day was removed from the daily net surface heat flux of the domain. This correction proved to yield consistent results with the heat fluxes computed directly using atmospheric observations acquired by ships-of-opportunity. [Clancy, et.al., 1980] In another study, comparison of the FNOC heat fluxes with those calculated by Nate Clark indicated a cold bias believed to be mainly the result of excessive latent heat loss. The problem of heat bias is extremely evident in such data sparse

areas as the high latitudes. For example, TEOTS SST's in the Sea of Okhotsk, the Bering Sea, and the Labrador Sea have in the past exhibited a warm bias, running as much as 6C above those of conventional EOTS (essentially representative of climatology within these areas). [Clancy, et.al, 1982]

In the simulations presented, the initial conditions and forcing for the first two days were supplied to TOPS by the PE model. On 3 August, NOGAPS replaced the PE model. However, any spurious heat available in the PE model entered into the simulation prior to bringing NOGAPS online. Once introduced into the run, it is unlikely that the heat could be removed without much mixing or surface cooling (due to the Second Law of Thermodynamics). NOGAPS' contribution to the spurious heating is unknown, though it's clear that the heating trend was not corrected over the short run time. (It is as yet unknown whether NOGAPS has a heat bias of any kind.)

Examining the TEOTS SST anomalies (TEOTS - climatology) for some of the cruise days as well as for a number of days following the cruise, and following the 'return to climatology' adjustment installed in TOPS on 20 September (Table IV) revealed an excess of 2-3C in the study domain as compared to conventional EOTS.

TABLE IV
TEMPERATURE ANOMALIES

DATE	TEMPERATURE ANOMALY (C)	
	TEOTS	EOTS
820730	2	
820803	NOGAPS Online	
820804	2	-1
820808	2	0
820811	3	
820814	2	
820819	3	
820827	2	
820828	System Restart	
820910	1.7	
820920*	1.4	
820923	1.9	

*Return to climatology adjustment installed

The warmer SST's along with the an identified tendency for the turbulent parameter scheme used in TOPS to underpredict the MLD's [Martin, 1982] might be important in explaining the trend in the TOPS' profiles. The difference between various model profiles with depth is believed to be the result of the strong connection TEOTS has with climatology.

To make a strict comparison of model results (assuming ideally that the model forcing is the same, as it should be), one should interpolate between FNOC gridpoints to the locations of XBT 96.

It is felt , however, that the heating difference is not totally a function of distance. Erroneous heat fluxes, strong dependence upon climatology, and advection (associated with mesoscale variability) are thought to play important roles in the results.

V. SUMMARY AND CONCLUSIONS

The Garwood and Mellor level-2.5 simulations resulted in cooling and deepening of the mixed layer over time, and exhibited a likeness to the observations. The TOPS model, receiving different forcing, produced warmer profiles with a substantial warming trend over the 13 days.

The exhibited differences of the TOPS profiles with respect to the profiles produced by the other models are believed to be more than a result of location. They are believed to be due to a) a heat bias in FNOC's atmospheric PE model, b) too much dependence upon climatology, and c) advection and the subgrid scale variability existing in the region.

The autocorrelation functions for SST and MLD indicated a maximum correlation distance of 35 km. However, TOPS uses a standard FNOC grid with spacing 381 km at 60N. Hence, though interpolation should be carried out when looking at regions between the gridpoints, it seems highly unlikely to be able to recover the small scale variability dominating the region.

VI. RECOMMENDATIONS

First of all, numerous recommendations are in order concerning the data acquisition on future cruises. Most importantly, all easily observed data should be recorded regardless of the immediate mission of the cruise. (e.g., wet bulb temperature) The equipment should be in a working status, and be sufficiently backed-up with manual logs. Underway analysis should be carried out in a consistent manner wherever possible to avoid excessive reworking of the data ashore. A thorough scientific crew indoctrination period is, therefore, in order.

From the modeling aspect, many more evaluations of TOPS are necessary under numerous varied conditions prior to its full acceptance by the scientific community. It is important that the TOPS products be interpolated to the observed position and time of the study domain prior to any further evaluations of the model's performance. Design tests should be carried out with control over the variables. Independent, direct measures of atmospheric forcing should be made to drive the research and operational models. (Simulations should be produced using both sets of forcing values). Additionally, it would be of interest to attempt to predict SST and MLD from one realization to the next, and to examine the changes in the profiles in the (z,x,t) domain instead of

merely the (z,day) domain. All of these tests and comparisons should also be performed on the 60 km and 20 km grids of the future.

In addition, other operational models and their products are becoming more important both in the Navy and in the civilian community. With their growing availability, so too must grow the amount and quality of verification testing accorded them, for they are an important asset of the future.

APPENDIX A

A. DATA PROCESSING PROCEDURES

Working with a new data set is rarely an easy task. The data must be edited and processed into a usable format. Here, the editing procedures used to produce the five required inputs for the version of the Garwood model at hand are described in more detail to better assess the model inputs and results.

The procedure applied to the DAS data was as follows. First, the data on magnetic tape was dumped onto mass storage and filtered for blocks of zeros and gross errors in latitude and longitude. Following this, the data from the entrance and exit tracks to the cruise grid were deleted so as to confine the data to the study domain. Finally, the finer errors in temperature, wind speed, etc. were deleted. The resulting air temperature data were then averaged over three-hour intervals to yield the required eight daily air temperatures. Averages were computed over bins containing from 6 to 299 values with the maximum standard deviation for any resultant value being 1.67C and the minimum being 0.0005C. Only three of the averaged values possessed standard deviations over 1C. Procedures used to obtain missing values within cruise days were based on the assumptions described previously. For days in port, the air temperatures were held at a representative constant value. (This could be improved upon with reasonable means to predict gaps.)

The dewpoint temperatures were erroneous due to equipment failure. The required eight values of dewpoint per day were calculated by assuming a relative humidity of 90% and using the procedure described in Bolton (1980). This value for relative humidity was chosen to correspond with the intermittently hazy/foggy conditions.

Cloud cover indications from the ship's log were either in tenth of sky cover or in descriptive terms. The first step taken was to convert the descriptors to tenths of sky cover using Bowditch's American Practical Navigator and the experience of the R/V ACANIA's first mate. The tenths of sky cover were then converted to octals, and averaged over three hour intervals. Missing values during cruise days were not a problem as they had been with the air and dewpoint temperatures. The cloud cover during the in-port days was held at a constant five tenths.

Winds could have been obtained in two ways. The DAS recorded winds could have been converted to true winds and averaged as was done with the air temperatures. The other way winds could have been obtained was by interpolating the daily analyzed TEOTS 39.05N, 127.75W wind to the necessary three-hour interval. The TEOTS analyzed winds over both CCSII and CCSIII are depicted in Figs. 25 and 26 with the latter time series containing the interpolated eight three-hourly values. (The symbol denotes the value at 00 Zulu) The latter method was chosen for convenience as well as to

facilitate the comparison of the results of the TOPS, Mellor level-2.5, and Garwood models. Some of the 'CTD station winds' (already assumed to be true winds due to the 'zero' speed of advance of the ship) were plotted against the FNOC archived winds to observe whether or not the latter could 'reasonably' be applied to the cruise area. The CTD winds were found mainly to fluctuate around the FNOC winds except for the first day and a half when the 'CTD winds' were exceeded by the FNOC winds. The FNOC winds were (Fig. 86) employed in subsequent runs. (The triangles represent 'CTD winds' recorded along with suspect data; leading to a possible suspicion in the winds.) A sensitivity analysis was done to assess the importance of the wind stress as a boundary condition, and in so doing, ascertain the magnitude of possible problems introduced by using winds recorded at 19.5m vice 10.0m. The procedure and results were described in Chapter IV.

The final input required was SST. The SST's were available from a number of sources. DAS recorded boom temperatures could have been averaged. This route was not chosen, because of the possible problems posed by the boom varying in its depth in the water (interaction with the ship's wake). Alternatives included the use of the bucket or XBT surface temperatures, averaged or singly, at the required times. For the initial runs, the XBT SST's recorded by DAS were used: this was believed to be the least subjective

FNOC WINDS AND LOGGED CTD WINDS

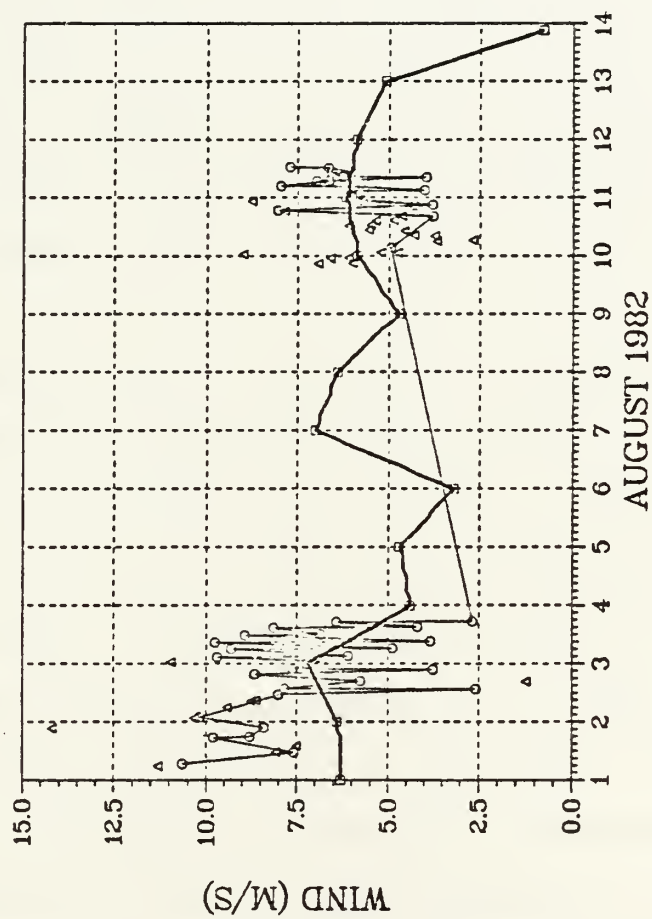


Figure 86. Time series of FNOC analyzed winds vs DAS logged winds

approach. The bucket temperatures were subject to the experience of the watchstander, as were the XBT SST's recorded in the XBT logs. The validity of the latter were found to strongly depend upon the existence of a surface thermocline, either 'real' or possibly due to the initially nonlinear slow response rate of the XBT recorder. The XBT temperatures were taken from those launched closest to the required input time. (usually within 30 minutes--sometimes linear interpolations were performed.) Averages were not made for the three-hour transit of the ship across possible fronts.

Finally it was necessary to input an initial temperature profile into Garwood and Mellor level-2.5 models. Temperatures were interpolated to intervals of one meter to a depth of 200M. The first runs were made using an interpolated TEOTS profile corresponding to 1 August. (The original TEOTS analyzed temperature profiles consisted of 13 temperature depth values. Surface values were not available; the temperature at one meter was used at the surface.) Subsequent runs were made using XBT 96 as the initial temperature profile for the Garwood and Mellor level-2.5 models. This XBT was chosen, because of its proximity to the FNOC gridpoint of interest. More importantly, however, it was chosen because of its common position with an XBT, 216, launched six days later. XBT's 96 and 216 were launched on 4 and 10 August, respectively, thus spanning a part of both cruises.

APPENDIX B

TABLE V

VERTICAL RESOLUTION OF TOPS

Level	Depth(m)
1	2.5
2	7.5
3	12.5
4	17.5
5	25.0
6	32.5
7	40.0
8	50.0
9	62.5
10	75.0
11	100.0
12	125.0
13	150.0
14	200.0
15	300.0
16	400.0
17	500.0

TOPS is run on the Cyber 205 computer on a standard 63x63 FNOC global grid. Values of T, S, U, and V are defined with this horizontal resolution at each of the seventeen levels listed above. All spatial derivatives are centered in space. The horizontal advection components are defined on a staggered grid; they are forward-differenced in time. Vertical eddy fluxes and W are defined midway between these levels. The former are differenced backward in time, while the latter (as well as the Coriolis term) is differenced trapezoidally in time.

Additionally, TOPS is quasi-three-dimensional model. (though a nonadvective version is kept on the Cyber 175 as a backup.) Advection, as previously mentioned, is by climatologically averaged geostrophic currents and instantaneous wind drift. The geostrophic currents are updated monthly using density fields computed from monthly temperature and salinity climatology and the thermal wind equations integrated upward from a predetermined "level of no motion". The geostrophic currents are nondivergent. The sole contributor to the vertical advection component is, therefore, the instantaneous wind drift via the Ekman suction mechanism.

LIST OF REFERENCES

- Denman, K.L. and Miyake, M. (1973): Upper Layer Modification
Papa: Observations and Simulation, J. Phys. Oceanogr., 3,
185-196.
- DeSzoek, R.A. (1980): On the Effects of Horizontal
Variability of Wind Stress on the Dynamics of the Ocean
Mixed Layer, J. Phys. Oceanogr., 10, 1439-1440, 1451-1452.
- Garwood, R.W. and Camp, N.T. (1977): Comments on
"Climatological Numerical Models of the Surface Mixed Layer
of the Ocean", J. Phys. Oceanogr., 7, 469-470.
- Haney, Robert L. (1979): Numerical Models of Ocean
Circulation and Climate Interaction, Rev. Geophys. Space
Phys., 17, 1494-1499.
- Haney, Robert L. and Davies, R.W. (1976): The Role of
Surface Mixing in the Seasonal Variation of the Ocean
Thermal Structure, J. Phys. Oceanogr., 6, 504-510.
- Miller, J.R. (1976): The Salinity Effect in the Mixed Layer
Ocean Model, J. Phys. Oceanogr., 6, 29-35.

BIBLIOGRAPHY

- Alexander, R.C. and J.W. Kim (1976): Diagnostic Model Study of Mixer-Layer Depths in the Summer North Pacific, J. Phys. Oceanogr., 6, 293-298.
- Barnett, T.P., D.R. McLain, S.E. Larson, and E.J. Steiner (1980): Comparison of Various Sea Surface Temperature Fields, COSPAR/SCOR/IUCRM Symposium on Oceanography from Space, Venice, Italy, May, 11p.
- Bathymetric Atlas of Northern Pacific Ocean, 1978, Naval Oceanographic Office, NSTL Station, Bay St. Louis, MS 39522.
- Benjamin, T.B. (1963): The Threefold Classification of Unstable Disturbances in Flexible Surfaces Bounding Inviscid Flows, J. Fluid Mech., 16, 435-450.
- Bolton, D. (1980): The Computation of Equivalent Potential Temperature, Mon. Weather Rev., 108, 1046-1053.
- Bowditch, N. (1977): American Practical Navigator, Vol. 1, DMAHC, 855-861.
- Budd, B.W. (1980): Prediction of the Spring Transition and Related Subsurface Anomalies, M.S. Thesis, Naval Postgraduate School, Monterey, CA., 95p.
- Camp, N.T. and R.L. Elsberry (1978): Oceanic Thermal Response to Strong Atmospheric Forcing II. The Role of One-Dimensional Processes, J. Phys. Oceanogr., 8, 215-224.
- Chou, P.Y. (1945): On Velocity Correlations and the Solutions of the Equations of Turbulent Fluctuations, Quant. Appl. Math., 3, p. 38.
- Clancy, R.M. and P.J. Martin (1979): The NORDA/FLENUMOCEANCEN Thermodynamical Ocean Prediction System (TOPS): a Technical Description, NORDA Technical Note 54, Naval Ocean Research and Development Activity, NSTL Station, MS, 28p.
- Clancy, R.M. and P.J. Martin (1981): Synoptic Forecasting of Oceanic Mixed Layer Using the Navy's Operational Environmental Data Base: Present Capabilities and Future Applications, Bull. Amer. Meteor. Soc., 62, 770-784.
- Clancy, R.M., P.J. Martin, S.A. Piacsek, and K.D. Pollak (1981): Test and Evaluation of an Operationally Capable Synoptic Upper-Ocean Forecast System, NORDA Technical Note 92, Naval Ocean Research and Development Activity, NSTL Station, MS, 66p.

- Clancy, R.M. and K.M. Pollak (1982): A Real-Time Synoptic Ocean Thermal Analysis/Forecast System (in preparation), 71p.
- Davis, R.E., R. DeSzoeka, D. Halpern, and P. Niiler (1981): Variability in the Upper Ocean during MILE. Part I: The Heat and Momentum Balances, Deep-Sea Res., 28, 1427-1451.
- Davis, R.E., R. DeSzoeka, and P. Miller (1981): Variability in the Upper Ocean during MILE. Part II: Modeling and Mixed Layer Response, Deep-Sea Res., 28, 1453-1475.
- Denman, K.L. (1973): A Time-Dependent Model of the Upper Ocean, J. Phys. Oceanogr., 3, 173-184.
- DeSzoeka, R.A. and P.B. Rhines (1976): Asymptotic Regimes in Mixed-Layer Deepening, J. of Mar. Res., 34, 111-114.
- Dobryshman, E.M. (1972): Review of Forecast Verification Techniques, WMO Technical Note 120, WMO, Geneva, Switzerland, 51p.
- Elsberry, R.L., P.C. Gallacher, and R.W. Garwood (1979): One-Dimensional Model Prediction of Ocean Temperature Anomalies During Fall 1976., Technical Report NPS 63-79-003, Naval Postgraduate School, Monterey, CA., 30p.
- Elsberry, R.L. and R.W. Garwood (1980): Numerical Ocean Prediction Models-Goal for 1980s, Bull. Am. Meteor Soc., 61, 1556-1566.
- Garwood, R.W. Jr. (1979): Air-Sea Interaction and Dynamics of the Surface Mixed-Layer, Rev. Geophys. Space Phys., 17, 1507-1515.
- Garwood, R.W. Jr. (1977): An Oceanic Mixed Layer Model Capable of Simulating Cyclic States, J. Phys. Oceanogr., 7, 455-468.
- Garwood, R.W. and D. Adamec (1982): Model Simulations of Seventeen Years of Mixed Layer Evolution at Ocean Station Papa, NPS68-82-006, NORDA, NSTL Station, Mississippi, 30p.
- Gill, A.E. and J.S. Turner (1976): A Comparison of Seasonal Thermocline Models with Observation, Deep-Sea Res., 23, 391-401.
- Grabowski, N.J. and G.T. Hebenstreit (1980): A Review of One-Dimensional Upper Ocean Models (unpublished report), SAI, McLean, Virginia.

- Halpern, D. (1974): Observations of Deepening of the Wind-Mixed Layer in the Northeast Pacific Ocean, J. Phys. Oceanogr., 4, 454-466.
- Halpern, D. (1976): Measurements of Near-surface Wind Stress over an Upwelling Region Near the Oregon Coast, J. Phys. Oceanogr., 6, 108-112.
- Heinmiller, R., C. Ebbesmeyer, B. Taft, D. Olsen, and O. Nikitin (1982): Systematic Temperature and Depth Differences between Conductivity Temperature-Depth (CTD) and Expendable Bathythermograph (XBT) Profiles (Unpublished manuscript), 37p.
- Hickey, B.M. (1978): The California Current System-hypotheses and facts, Progress in Oceanography, 8, 193-241.
- Husby, D.M. and C. Nelson (1982): Turbulence and Vertical Stability in the California Current, Calcofi Report, XXIII, 113-129.
- Kim, J.W. (1976): A Generalized Bulk Model of the Oceanic Mixed Layer, J. Phys. Oceanogr., 6, 686-695.
- Klein, Patrice (1980): A Simulation of the Effects of Air-Sea Transfer Variability on the Structure of Marine Upper Layers, J. Phys. Oceanogr., 10, 1824-18.
- Klein, P. and M. Coantic (1981): A Numerical Study of Turbulent Processes in the Marine Upper Layers, J. Phys. Oceanogr., 11, 849-862.
- Kochergin, V.P., V.I. Klimck, and V.A. Sukhorukov (1976): A Turbulent Model of the Ocean Ekman Layer Sb. Shisl. Metody Mekhan. Sploshnoi Sredy, 7, 72-81.
- Kondo, J., J. Sasano, and T. Ishii (1979): On Wind-Driven Current and Temperature Profiles with Diurnal Period in the Oceanic Planetary Boundary Layer, J. Phys. Oceanogr., 9, 360-372.
- Kraus, E.B. and J.S. Turner (1967): A One-Dimensional Model of the Seasonal Thermocline, Part II, Tellus, 19, 98-105.
- Larsen, D.G. (1982): Oceanic Data Assimilation Tests with a One-Dimensional Model, M.S. Thesis, Naval Postgraduate School, Monterey, CA., 4 p.

- Marchuk, G.I., V.P. Kochergin, V.I. Klimok, and V.A. Sukhorukov (1977): On the Dynamics of the Ocean Surface Mixed Layer, J. Phys. Oceanogr., 7, 865-866.
- Martin, P.J. (1982): A Comparison of One-Dimensional Mixed-Layer Models at Ocean Stations Papa and November, (In preparation).
- Mellor, G. and P. Durbin (1975): The Structure and Dynamics of the Ocean Surface Mixed Layer, J. Phys. Oceanogr., 5, 718-728.
- Mellor, G.L. and T. Yamada (1974): A Hierarchy of Turbulence Closure Models for Planetary Boundary Layers, J. Atmos. Sci., 31, 1791-1806.
- Mellor, G. and T. Yamada (1982): Development of a Turbulence Closure Model for Geophysical Fluid Problems, Rev. Geophys. Space Phys., 20, 851-861, 870-873.
- Munk, W.H. and E.R. Anderson (1948): Notes on a Theory of the Thermocline, J. Mar. Res., 7, 276-295.
- Nelson, C.S. (1977): Wind Stress and Wind Stress Curl over the California Current, NOAA Technical Report NMFS SSRF-714, 87p.
- Nelson, C.S. and D.M. Husby (1981): Climatology of Surface Heat Fluxes over the California Current Region, NOAA Technical Report NMFS SSRF 763, 155p.
- Niiler, P.P. (1975): Deepening of the Wind-Mixed Layer, J. Mar. Res., 33, 405-422.
- Niiler, P.P. and E.B. Kraus (1977): One-Dimensional Models of the Upper Ocean, Modelling and Prediction of the Upper Layers of the Ocean, E.B. Kraus Ed., Pergamon Press, 143-172.
- Phillips, O.M. (1977): The Dynamics of the Upper Ocean, 2nd Edition, Cambridge, Univ Press, London.
- Pollard, R.T. (1977): Observations and Models of the Structure of the Upper Ocean, Modelling and Prediction of the Upper Layers of the Ocean, E.B. Kraus Ed., Pergamon Press, 102-117.
- Pollard, R.T. and R.C. Millard (1970): Comparison Between Observed and Simulated Wind-Generated Inertial Oscillations, Deep-Sea Res., 17, 813-821.

Pollard, R.T., P.B. Rhines, and R.O.R.Y. Thompson (1973): The Deepening of the Wind-Mixed Layer, Geophys. Fluid Dyn., 3, 381-404.

Price, J.F. (1977): Observation and Simulation of Storm Driven Mixed Layer Deepening, Ph.D. Thesis, University of Miami, 192p.

Price, J.F., C.N.K. Mooers, and J.C. Van Leer (1978): Observation and Simulation of the Storm-Induced Mixed Layer Deepening. J. Phys. Oceanogr., 8, 582-599.

Reid, J.L., Jr., G.I. Roden, and J.G. Wyllie (1958): Studies of the California Current System, Calif. Coop. Oceanic Fish Invest., Prog. Rep., 1 July 1956 to 1 January 1958, 27-57.

Resnyanskiy, Y.D. (1975): Parameterization of the Integral Turbulent Energy Dissipation in the Upper Quasihomogeneous Layer of the Ocean. Izv. Atmos. Oceanic Phys., 11, 726-733.

Shook, R.E. (1980): The One-Dimensionality of the Upper Ocean Mixing and the Role of Advection during the POLE Experiment, M.S. Thesis, Naval Postgraduate School, Monterey, CA., 69p.

Steiner, E.F. (1981): The One-Dimensional Model Predictions of Upper Ocean Temperature Changes between San Francisco and Hawaii, M.S. Thesis, Naval Postgraduate School, Monterey, CA., 77p.

Sverdrup, H.U., M.W. Johnson, and R.H. Fleming (1942): The Oceans, Prentice Hall, Inc., Englewood Cliffs, N.J., 1087p.

Tennekes, H. and J.L. Lumley (1972): A First Course in Turbulence, the MIT Press, Cambridge, Mass., 287p.

Thompson, R.O.R.Y. (1975): Climatological Numerical Models of the Surface Mixed Layer of the Ocean, J. Phys. Oceanogr., 6, 496-503.

Thompson, R.O.R.Y. (1976): Climatological Numerical Models of the Surface Mixed Layer of the Ocean, J. Phys. Oceanogr., 6, 496-503.

Thompson, R.O.R.Y. (1977): Reply to Garwood and Camp. J. Phys. Oceanogr., 7, 470-471.

Vager, B.G. and S.S. Zilitinkevich (1968): A Theoretical Model of the Diurnal Variations of the Meteorological Fields, Meteorolo. i. Gidrol., 7.

Warn-Varnas, A., M. Clancy, M. Morris, P. Martin, and S. Horton (1982): Studies of Large-scale Thermal Variability with a Synoptic Mixed-Layer Model, NORDA Technical Note 156, Naval Ocean Research and Development Activity, NSTL Station, MS, 33p.

Warrenfeltz, L.L. (1980): Data Assimilation in a One-Dimensional Oceanic Mixed Layer Model, M.S. Thesis, Naval Postgraduate School, Monterey, CA., 108p.

Zilitinkevich, D.V. Chalikov, and Yu. D. Resnyansky (1979): Modelling the Oceanic Upper Layer, Oceanologica Acta, 2, 219-237.

INITIAL DISTRIBUTION LIST

	No. Copies
1. Defense Technical Information Center Cameron Station Alexandria, VA 22314	2
2. Library, Code 0142 Naval Postgraduate School Monterey, CA 93943	2
3. Professor Robert J. Renard, Code 63Rd Department of Meteorology Naval Postgraduate School Monterey, CA 93943	1
4. Professor Christopher N.K. Mooers, Code 68Mr Department of Oceanography Naval Postgraduate School Monterey, CA 93943	19
5. Dr. Roland W. Garwood, Jr., Code 68Gd Department of Oceanography Naval Postgraduate School Monterey, CA 93943	1
6. LTJG Diane C. Durban NAVOCEANCOMFAC, Keflavik, IC Naval Station FPO, New York, N.Y. 09571	2
7. Director Naval Oceanography Division Naval Observatory 34th and Massachusetts Avenue, N.W. Washington, D.C. 20390	1
8. Commander Naval Oceanography Command Central NSTL Station Bay St. Louis, MS 39522	1
9. Commanding Officer Naval Oceanographic Office NSTL Station Bay St. Louis, MS 39522	1
10. Commanding Officer Fleet Numerical Oceanography Center Monterey, CA 93940	1

11. Commanding Officer 1
Naval Ocean Research and Development
Activity
NSTL Station
Bay St. Louis, MS 39522
12. Commanding Officer 1
Naval Environmental Prediction Research
Facility
Monterey, CA 93940
13. Chairman, Oceanography Department 1
U.S. Naval Academy
Annapolis, MD 21402
14. Professor Jerome Williams 1
Oceanography Department
U.S. Naval Academy
Annapolis, MD 21402
15. Chief of Naval Research 1
800 N. Quincy Street
Arlington, VA 22217
16. Office of Naval Research (Code 480) 1
Naval Ocean Research and Development
Activity
NSTL Station
Bay St. Louis, MS 39522
17. Scientific Liaison Office 1
Office of Naval Research
Scripps Institution of Oceanography
La Jolla, CA 92037
18. Library 1
Scripps Institution of Oceanography
P.O. Box 2367
La Jolla, CA 92037
19. Library 1
Department of Oceanography
University of Washington
Seattle, WA 98105
20. Library 1
CICESE
P.O. Box 4803
San Ysidro, CA 92073

21. Library 1
School of Oceanography
Oregon State University
Corvallis, OR 97331
22. Commander 1
Oceanographic Systems Pacific
Box 1390
Pearl Harbor, HI 96860
23. Mr. Ken Pollak 1
Bldg 13
Fleet Numerical Oceanography Center
Monterey, CA 93940
24. Dr. S.A. Piaczek (Code 480) 1
Naval Ocean Research and Development
Activity
NSTL Station
Bay St. Louis, MS 39522
25. LCDR D. R. Leath, USN 1
Fleet Numerical Oceanography Center
Monterey, CA 93940
26. LCDR M. Frost, RN 1
Fleet Numerical Oceanography Center
Monterey, CA 93940
27. Professor Allan R. Robinson 1
Center for Earth and Planetary Physics
100D Pierce Hall
Harvard University
Cambridge, MASS 02138
28. Dr. M. M. Rienecker (Code 68) 1
Oceanography Department
Naval Postgraduate School
Monterey, CA 93943
29. Professor George L. Mellor 1
Geophysical Fluid Dynamics
Program
Princeton University
Post Office Box 308
Princeton, New Jersey 08540

2L8168

Thesis

D7991 Durban

c.1 Analysis of observed
and modeled mixed lay- ved
ers: NOCAL region. ay-

14 MAR 86

31507

206168

Thesis

D7991 Durban

c.1 Analysis of observed
and modeled mixed lay-
ers: NOCAL region.



thesD7991

Analysis of observed and modeled mixed l



3 2768 001 89611 1

DUDLEY KNOX LIBRARY